

**Design and Synthesis of Antisense Peptide Nucleic Acid Conjugated MR
Contrast Agents**

**Design und Synthese von Antisense Peptid-Nukleinsäure konjugierten
MR Kontrastmitteln**

DISSERTATION

der Fakultät für Chemie und Pharmazie
der Eberhard-Karls-Universität Tübingen

zur Erlangung des Grades eines Doktors
der Naturwissenschaften

2007

vorgelegt von

Wu Su

Tag der mündlichen Prüfung

26. Oktober 2007

Dekan

Prof. Dr. Lars Wesemann

1. Berichterstatter

Prof. Dr. K. Albert

2. Berichterstatter

Prof. Dr. K.-H. Wiesmüller

Acknowledgements

The work described in this thesis is a result from the collaboration between the department of High-Field Magnetic Resonance Center at the Max Planck Institute for Biological Cybernetics, under the supervision of Prof. Dr. Kamil Ugurbil, and the Institute for Organic Chemistry at Eberhard-Karls University of Tuebingen, under the supervision of Prof. Dr. Klaus Albert and Prof. Dr. Karl-Heinz Wiesmüller. First of all, I would like to thank all of my three supervisors for their excellent guidance during my PhD period in Tuebingen. Prof. Dr. Kamil Ugurbil provided the opportunity, funding and intellectual support for my PhD study. Prof. Dr. Karl-Heinz Wiesmüller taught me every aspect about peptide chemistry with his limitless patience. Prof. Dr. Klaus Albert gave me generous advice on the characterization of peptide by NMR and reviewed the doctoral thesis. Thank you to the rest of my committee: Prof. Dr. Martin E. Maier and Prof. Dr. Hermann A. Mayer. It is my honor to have such a renowned group of scientists in my committee.

I would like to thank Dr. Joern Engelmann for his helpful advice during my study and living in Tuebingen. Joern gave me innumerable valuable suggestions about the research work. With his limitless patience, he never denied me whenever I want to discuss with him. His generous advice, constant encouragement and thoughtful temper helped me to improve my knowledge in various aspects. I appreciate all the reference letters you wrote for me and the proofreading for this thesis.

I express my special thanks to our cell biology group: Dr. Joern Engelmann, Ms. Ritu Mishra and Ms. Hildegard Schulz. Dr. Joern Engelmann directed all the biological studies. Ms. Ritu Mishra and Ms. Hildegard Schulz performed all the cell biological experiments. The work in this thesis would not have been possible without their collaboration.

I would like to thank Dr. Josef Pfeuffer for his help and advice at the beginning of this project and still after he has left the institute.

Acknowledgements

Thanks to all the chemists of our bioconjugate group: Dr. Goran Angelovski, Dr. Ilgar Mammadov, Aneta Brud, Anurag Mishra, Deepti Jha, and Kirti Dhingra. Your idea, support and suggestion are greatly appreciated.

Thanks to Dr. Rolf Pohmann and Dipl.-Ing. Michael Beyerlein for performing MRI measurements. Thanks to Ms. Tina Schröder for all the help on the administrative arrangement.

Many good friends of mine, such as Dr. Xiao-zhe Zhang, Dr. Mingrui Wu and Xiaohai Sun et al, have enriched my academic and social activity in Tuebingen. I will never forget your help, optimism and energy.

I would like to pay tribute to the support of my parents and brother for their love, understanding and encouragement throughout my life. I especially thank my girlfriend, Dr. Yujun Di, who is the best friend of mine. Her constant support and understanding help me through difficult times and make good times even better.

Time runs so fast. It has been almost three years for me to study and live in such a lovely and beautiful city – Tuebingen. It is always like a dream to me to work at Max-Planck Institute and to live in the cultural rich city. I will never forget the beautiful memory: the mild weather, the green mountains, the quiet Neckar valleys, the clean historic downtown, and most importantly, the kindly people.

Abstract

Magnetic Resonance Imaging (MRI) is one of the most important diagnostic tools available in medicine. The specificity and sensitivity of MRI can be further enhanced by the introduction of contrast agents. As many clinically valuable targets reside inside the cell membrane, therefore, developing efficient intracellular targeted MR contrast agent is required. The objective of the present project is to construct novel targeted intracellular MR contrast agents aiming to image mRNA transcription by MRI.

The first part of this thesis takes an effort to search for an optimal vector for the intracellular delivery of MR contrast agents. Eight intracellular MR contrast agents, which conjugate different cell-penetrating peptides (CPP) with FITC and Gd(III) complexes, were synthesized by a continuous solid phase synthesis scheme. The key intermediates and final products were characterized by ESI-MS. Relaxivities of these MR contrast agents were measured at a frequency of 123 MHz and a magnetic field of 3 T. The comparison studies of the uptake and toxicity on NIH/3T3 cells suggest that D-Tat₅₇₋₄₉ contrast agent could label cells sufficient to enhance significantly relaxation rates R_1 and R_2 for MR measurements, thus D-Tat₅₇₋₄₉ peptide proves to be a useful CPP for the development of new intracellular MR contrast agents.

The second part of this thesis describes the design and synthesis of antisense MR contrast agents, which conjugate PNA with CPP, Gd-DOTA and FITC. The intracellular uptake was confirmed by fluorescence spectroscopy, fluorescence microscopy and MR imaging on NIH/3T3 mouse fibroblasts as well as on transgenic dsRed cells. A subtoxic labeling concentration of 0.5 μM is sufficient to enhance significantly MR imaging contrast. The intracellular Gd(III) contents are at the range of $10^{-9}\sim 10^{-8}$ mol Gd/ 10^7 cells. An *in vitro* PNA-DNA binding assay confirmed that there is a significant higher specificity of the dsRed antisense contrast agent in comparison to its non-sense counterpart. However, no specific accumulation of the antisense dsRed CA in comparison to the non-sense CA could be detected in the target containing dsRed cells. Fluorescence microscopy studies have showed an exclusive endosomal localization of the contrast agents. Thus, further modifications of the contrast agents are required to achieve the release from endosomes or a direct uptake into the cytosol.

Table of Contents

| | |
|---|-------------|
| Acknowledgements | I |
| Abstract | III |
| Table of Contents | V |
| Abbreviations | VIII |
| Chapter 1. Introduction | 1 |
| 1.1 MR imaging and MR contrast agents | 1 |
| 1.2 Labeling of cells with MR contrast agents | 5 |
| 1.3 Antisense imaging | 9 |
| 1.4 Synthesis schemes of PNA-peptide conjugates | 13 |
| 1.5 Aim of the project | 17 |
| Chapter 2. Synthesis and screening of cell penetrating peptides for the intracellular delivery of MR contrast agents | 19 |
| 2.1 Research design | 19 |
| 2.2. Results | 21 |
| 2.2.1 Synthesis and characterization of CPP conjugated MR contrast agents | 21 |
| 2.2.2 Determining the concentration and relaxivity of CPP conjugated contrast agents in aqueous solution | 27 |
| 2.2.3 <i>In vitro</i> studies of Gd-DTPA conjugates with L-Tat ₄₉₋₅₇ , D-Tat ₅₇₋₄₉ , PTD-4 and NLS | 28 |
| 2.2.4 <i>In vitro</i> comparison studies of Gd-DTPA and Gd-DOTA conjugates of L-Tat ₄₉₋₅₇ , D-Tat ₅₇₋₄₉ , and Orn- D-Tat ₅₇₋₄₉ | 32 |
| 2.3. Discussion | 35 |
| 2.3.1 Synthesis of CPP conjugated, dual-labeled Gd(III)-based MR contrast agents | 35 |
| 2.3.1.1 Optimization of the coupling scheme for Fluorescein labeling | 35 |
| 2.3.1.2 Conjugate DTPA dianhydride with peptides | 35 |
| 2.3.1.3 Formation of Gd-complexes | 36 |
| 2.3.1.4 Relaxivity of CPP conjugated MR contrast agents | 37 |
| 2.3.2 Intracellular delivery of CPP conjugated MR contrast agents | 38 |
| 2.4. Summary | 40 |

Table of Contents

| | |
|--|-----------|
| Chapter 3: Design, synthesis and in vitro evaluation of antisense PNA conjugated intracellular MR contrast agents | 41 |
| 3.1 Research design | 41 |
| 3.2 Results | 43 |
| 3.2.1 Design of antisense PNA-CPP conjugates | 43 |
| 3.2.2 Synthesis of Gd-DOTA-Lys(FITC)-PNA-CPP conjugates | 46 |
| 3.2.3 Chelating with gadolinium and purification | 47 |
| 3.2.4 Determining the concentration and relaxivity of PNA conjugated contrast agents | 48 |
| 3.2.5 <i>In vitro</i> fluorescence studies on NIH/3T3 embryonic mouse fibroblasts | 49 |
| 3.2.6 <i>In vitro</i> MR studies on NIH/3T3 embryonic mouse fibroblasts | 52 |
| 3.2.7 Determination of intracellular Gd ³⁺ content | 53 |
| 3.2.8 <i>In vitro</i> test of antisense PNA hybridizing with target sequence | 57 |
| 3.2.9 <i>In vitro</i> biological studies on a transgenic cell line expressing dsRed | 58 |
| 3.3 Discussion | 60 |
| 3.3.1 PNA synthesis and cleavage | 60 |
| 3.3.2 Determining the relaxivity of PNA conjugated contrast agents in solution and in labeled cells. | 62 |
| 3.3.3 Intracellular uptake of PNA conjugated MR contrast agent | 62 |
| 3.3.3 Antisense imaging by MRI | 65 |
| 3.4. Outlook | 67 |
| 3.5 Summary | 68 |
| Chapter 4. Experimental | 69 |
| 4.1 General | 69 |
| 4.2 Synthesis of CPP conjugated, dual-labeled Gd(III)-based MR contrast agents | 69 |
| 4.2.1 Gd-DTPA-Lys(FITC)-L-Tat ₄₉₋₅₇ -OH (1) | 70 |
| 4.2.2 Gd-DTPA-Lys(FITC)-D-Tat ₅₇₋₄₉ -OH (2) | 72 |
| 4.2.3 Gd-DTPA-Lys(FITC)-Orn-D-Tat ₅₇₋₄₉ -OH (3) | 73 |
| 4.2.4 Gd-DTPA-Lys(FITC)-NLS-OH (4) | 74 |
| 4.2.5 Gd-DTPA-Lys(FITC)-PTD-4-OH (5) | 74 |

Table of Contents

| | |
|--|-----------|
| 4.2.6 Synthesis of 4,7,10-tricarboxymethyl- <i>tert</i> -butyl ester 1,4,7,10-tetraaza cyclododecane-1-acetate (DOTA-(tBu) ₃) | 75 |
| 4.2.7 Gd-DOTA-Lys(FITC)-L-Tat ₄₉₋₅₇ -OH (6) | 76 |
| 4.2.8 Gd-DOTA-Lys(FITC)-D-Tat ₅₇₋₄₉ -OH (7) | 77 |
| 4.2.9 Gd-DOTA-Lys(FITC)-Orn-D-Tat ₅₇₋₄₉ -OH (8) | 78 |
| 4.3 Synthesis of PNA-CPP conjugated MR contrast agents | 78 |
| 4.3.1 PNA synthesis | 78 |
| 4.3.2 Conjugate DOTA tris(<i>tert</i> -butyl) ester (DOTA-(tBu) ₃) with PNA-CPP conjugates | 80 |
| 4.3.3 Labeling PNA-CPP conjugate with FITC | 80 |
| 4.3.4 Chelating with gadolinium | 80 |
| 4.4 Cellular uptake assay | 81 |
| 4.5 Determination of intracellular Gd ³⁺ content | 82 |
| 4.6 In vitro test of antisense PNA hybridizing with target sequence | 83 |
| 4.7 <i>In vitro</i> MR studies | 83 |
| 4.8 Data analysis | 84 |
| References | 86 |
| Lebenslauf von Wu Su | 95 |

Abbreviations

Abbreviations

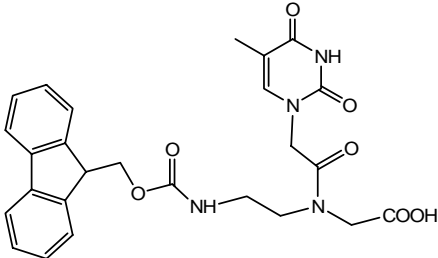
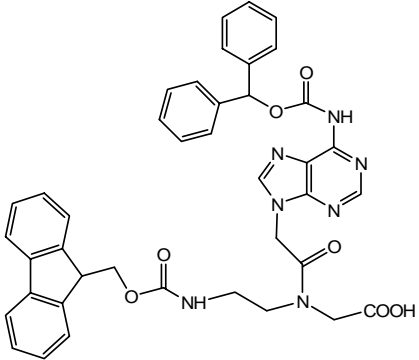
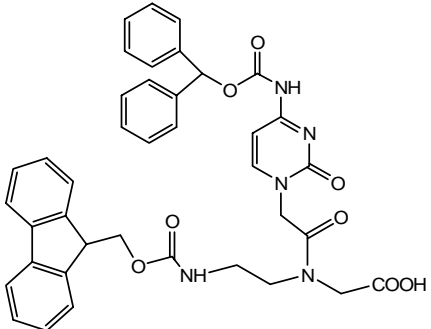
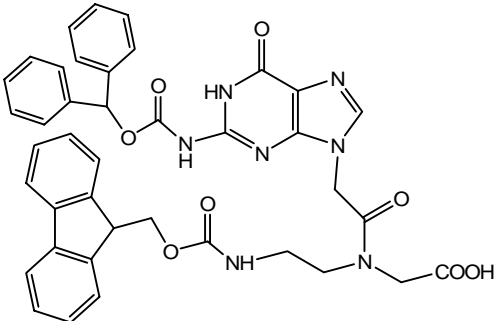
| Abbreviation | Name |
|---------------------------------|---|
| A | adenine |
| A (ala) | alanine |
| AEEA | aminoethoxyethoxyacetic acid |
| Boc | butoxycarbonyl |
| Bhoc | benzhydryloxycarbonyl |
| BLAST | basic local alignment and search tool |
| C | cytosine |
| CA | contrast agent |
| CLIO | cross-linked iron oxide particle |
| CPP | cell penetrating peptide |
| cyclen | 1,4,7,10-tetraazacyclododecane |
| DCM | dichloromethane |
| DIEA | N,N'-diisopropylethylamine |
| DMF | dimethylformamide |
| DOTA | 1,4,7,10-tetraazacyclododecane-N,N',N'',N'''-tetraacetic acid |
| DOTA (tris- <i>t</i> -Bu ester) | 1,4,7,10-tetraazacyclododecane-1,4,7-tris(acetic acid- <i>tert</i> -butyl ester)-10-acetic acid |
| DTPA | diethylenetriaminepentaacetic acid |
| EPC | endothelial progenitor cell |
| ESI-MS | electrospray ionization mass spectrometry |
| FITC | fluorescein isothiocyanate |
| Fmoc | 9-fluorenylmethoxycarbonyl |
| G | guanine |
| HATU | 2-(1-H-7-azabenzotriazol-1-yl)-1,1,3,3-tetramethyluronium hexafluorophosphate |
| HBTU | 2-(1H-benzotriazol-1-yl)-1,1,3,3-tetramethyluronium |

Abbreviations

| | |
|-------------|---|
| | hexafluorophosphate |
| HBSS | Hanks' balanced salt solution |
| HIV | human immunodeficiency virus |
| HOBt | 1-hydroxybenzotriazole |
| HSA | human serum albumin |
| K (Lys) | lysine |
| MION | monocrystalline iron oxide nanoparticle |
| MR | magnetic resonance |
| MRI | magnetic resonance imaging |
| NIH/3T3 | mouse embryonic fibroblast |
| NMR | nuclear magnetic resonance |
| O (Orn) | ornithine |
| ODN | oligodeoxynucleotide |
| P (Pro) | proline |
| PAMAM | polyamidoamine |
| Pbf | 2,2,4,6,7-pentamethyldihydrobenzofuran-5-sulfonyl |
| PBS | phosphate buffered saline |
| PNA | Peptide Nucleic Acid |
| Q (Gln) | glutamine |
| R (Arg) | arginine |
| SPIO | superparamagnetic iron oxide |
| T | thymine |
| <i>t</i> Bu | <i>tert</i> -butyl |
| TFA | trifluoroacetic acid |
| TIS | triisopropylsilane |
| Trt | trityl |
| USPIO | ultrasmall superparamagnetic iron oxide |
| UV | ultraviolet |
| V (Val) | valine |
| Y (Tyr) | tyrosine |

Abbreviations

PNA Monomers

| Common Name | Structure |
|---|--|
| <p>Fmoc-PNA-T-OH $C_{26}H_{26}N_4O_7$ MW: 506.51</p> |  |
| <p>Fmoc-PNA-A(Bhoc)-OH $C_{40}H_{35}N_7O_7$ MW: 725.75</p> |  |
| <p>Fmoc-PNA-C(Bhoc)-OH $C_{39}H_{35}N_5O_8$ MW: 701.72</p> |  |
| <p>Fmoc-PNA-G(Bhoc)-OH $C_{40}H_{35}N_7O_8$ MW: 741.75</p> |  |

Chapter 1. Introduction

1.1 MR imaging and MR contrast agents

Magnetic Resonance Imaging (MRI) is one of the most versatile imaging techniques based on the principles of nuclear magnetic resonance (NMR). With its excellent spatial resolution, noninvasive nature and so far unsurpassed ability in distinguishing soft tissues, MRI has therefore become one of the most important diagnosis tools available in medicine (1, 2). MRI offers high three-dimensional spatial resolution down to the 10- μm range (3, 4), complete body coverage, and the opportunity to determine additional physiologic parameters noninvasively (e.g., blood flow, perfusion, and diffusion). All these characterize MRI to contain considerable potential for molecular imaging (5). The MRI signal is created through the interaction of the total water signal (proton density) and the magnetic properties (T_1 : the longitudinal relaxation time, and T_2 : the transverse relaxation time) of the tissues being imaged. Differential contrast in soft tissues depends on endogenous differences in water content, relaxation times, and/or diffusion characteristics in the tissue of interest. T_1 and T_2 weighted images display the best contrast for soft tissues, as proton spin density is essentially invariant while relaxation times vary greatly from one tissue to the other (6, 7).

Nevertheless, there remains the possibility of poor contrast between healthy and damaged tissue due to a too small variation in relaxation times. MR contrast agents are chemicals, which are able to enhance the relaxation rates of water protons (8). They are applied in MR imaging to increase the signal difference between the area of interest and the background. Indeed, the influence of MR contrast agents on the relaxation times of proton spins has a marked effect on the signal intensity thereby increasing the contrast of the images and better delineating the objective regions.

MR contrast agents do not appear themselves on MR images but affect longitudinal and transverse relaxation of the surrounding nuclei, mainly the water solvent protons (9). The addition of a contrast agent results in an increased relaxation rate of the surrounding nuclei that appear as a bright spot of increased intensity in T_1 -weighted images or as a region of decreased brightness in T_2 -weighted images (10). MR contrast agents are thus classified as positive or negative, T_1 or T_2 , contrast agents. The two major classes of MR

Chapter 1. Introduction

contrast agents are paramagnetic contrast agents, usually based on the chelates of Gd(III) generating T_1 positive signal enhancement (11, 12), and super-paramagnetic contrast agents that use mono- or polycrystalline iron oxide to generate strong T_2 negative contrast in MR images (13).

Most of MR contrast agents, which have already approved for clinical use, are complexes of gadolinium (III) as this ion has a high magnetic moment and a long electronic relaxation time. The choice of Gd(III) would be expected, for no other ion has seven unpaired electrons. But there is a much more subtle reason it performs so well. The symmetric S-state of Gd(III) is a hospitable environment for electron spins, leading to a much slower electronic relaxation rate. In the intricate effect that gives rise to relaxivity, water protons hardly feel the effects of ions such as Dy(III); Gd(III) electrons, on the other hand, are more closely in tune with the proton's frequency (10). Thus Gd(III) exhibits the strongest effect of all elements on the longitudinal relaxation time T_1 . Water exchanges quite readily on Gd(III) aqua complexes. The rate of exchange between aqua ligands on octadenate-chelated Gd(III) is approximately $3 \times 10^6 \text{ s}^{-1}$, which allows thousands of water molecules to transiently coordinate to a single ion on the MRI time scale. Therefore, the effect of the metal fragment on relaxation times is widespread, and only low concentrations (0.1-0.3mmol/Kg) are necessary to be effective.

Since T_1 weighted protocols in MRI have rapid pulse sequences, the advances in MRI have strongly favored T_1 agents and thus Gd(III) (10). Faster scans with higher resolution require more rapid radio frequency pulsing and are thus generally T_1 -weighted since the MR signal in each voxel becomes saturated. T_1 agents relieve this saturation by restoring a good part of the longitudinal magnetization between pulses. At the same time, a good T_1 agent would not significantly affect the bulk magnetic susceptibility of the tissue compartment in which it is localized, thus minimizing any inhomogeneities which can lead to image artifacts and/or decreased signal intensity. Small iron particles can function as T_1 agents using very T_1 -weighted scans, but the resulting changes in magnetic susceptibility are much larger than that for Gd(III) chelates.

However, since the free metal ion of Gd (III) being toxic, its complexation is needed in order to ensure the innocuousness of the agent during its travel through the body of the patient. Gadolinium chelate remains in the body several days after intravenous

administration. Coordinating the metal to ligands can reduce its toxicity if the chelates are too obstinate to be displaced by water (12). Currently, all Gd(III)-based chelates approved for clinic application in MRI are eight or nine-coordinated complexes. One or two coordination sites must be open for water molecules, to allow inner sphere spin transitions, or transitions between the metal nuclei and a ligand to which they are directly bound. The formation of kinetically inert and thermodynamically stable complexes of Gd (III) has been demonstrated with chelating agents such as diethylenetriaminepentaacetic acid (DTPA) and 1,4,7,10-tetracarboxymethyl-1,4,7,10-tetraazacyclododecane (DOTA) (Figure 1). The metal ion is buried in the cage, so it is unlikely to bind to donor groups in proteins and enzymes. There is nothing in the chemical structure of the ligand that a good nucleophile or electrophile can attack. They actually do remain chelated in the body and are excreted intact. Apparently, the off-the-shelf ligands such as DTPA or DOTA form complexes strong enough so that, for the period that the agents are in the body, there is no detectable dissociation. This is in the face of significant amounts of phosphate, citrate, transferrin, and other chelating substances. Since the approval of $[\text{Gd}(\text{DTPA})(\text{H}_2\text{O})]^{2-}$ in 1988, it can be estimated that gadolinium chelates have been administered to millions of patients worldwide. Currently, approximately 30% of MRI examinations include the use of contrast agents, and this is projected to increase as new agents and applications arise (10).

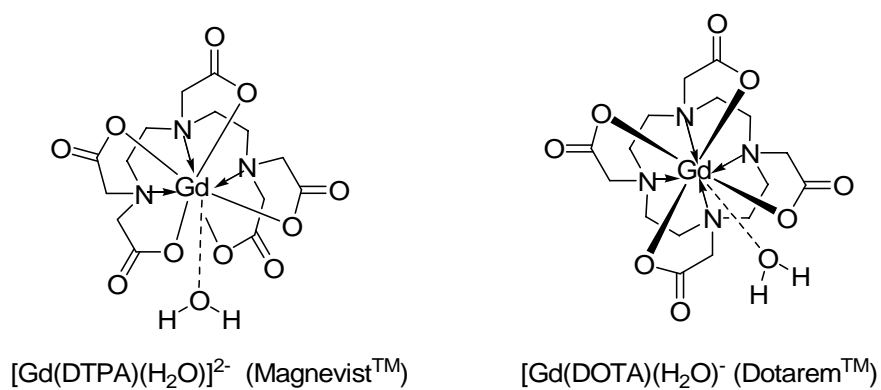


Figure 1. Chemical structures of $[\text{Gd}(\text{DTPA})(\text{H}_2\text{O})]^{2-}$ and $[\text{Gd}(\text{DOTA})(\text{H}_2\text{O})]^{-}$

Iron-oxide-based contrast agents usually consist of a monocrystalline (MION) or small polycrystalline (SPIO) magnetic core with a diameter of 5 to 30 nm embedded with a polymer coating (such as dextran or other polysaccharides) for a total particle diameter of

Chapter 1. Introduction

17-50 nm, respectively. Generally, the relaxation properties of these contrast agents depend on the molecular size of the carrier and larger molecules have a higher relaxivity per molecule. Therefore to improve the sensitivity of detection, it is feasible to use large, highly efficient contrast agents. For example, SPIO particles can be detected at micromolar concentrations of iron, and offer sufficient sensitivity for T₂-weighted imaging. On the other hand, the large molecular size can prevent effective extravasation of the contrast agent molecules from the vasculature, and reduce diffusion of the contrast agent through the interstitium (13, 14).

These contrast agents discussed above are all non-specific, even if their distribution in the body is far from homogeneous, and their efficacy in enhancing contrast stems from their preferential distribution in the blood stream because they are all quite hydrophilic. Nonspecific contrast agents are widely available for clinical use. They show a nonspecific distribution pattern that allows measurement of tissue perfusion, vascular permeability, or vascular volume in a given voxel. These parameters can be extracted by fast imaging techniques and pharmacologic modeling or steady-state imaging techniques (15, 16). However, true molecular targets can not be imaged with this approach. Thus, there remains the need for novel compounds of improved performances. Increased efficacy, exclusive blood distribution, targeting, and sensing are some of the exciting properties of the new molecules developed in the last few years (17, 18). These novel MR contrast agents can be basically divided into smart and targeted probes according to their dynamic mechanism.

Smart contrast agents might change MR signals, which depend on some variables in their immediate environment. Various stimuli, ranging from pH to enzymes, have been exploited for generating intelligent agents (19 - 21). The most important factor for obtaining an efficient smart contrast agent is that the percent change in relaxivity, and not its absolute value. Usually, smart contrast agents have been built on Gd(III) systems because their relaxivity can be dictated by their environment. The numbers of water molecules in the first coordination sphere, the water exchange rate and the rotational correlation time have a strong effect on the relaxivity of the compounds and can be influenced by many other factors.

Targeted MR contrast agents are linked to specific affinity ligands such as peptides, antibody fragments, or small molecules imparting molecular specificity to the probe. Combining efficient targeting strategies with sensitive imaging techniques may help to resolve molecular targets in the nanomolar range *in vivo*. Thus, the detection of cell surface proteins (e.g., tumor associated receptors) is feasible (22). Approaches to increase the sensitivity of MR with targeted contrast agents were presented by Wickline et al. (23) who significantly amplified the number of reporter molecule per nanoparticle (up to 90,000 gadolinium chelates per nanoparticle). The nanoparticles can be targeted with high affinity to specific molecules via antibodies. This scheme was exploited for visualization of fibrin in vascular plaques and vascular expression of integrins in tumors (23). Other studies have reported targeted contrast agents for imaging Alzheimer amyloid plaques, the human transferrin receptor, and the secretin receptor or the endothelial integrin $\alpha_v\beta_3$ (24, 25). More recently, an antibody-conjugated gadolinium chelate was applied for *in vivo* MR imaging of HER-2/neu receptors in a mouse xenograft model (26, 27). Biotinylated anti-HER-2/neu antibody was administered first followed by a gadolinium chelate complexed with avidin; the amplified R_1 lengthening effect indicates that the agent is localized to tumor areas in which the HER-2/neu receptor is expressed.

1.2 Labeling of cells with MR contrast agents

Due to its high spatial resolution capabilities and excellent soft tissue contrast, MR imaging is excellently suited for cell tracking application. MRI contrast agents can be incorporated into cells by electroporation, and passive or active targeting mechanisms such as phagocytosis, pinocytosis, receptor mediated endocytosis, transporters, and cell penetrating peptide mediated intracellular uptake (28). Passive targeting agents primarily highlight phagocytic cells and organs naturally responsible for particle clearance within the body. Active targeting refers to ligand-directed, site-specific accumulation of contrast and /or therapeutic agents.

Electroporation has recently been used to label cells with Gd chelates and SPIO nanoparticles (29). Electroporation is commonly used to introduce DNA into the cell genome and is known to be associated with cell stress due to chemical imbalances and efflux or influx of chemicals from within the cell and surrounding media altering the cells

Chapter 1. Introduction

viability and survival. There is relatively little experience using this approach with MRI contrast agents to label cell, and it is unclear as to the long-term effects on reactive oxygen species (ROS) or cell viability when using this method. It has been demonstrated that a significant amount of cell lysis and death occurred during electroporation, and following labeling of contrast agents (30).

Phagocytosis is a special form of endocytosis in which particles are ingested through the formation of a large endocytic vesicle. In principle this appears the route of choice for labeling cell endowed with efficient phagocytic activity, as it would allow single step internalization of large amount of contrast agent. Whereas the entrapment of iron oxide particles by this process is immediately effective in inducing marked change in MR contrast of labeled cells, in the case of Gd containing particles, it is necessary to foresee its further solubilization in order to fully exploit the potential of the imaging probe based on paramagnetic Gd-chelates (31).

Pinocytosis, also called fluid endocytosis, is the process through which the cell entraps portions of the extracellular fluid by means of the progressive invaginations of the membrane, to form vesicles that evolve from early to late endosomes eventually to end up into lysosomes. Incubation of cells in a medium containing MR contrast agents at sufficiently high concentration leads to its internalization at amounts that may be sufficient for MR imaging (32).

Receptor mediated endocytosis is the most widely applied scheme to internalize MR contrast agents into cells as it is expected to occur anytime a ligand is modified by attaching one or more metal-chelate moieties. Receptor mediated endocytosis is the mechanism of choice for the internalization of dendritic polymers containing a high number of Gd(III) complexes. The first example of receptor-mediated endocytosis of Gd(III) complexes dendritic polymers dealt with the targeting of tumor cells overexpressing the high affinity folate receptor (hRF) (33). It showed that the uptake of folate-conjugated dendrimers into cells occurs with a sigmoidal dose-responsive curve as expected for a specific uptake. Other samples of receptor-mediated endocytosis of MR contrast agent included β -D-galactose receptor, cholecystokinin receptor and somatostatin analogs.

Transporters' scheme appears an interesting one as such systems are intrinsically devoted to cell internalization of large quantities of substrate molecules. Gd-DTPA-glutamine has been tested to differentiate tumor from healthy cells. After a few hours of incubation, the amount of Gd-chelate internalized in tumor cells is 4-5 times higher than that taken up by healthy hepatocytes (34).

Cell penetrating peptides (CPPs) have been extensively utilized to achieve intracellular delivery (35-37). CPPs usually consist of short, typically basic, peptide sequences of 7–34 amino acids in length that are capable of crossing the cell membrane either alone or attached to a molecular cargo. Early observations revealed that these cell-penetrating peptides rapidly translocate into various cell types. Included among such peptides are the third helix of the homeodomain of Antennapedia (38), polyarginines (39), guanidinium peptides (40), and viral proteins such as herpes simplex virus VP22 (41), HIV-1 Rev protein (42), and the basic domain of HIV-1 Tat protein (43). When administered in non-toxic concentrations, CPPs can be used to transport genes, therapeutic drugs and diagnostic probes into the intracellular compartment. Although the exact mechanism for membrane translocation of CPPs remain under investigation, successful utilization of CPPs not only for molecular imaging, but also for therapeutic and combined applications, is progressing in numerous fields of research.

Delivering imaging agents to intracellular compartments by peptides would allow for selective retention and signal amplification, thereby opening up a broad range of novel molecular imaging applications (44). CPPs have been explored to carry MR contrast agents into cells. Bhorade *et al.* reported that Gd-DOTA bound to HIV-Tat peptide is efficiently internalized into mammalian cells (45). For this application, DOTA is conjugated to a Lys C-terminally appended to Tat using orthogonal synthetic strategies and stably complexed with Gd under standard conditions (Figure 2). T₁-weighted spin-echo MR images of cells embedded in agar indicated the presence of enhanced intracellular relaxivity, consistent with transduction of Gd-DOTA-Tat peptide into the cell interior. The intracellular localization of the Gd complex was confirmed with a fluorescein-conjugated Tat peptide that showed cytosolic localization. Furthermore, intracellular delivery of the Gd-DOTA complex using other CPPs such as poly-Arg peptides has been reported (46). The permeation, relaxivity, and enhanced retention

Chapter 1. Introduction

properties of the Gd-DOTA poly-Arg peptide were well characterized in several cell types using inductively coupled plasma mass spectrometry (ICP-MS) and T_1 relaxivity measurement (47).

Gly - Arg - Lys - Lys - Arg - Arg - Gln - Arg - Arg - Arg - Gly - Tyr - Lys - NH₂

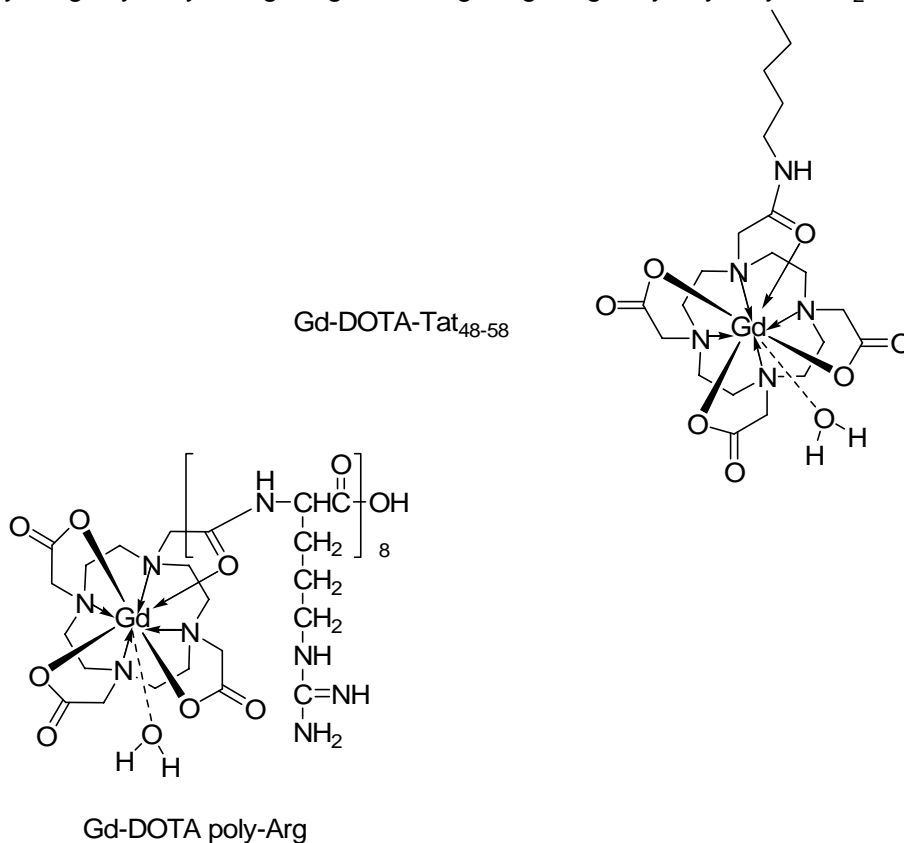


Figure 2. CPP conjugated intracellular MR contrast agents

The Tat peptide has also been used to mediate delivery of biocompatible cross-linked iron oxide particles (CLIO) and superparamagnetic nanoparticles into cells (48). The derivatized particles have been shown to internalize into mouse spleen lymphocytes greater than 100-fold more efficiently than nonmodified particles. By labeling CLIO particles with FITC, cytoplasmic and nuclear localization was demonstrated. CLIOs affect the transverse relaxation time (T_2) by introducing large susceptibility effects, which alter the local magnetic field homogeneity and result in signal loss where CLIOs are located. The strong decrease in signal by MR imaging enables the magnetically labeled cells to be tracked *in vivo*. These results demonstrate that CPP can be used to ferry

magnetic particles efficiently into cells; and labeled cells can be visualized by MR imaging at the single-cell level *in vitro* and/or induce signal intensity changes detectable in whole organs (48).

1.3 Antisense imaging

Real-time imaging of gene expression *in vivo* at high spatial resolutions has been a long-cherished goal in molecular research (49). If such techniques were available, both endogenous and exogenous (for example, gene therapy) expression could be studied in live animals and potentially in a clinical setting. Currently, the most widely used strategies for imaging gene expression are termed “direct” and “indirect” approaches (50). Direct molecular imaging can be defined in terms of a probe–target interaction, whereby the resultant image of probe localization and magnitude (image intensity) is directly related to its interaction with the target epitope or enzyme. A recent direct imaging strategy involves the development of antisense and aptamer oligonucleotide probes that specifically hybridize to target mRNA or proteins *in vivo*. Radiolabeled antisense probes (RASONS) have been developed to directly image endogenous gene expression at the transcriptional level. RASONS are small oligonucleotide sequences that are complementary to a small segment of target mRNA or DNA and could potentially target any specific mRNA or DNA sequence. In this context, imaging specific mRNAs with RASONS produces “direct” images of specific molecular-genetic events. Direct imaging of mRNA can provide information on cellular gene expression patterns and may have the potential to detect molecular changes in disease states at relatively early stages, providing opportunities for pre-emptive therapeutic interventions.

The concept of using antisense molecules to inhibit gene expression was introduced in 1967, as a result of the elucidation of the rules of Watson-Crick and Hoogsteen base pair formation between nucleic acids (51); the basis of this promise was that specific DNA or messenger RNA sequences could be arrested uniquely by relatively short complementary oligonucleotides for antigene or antisense therapy, respectively (Figure 3). The principles for application of antisense agents in antiviral and cancer therapy are now well defined (52). Theoretically, the same principles could serve as guidelines for the development of

Chapter 1. Introduction

labeled antisense oligonucleotide analogues for imaging gene expression. Therefore, antisense imaging should be highly specific from theoretical considerations.

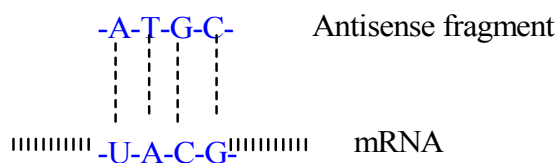


Figure 3. Base pairing between purines and pyrimidines

In 1994, Dewanjee produced the first non-invasive tumor image in a living animal model using a radiolabeled antisense oligonucleotide (53). Yet real-time, direct, *in vivo* imaging of endogenous gene expression has still not been demonstrated in a widespread and conclusive manner by this method. Various problems have exhibited such as: (i) low number of target mRNA/DNA molecules per cell; ii) limited tracer delivery (poor cell membrane and vascular permeability, cannot penetrate blood–brain barrier); (iii) poor stability (degradation by H-RNase); (iv) slow clearance (slow washout of nonbound oligonucleotides); and (v) comparatively high background activity and low specificity of localization (low target/background ratios). Recent developments in antisense imaging technology extend the possibility that this modality will become an extremely powerful tool for the noninvasive study of gene expression *in vivo*. These developments include: (i) new antisense analogues with superior properties for binding macromolecular nucleic acids, (ii) advances in radiolabeling chemistry to produce extremely high specific activity antisense imaging agents, (iii) novel drug targeting technology to improve *in vivo* specificity, and (iv) emerging optical imaging modalities for *in vitro* screening applications and real-time *in vivo* imaging of gene expression (54).

The first antisense agents were DNAs, but these oligonucleotides are rapidly degraded by nucleases *in vivo*, greatly limiting their utility for imaging applications. A number of novel oligonucleotide analogues, designed for improved stability, target binding, and antisense activity, have been synthesized and evaluated *in vitro* and *in vivo*. Methylphosphonate DNA, Phosphorothioate DNA, 2'-O-methyl RNAs (55), PNAs (peptide nucleic acids) (56), MORFs (morpholino) (57), and HypNA-pPNAs (trans-4-

hydroxy-L-proline nucleic acid-phosphono nucleic acid) (58) (Figure 4) bind complementary RNA with greater affinity, stability, and mismatch specificity than corresponding DNA:RNA duplexes, potentially rendering them more suitable for antisense imaging.

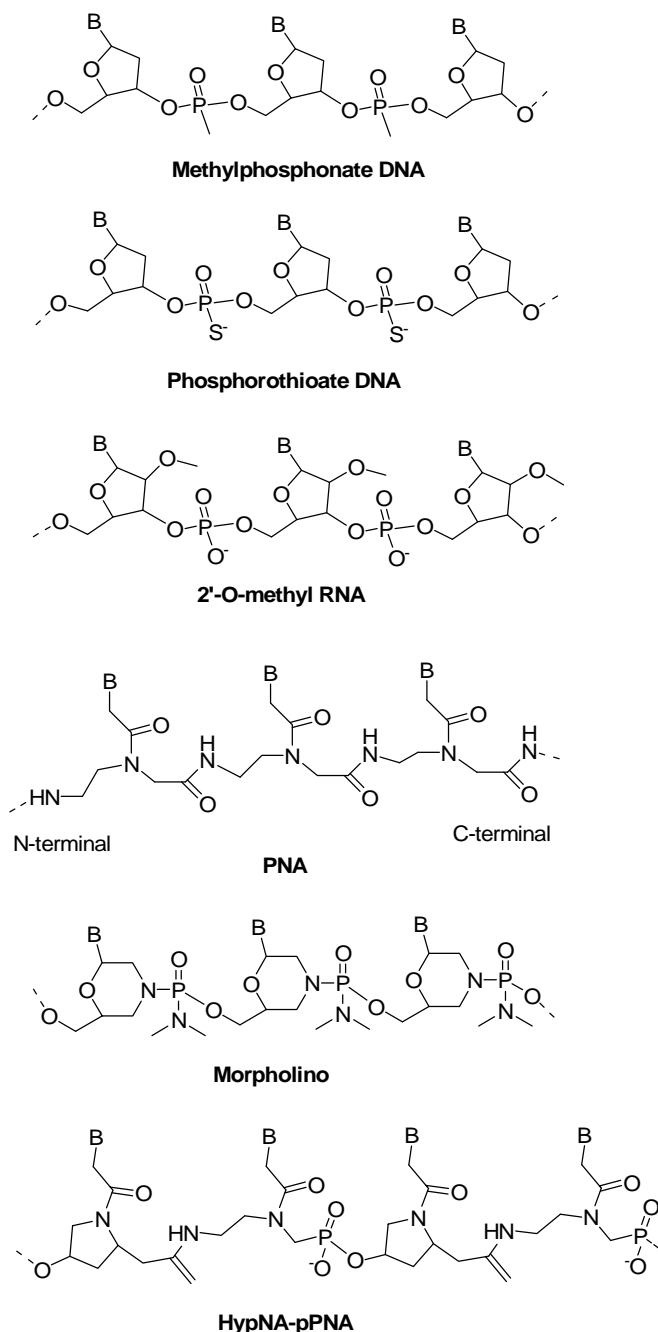


Figure 4. General structures of some DNA and RNA analogues for antisense imaging

Chapter 1. Introduction

PNA is a DNA mimic containing a pseudopeptide backbone that makes it extremely stable in biological fluids. Despite the radical difference in the chemical composition of the backbone, PNA not only retains but also improves the hybridization characteristics of DNA and RNA. In most cases PNA oligomers with mixed bases sequences form duplexes (by Watson-Crick base-pairing) with complementary DNA and RNA with higher thermal stability than corresponding DNA-DNA or DNA-RNA complexes and without sacrificing sequence specificity (59). These qualities make PNA a leading agent among ‘third generation’ antisense and antigene agents (60). For example, Pardridge *et al.* (61) reported the imaging of gene expression in the brain *in vivo* by a PNA-antisense probe. They synthesized an antisense-imaging agent comprised of a radio-iodinated PNA conjugated to a monoclonal antibody to the rat transferrin receptor by using avidin-biotin technology. The PNA is a 16-mer antisense to the sequence around the methionine initiation codon of the luciferase mRNA. The PNA conjugate was injected intravenously in animals with brain tumors and which were killed 2h later for frozen sectioning of brain and film autoradiography. Tumors were imaged in all rats administered the [¹²⁵I] labeled PNA that was antisense to the luciferase sequence. This study demonstrated that gene expression in the brain *in vivo* could be imaged with antisense radiopharmaceuticals that are conjugated to a brain drug-targeting system.

Tian *et al.* (62) also designed an antisense PNA probe, which conjugated PNA with an IGF1 peptide on the C-terminus, and a [^{99m}Tc] chelator on the N-terminus. The PNA is a 12-mer antisense to the sequence of the MYC mRNA. MCF7 xenografts in nude mice were visualized at 4 and 24h after tail vein administration of the [^{99m}Tc] PNA probe specific for MYC mRNA, but not with the mismatch control.

These results demonstrated that molecular imaging of oncogene mRNA in solid tumors with antisense PNA-peptide chimeras might provide additional genetic characterization of pre-invasive and invasive cancers.

Although there are a lot of publications which reported to image gene expression by radio labeled antisense imaging, MRI imaging of gene expression are usually achieved by two approaches: (i) imaging of introduced reporters or enzymes, which bind or metabolize paramagnetic substrates; or (ii) imaging of a unique spectroscopic signature (63).

Developing the antisense conjugated MRI contrast agent will propose a new method to image gene expression *in vivo*. In addition, development of targeted MR contrast agent directed to specific molecular entities could dramatically expand the range of MR applications by combining the noninvasiveness and high spatial resolution of MRI with specific localization of molecular targets.

In 2003, Heckl et al. (64) reported the first and to date the only results on an intracellular MR contrast agent, composed of a gadolinium complex, a *c-myc*-specific PNA sequence and a transmembrane carrier peptide, showing the potential of tracking cells *in vivo* by MRI using mRNA as target. In MR imaging, increased intracellular signal intensity in HeLa cells could be detected after just 10 min of incubation with Gd³⁺-complex and subsequently reached a maximum after 1h. This rapid increase in signal intensity after 10 min was also observed *in vivo* in Dunning prostate tumors independent of the specificity of PNA, and subsequently, reaching a maximum after 30 min. However, there is no further study reported. Whether improvements on this strategy can be achieved using different carrier peptides and/or contrast agent moieties remains an important question.

1.4 Synthesis schemes of PNA-peptide conjugates

The main hindrance to the effective use of PNA oligomers has been their relatively poor uptake by cells. A great deal of effort has gone into devising means for enhancing the intracellular delivery of oligonucleotides (65, 66), including viral vectors, cationic lipids and cationic liposomes. Although cationic lipids and polymer carriers have been widely used in the laboratory setting, a new approach involving conjugation of oligonucleotides to peptide vectors seems particularly promising. Peptide-oligonucleotide conjugates (67), unlike oligonucleotide complexes with cationic lipids or polymers, are of relatively modest molecular size. Thus, they are more likely to evade uptake by the phagocytes of the reticuloendothelial system and to attain a widespread biodistribution subsequent to *in vivo* administration.

Two different strategies have been adopted for the synthesis of PNA-peptide conjugates: On-line continuous solid-phase synthesis schemes and fragment conjugation schemes (68).

Chapter 1. Introduction

During continuous solid-phase synthesis scheme, PNA-peptide conjugates are synthesized by adaptation of established solid-phase peptide synthesis protocols (69). Commercially available PNA monomers have their back-bone amine group protected with either the 9-fluorenyl-methoxycarbonyl (Fmoc) or N-tert-butoxycarbonyl (Boc) group, while the exocyclic amines of the nucleobases (A, C and G) are protected by the benzhydryloxycarbonyl (Bhoc) or Benzyloxycarbonyl (Z) protecting groups. The solid-phase synthesis of a peptide-C-terminal to N-terminal-PNA conjugate commences with the immobilization of a PNA monomer to an acid labile linker on a suitable resin. Usually, the polyethyleneglycol-polystyrene (PEG-PS, linker=link amide) resin can be used for Fmoc/Bhoc chemistry synthesis scheme; whereas the PS resin (linker = methylbenzhydrylamine) resin is compatible with Boc/Z chemistry synthesis scheme. Removal of the N-terminal protecting group (with 20% piperidine/ DMF for Fmoc or 50% TFA for Boc, is followed by elongation with the next protected building block under the agency of a coupling reagent (e.g. HATU) and capping of residual amines with acetic anhydride, which leads to a PNA dimer. Repetition of this reaction cycle entailing deprotection, coupling and capping steps eventually leads to the construction of an immobilized fully protected PNA-peptide conjugate. End-capping of this construct (removal of the final protecting group and acetylation of the N-terminus) is carried to prevent the formation of PNA rearrangement or breakdown products. Finally, cleavage from the resin and deblocking of the protecting groups (TFA in the presence of scavengers (Fmoc); HF or 10% TFMSA/TFA and scavengers (Boc)) affords the target peptide-PNA conjugate.

In the fragment conjugation scheme, PNA oligomer and peptide oligomer are assembled separately on their own solid supports. After the synthesis and purification of individual PNA and peptide sequences, they are finally conjugated to each other chemoselectively (68). Different methods can be discerned on the basis of the type of linkage between the peptide and PNA fragments. The functional linkages commonly used in fragment conjugation included amide, disulfide, thioether, oxime, and thioester etc. The general reactions used to prepare some of the linkages are summarized in Figure 5.

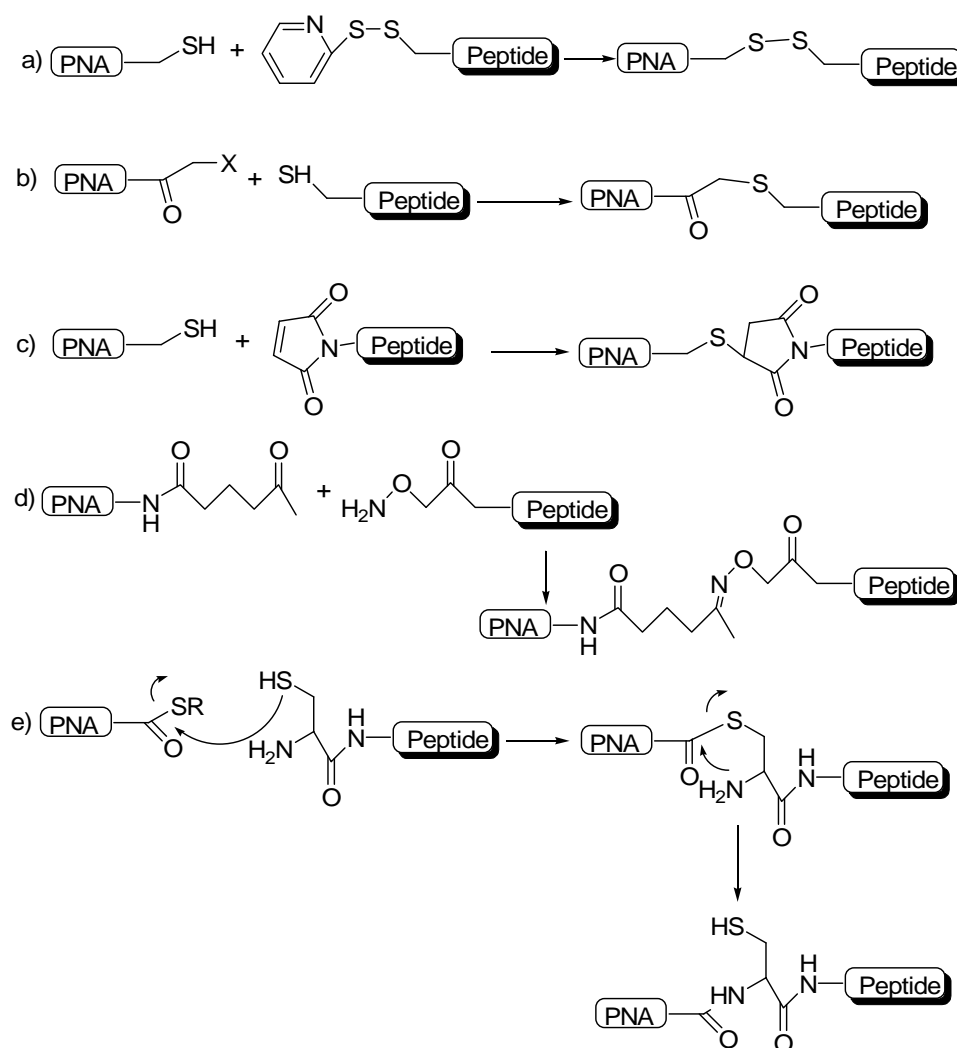


Figure 5. Schematic representation of the coupling strategies for PNA-peptide conjugates.

a) Disulfide formation by thiopyridyl activation. b) Thioether formation. c) Thioether bond formation by maleimide functional group. d) Oxime formation. e) Native chemical ligation.

A frequently used method is the linkage of fragments via a disulfide bond (70). The main reason is that disulfide bonds in PNA-peptide conjugates are vulnerable for cleavage in the reductive environment of the cytosol, thus releasing the free PNA sequence after intracellular uptake. For the formation of disulfide bond, both peptide and PNA fragments need to contain a thiol moiety, usually obtained by the incorporation of a

Chapter 1. Introduction

cysteine residue at either the C-terminal or N-terminal position. The preparation of disulfides originates from synthetic protocols developed in peptide chemistry and conducted following direct oxidation of two free thiols. This oxidative coupling method can give rise to the formation of symmetrical dimers, besides the desired product. The yield can be improved by the use of an excess of one of the fragments, which can give a more selective conversion. A more fruitful procedure to disulfide bond formation exploits the nucleophilicity of the thiol group of one of the fragments and activation of the other thiol group (71). An often-applied method to activate a thiol group towards nucleophilic substitution is its attachment to a thiopyridyl moiety. Nucleophilic substitution of this moiety by the incoming free thiol of the other fragment results in formation of the desired product. It is important to note that these coupling reactions should be carried out in an oxygen-free environment to prevent unwanted dimerization of molecules carrying a free thiol group.

The nucleophilicity of the thiol group can also be applied to prepare PNA-peptide conjugates having more stable thioether linkages (72). For example, the thiol containing segment can react in a Michael type reaction with double bond of a maleimide functional group of the other fragment to give a covalently linked conjugate. Other potential nucleophiles, such as the side-chain amines in peptides are protonated at pH 8, rendering them unreactive.

Chemoselective oxime formation is one of the most commonly used linkages in an alternative strategy to couple PNA and peptide fragments (73). This is because oxime formation is an efficient reaction, requires no harsh conditions, involves highly reactive functional groups, and introduction of the aldehydes and hydroxylamine on either fragment is relatively easy. In this strategy, a ketone functionality of one fragment was reacted with an amino-oxyacetic acid to the C-terminal side-chain amine functionality. The condensation was carried out in aqueous buffer at pH 4.2 and proceeds in a highly efficient manner.

Recently, an alternative approach for the synthesis of peptide-PNA conjugates (74) was reported using Kent's native chemical ligation strategy (75). This type of ligation is based on a reversible transthioesterification between two unprotected fragments, one containing a C-terminal thioester and the other an N-terminal cysteine. Rearrangement by a

proximity-driven nucleophilic attack of the cysteine amine on the thioester irreversibly leads to an amide linkage and causes depletion of the freely equilibrating thioester intermediates and the formation of a single ligation product.

In summary, the initial research motive of PNA-peptide conjugation was to improve the pharmacokinetic properties of therapeutically valuable PNA. Different types of peptides were used in the form of either noncovalent complexes or covalent conjugates to enhance the cellular uptake of PNA. The biological properties, for example, the antisense activity of similar conjugates, are shown to be influenced by the nature of the chemical linkage between the peptide and PNA fragments (76). The advance in both continuous solid-phase synthesis and chemoselective conjugation methods opens the way to the design and synthesis of PNA-peptide hybrids possessing combined functionalities. These synthetic developments may eventually lead to the design of therapeutic probes based on PNA, which are able to target specific cell types, penetrate the cellular membrane, direct to the right cellular compartment, and fulfill a predetermined task, such as antisense /antigene activity, selective cleavage of DNA or RNA target sequences or activation of transcription.

1.5 Aim of the project

Many clinically valuable targets reside inside the cell membrane. As most of the Gd(III) based MR contrast agents are extracellular, therefore, developing efficient intracellular targeted MR contrast agent is required. The objective of the present project is to construct a series of targeted intracellular MR contrast agents aiming to image mRNA transcription by MRI. This thesis includes two major parts of work:

The first part of this thesis takes an effort toward the design, synthesis, characterization, and *in vitro* testing of a series of CPP mediated intracellular MR contrast agents. Several typically applied CPPs would be selected as the transmembrane vectors to be conjugated with Gd(III) complexes as well as fluorescent dyes. Being labeled with fluorescent moiety, the dynamic transmembrane behavior, intracellular distribution and biocompatibility can be studied by fluorescence microscopy and spectroscopy in cells plated in 96well plates. In addition, after loading cells with MR contrast agents, the cellular relaxation rate and contrast enhancement data can be determined quantitatively. Comparison studies on the relative efficacy, toxicity and uptake mechanism of individual

Chapter 1. Introduction

CPP, allowed for screening an optimal CPP for the intracellular delivery of MR contrast agents.

Referred from the previous studies of Heckl (64) and Tian (62), there should be some kinetic differences between the antisense contrast agent and nonsense contrast agent when interacting with the target mRNA: the antisense contrast agents might have a longer retention time in the cells after binding with the target mRNA. The second part of this thesis is to design and synthesize antisense MR contrast agents, which conjugate PNA with cell penetrating peptides, Gd-DOTA and FITC. CPP will facilitate the intracellular delivery of the designed contrast agents. PNA fragment is the antisense to the targeting mRNA, which can specifically bind to complementary sequence in mRNA. With FITC and Gd-DOTA, fluorescent optical imaging as well as MR imaging can visualize the labeled cells. *In vitro* cell biological evaluations can be made on normal NIH/3T3 mouse fibroblasts to confirm the intracellular uptakes of the designed contrast agents and their biocompatibility using MR and fluorescent optical imaging techniques. The intracellular content of the antisense PNA contrast agents can be determined by MR or ICP-MS after the labeled cells were treated by concentrated HCl or nitric acid. The specificity of the antisense PNA contrast agents to the target sequence can be demonstrated by an *in vitro* hybridizing test. These preliminary studies on the antisense probes should support some helpful data for the further rational design and modification of intracellular targeted MR contrast agents. Further studies on transgenic cells which express target mRNA are needed to prove the specific accumulation of the antisense contrast agent by binding with the target mRNA. The long run goal of this research program is to track specific cells noninvasively by MR imaging using mRNA as the target.

Chapter 2. Synthesis and screening of cell penetrating peptides for the intracellular delivery of MR contrast agents

2.1 Research design

Aiming to screen an optimized vector for the intracellular delivery of MR contrast agents, five kinds of typically applied CPPs were selected: L-Tat₄₉₋₅₇ (derived from HIV-1 Tat peptide) (77), D-Tat₅₇₋₄₉ (retro-inverso isomer of Tat peptide), Orn-D-Tat₅₇₋₄₉ (substitution of Glutamine (q) residue with Ornithine (o) residue) (78), PTD-4 (a synthetic protein transduction domain) (79) and NLS (nuclear localization sequence of SV 40T-antigen) (80).

Compared to the Boc/benzyl based scheme, Fmoc/tBu based solid phase peptide synthesis scheme has offered more flexibility for the modification of the peptide chain, more specificity in the cleavage of the N^α versus the side-chain protecting groups, and milder cleavage conditions. Therefore, Fmoc/tBu chemistry is selected in the peptide syntheses.

One lysine residue is added at the N-terminal of every CPP as a linker. The Gd(III) chelate (DTPA or DOTA) is conjugated at the α-NH₂ group of Lys, whereas FITC is conjugated on the ε-NH₂ group of Lys (Figure 6). Therefore, the designed MR contrast agents can label cells for optical as well as MR studies. The intracellular uptake efficiency of these contrast agents can be quantified with fluorescent spectroscopy and MR measurements; furthermore, the intracellular distribution of these probes could be demonstrated by fluorescent microscopy.

Chapter 2. Screening of CPP

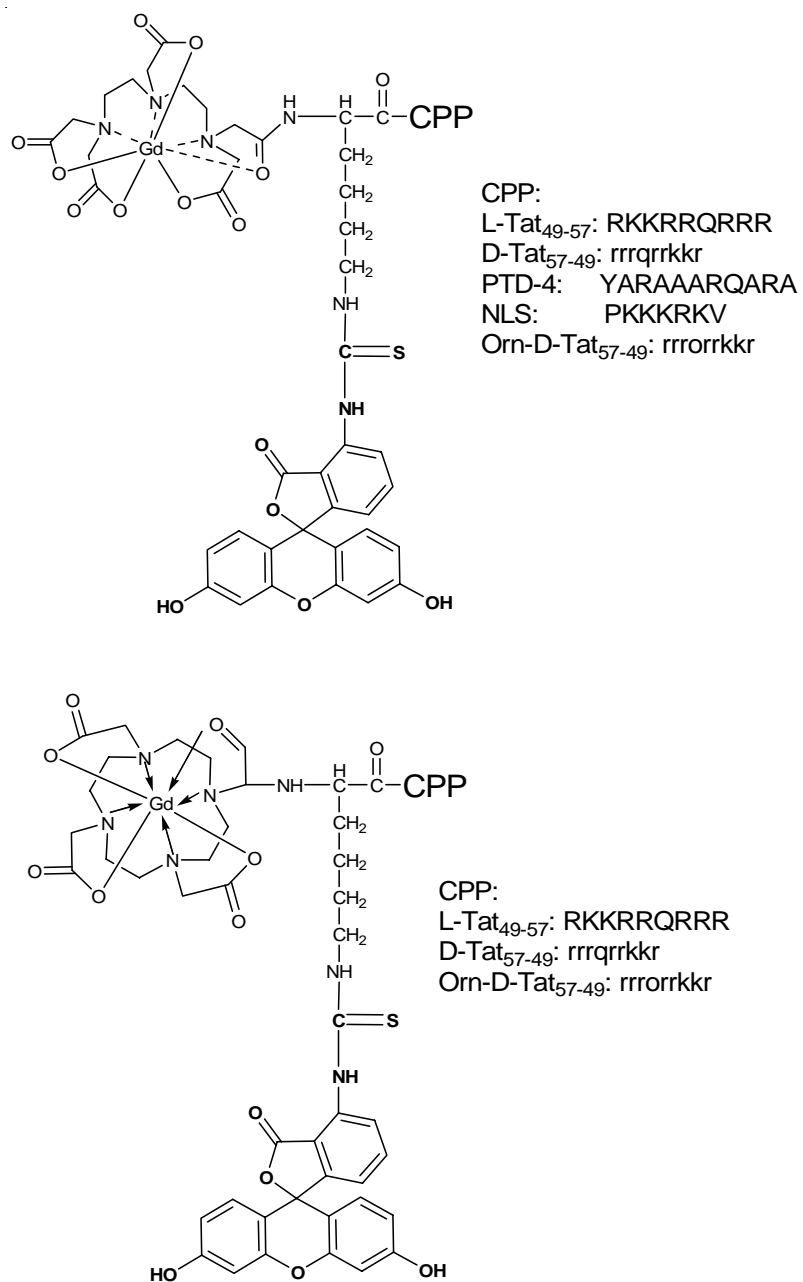


Figure 6. Schematic structures of Gd-DTPA and Gd-DOTA conjugated intracellular MR contrast agents

2.2. Results

2.2.1 Synthesis and characterization of CPP conjugated MR contrast agents

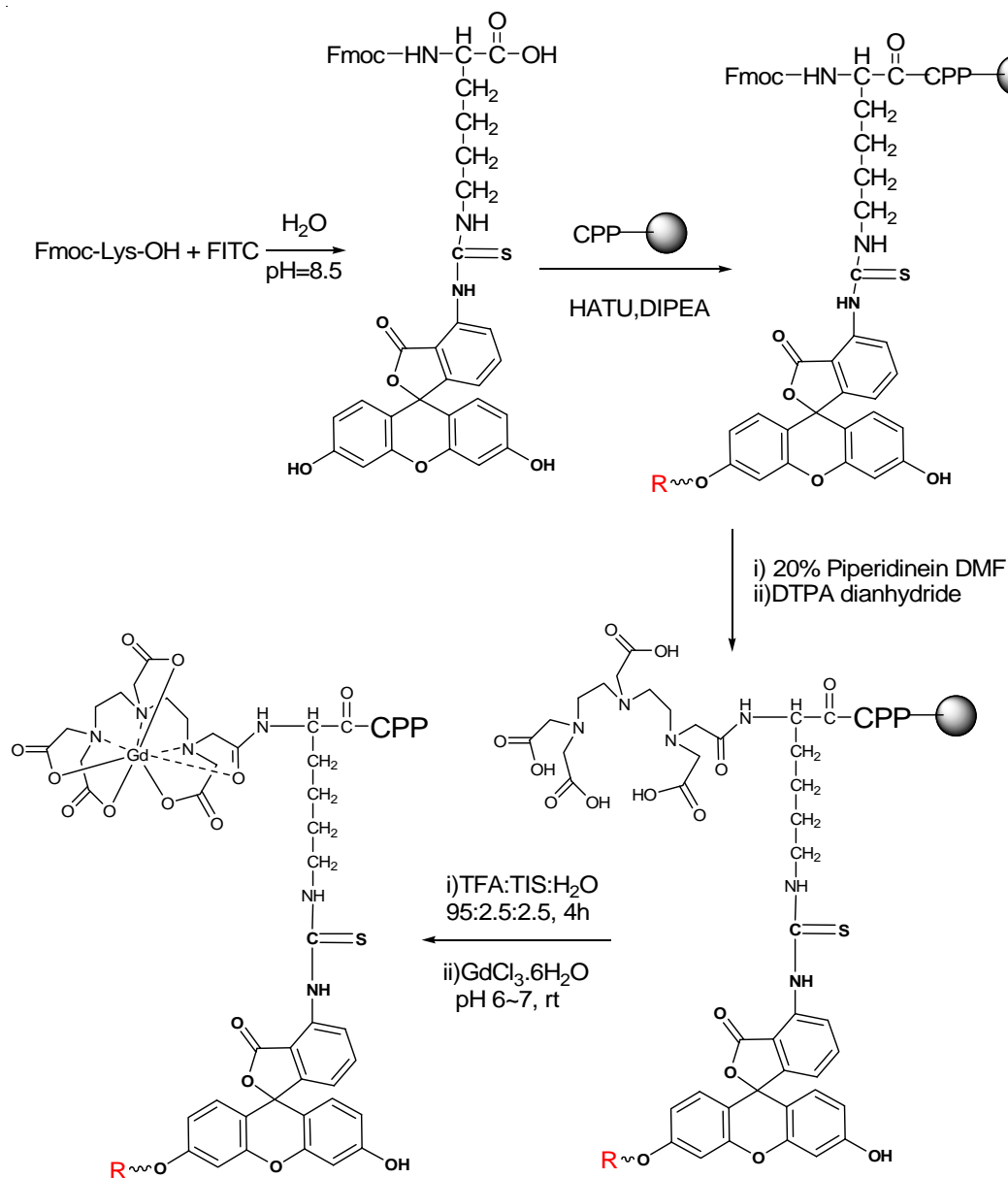
Two different schemes were tried to synthesize the CPPs conjugates: fragment conjugation scheme and on-line continuous solid-phase synthesis scheme.

In the fragment conjugation scheme, we planned to prepare three fragments: Fmoc-Lys(FITC)-OH, peptide, and DTPA dianhydride. First, CPP was synthesized by solid-phase synthesis scheme on Wang resin using Fmoc/tBu protected amino residues. Fmoc-Lys(FITC)-OH was synthesized by conjugating FITC with Fmoc-Lysine in solution. The resulting product Fmoc-Lys(FITC)-OH can be applied as a building block to be conjugated with CPPs. Afterwards, DTPA dianhydride coupled on the α -NH₂ group of Lys to obtain the whole CPP conjugated ligand (Scheme-1). However, there is an unprotected phenol hydroxyl group in FITC. In the next steps of coupling Fmoc-Lys(FITC)-OH with CPP or conjugate DTPA dianhydride with Lys, side products were formed which are derived from the carboxyl group coupling with the phenol group in FITC. Therefore, the yield of this scheme is very low. Further optimizations of this scheme were tried, such as protecting the phenol hydroxyl group in FITC. When the phenol hydroxyl group in FITC was protected with Trt, the over coupling side products was prevented. Therefore, the yield of the optimized scheme was much better than that of in unprotected scheme (For example, DTPA-Lys(FITC)-NLS-OH, the yield of unprotected scheme was 8%; the yield of protected scheme was 24%).

In comparison, we have developed an on-line continuous solid-phase synthesis scheme: CPP was synthesized by solid-phase Fmoc/tBu-chemistry scheme on Wang resin using HATU or HBTU as the coupling reagents. After then Fmoc-Lys(Dde)-OH was applied as a linker. FITC was coupled on the ϵ -NH₂ group of Lys on resin. Different bases, such as DIEA and triethylamine, were tested under different coupling condition. Finally, the optimal condition to couple FITC with Lys on resin is: 4eq FITC, 8eq DIEA for 7 hours (Scheme-2). The advantage of this scheme was that all coupling reactions were performed under mild conditions; and coupling FITC in the last step prevented the formation of side products, such as excess coupling on the phenol group of FITC. In addition, this continuous scheme allows the coupling process to be carried out by a fully

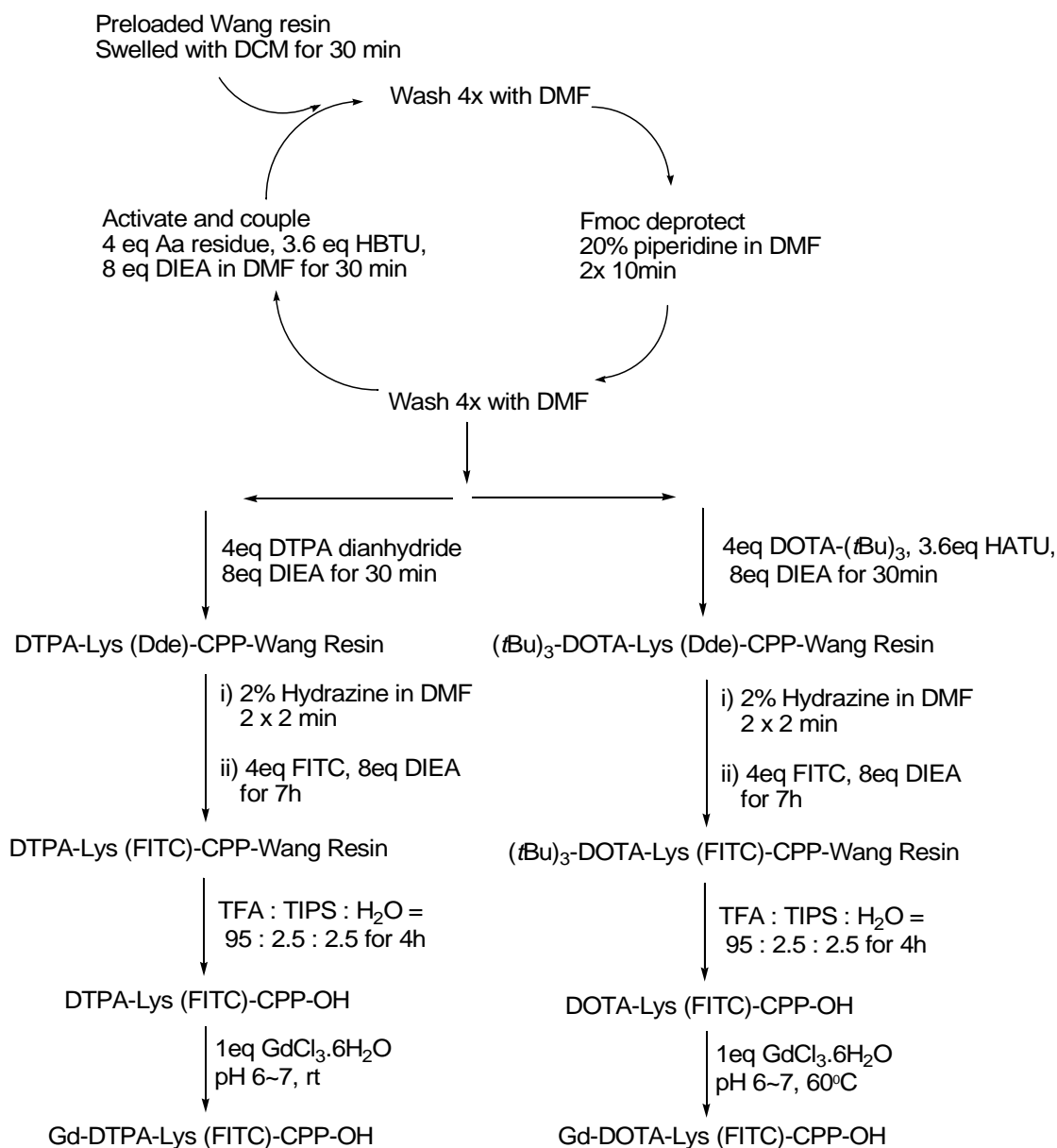
Chapter 2. Screening of CPP

automated synthesizer. Therefore, the on-line continuous solid-phase synthesis scheme was selected as the optimal scheme for the synthesis of CPP conjugated contrast agents.



Scheme-1. Synthesis of CPP conjugated MR contrast agents by fragment conjugation scheme

R could be Fmoc-Lys(FITC)- or DTPA



Scheme-2. Synthesis of CPP conjugated MR contrast agents by continuous solid-phase synthesis scheme

In the on-line continuous solid-phase synthesis scheme, peptides were synthesized on Wang resin at the substitution about 0.50-0.60 mmol/g. Then, a Fmoc-Lys(Dde)-OH residue was applied as a spacer. Afterwards, Fmoc group was deprotected selectively, and DTPA or DOTA tris(*tert*-butyl) ester was coupled on the α -NH₂ group of Lys.

Chapter 2. Screening of CPP

Finally, the Dde group was removed by treatment with 2% hydrazine in DMF; FITC was coupled on the ϵ -NH₂ group of Lys under the addition of DIEA. For every key intermediate, aliquots of the resin-bound conjugates were cleaved and side chain-deprotected with H₂O/TIS/TFA, and ESI-MS analysis was performed to confirm that the observed masses were consistent with the calculated molecular weights of the designed intermediates (e.g. Figure 7, Figure 8).

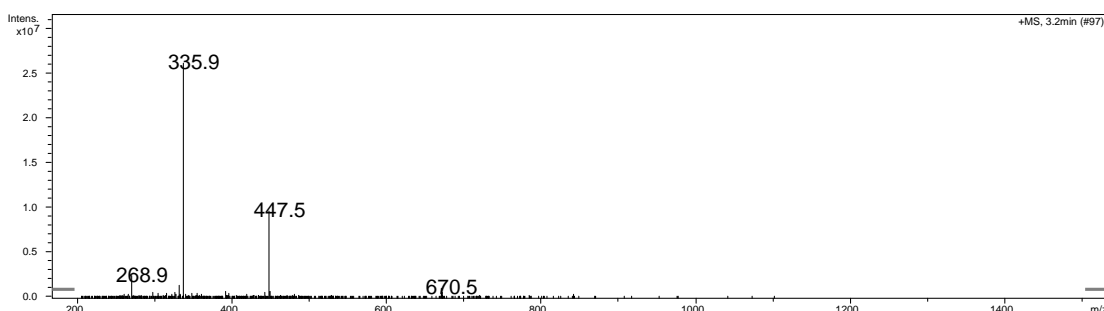


Figure 7. ESI-MS Spectrum of the Tat peptide. $m/z = 670.5$ ($(M+2H)^{2+}$), 447.5 ($(M+3H)^{3+}$), 335.9 ($(M+4H)^{4+}$), and 268.9 ($(M+5H)^{5+}$) were consistent with the calculated molecular weight (1339.6)

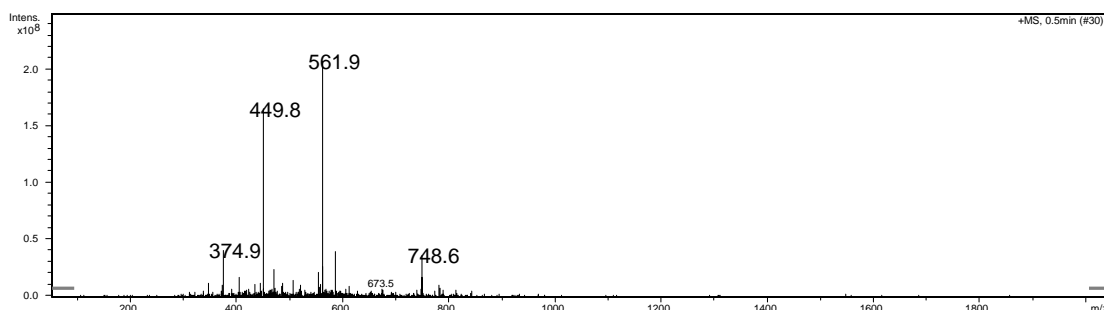


Figure 8. ESI-MS Spectrum of DOTA-Lys(FITC)-D-Tat₅₇₋₄₉-OH. Detected molecular ions at $m/z = 748.6$ ($(M+3H)^{3+}$), 561.9 ($(M+4H)^{4+}$), 449.8 ($(M+5H)^{5+}$), and 374.9 ($(M+6H)^{6+}$) were consistent with the calculated mass of the desired product (2244.56)

The conditions used to cleave the peptides from the resin simultaneously deprotected the *tert*-butyl esters on the DOTA ligands. After purified by RP-HPLC, the CPP conjugated ligands were characterized by ESI-MS (e.g. Figure 8). Then, CPP conjugates were all

successfully chelated with Gd^{3+} under mild conditions (for DTPA complex, 1eq of $GdCl_3 \cdot 6H_2O$ chelated at room temperature for 24h; whereas for DOTA complex, 1eq of $GdCl_3 \cdot 6H_2O$ chelated at $60^\circ C$ for 12 h). Final products were purified by HPLC and confirmed by ESI-MS (e.g. Figure 9, Table 1).

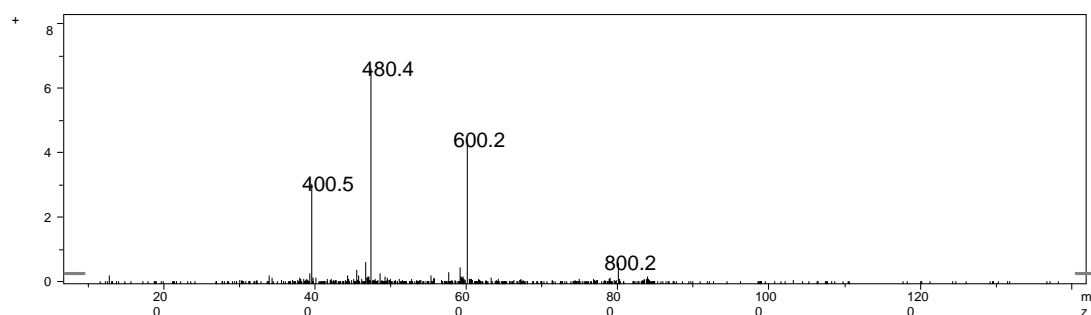


Figure 9. ESI-MS Spectrum of Gd-DOTA-Lys(FITC)-L-Tat-OH. Detected molecular ions at $m/z = 800.2((M+3H)^{3+})$, $600.2((M+4H)^{4+})$, $480.4((M+5H)^{5+})$, and $400.5((M+6H)^{6+})$ were consistent with the calculated molecular weight (2397.78).

When the ESI-MS was measured at negative polarity, the spectrum of CPP conjugated Gd-DTPA complex showed ions at $m/z = (M-1)^{1-}$ and $(M-2)^{2-}$ (Figure 10). This spectrum is well consistent with the structure of CPP conjugated Gd-DTPA. There are two negative charged positions: one from the Gd-DTPA, another from the C-terminal of peptide. If the ESI-MS spectrum is amplified, the isotopes of Gd can be observed clearly (Figure 11).

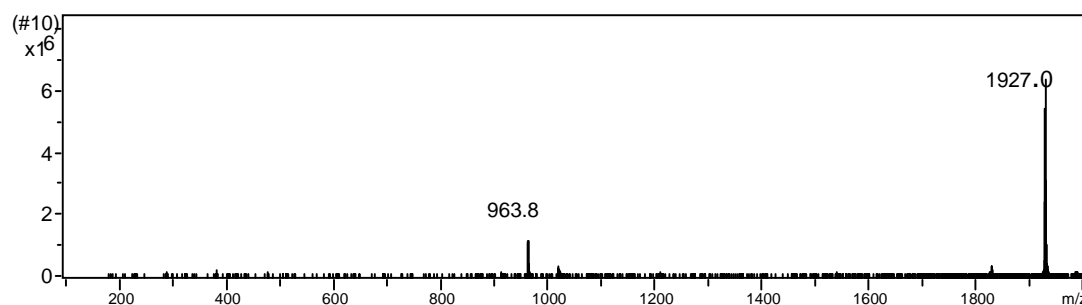


Figure 10. ESI-MS Spectrum of Gd-DTPA-Lys(FITC)-NLS-OH at negative polarity. Detected molecular ions at $m/z = 1927.0((M-1)^{1-})$ and $963.8((M-2)^{2-})$ were consistent with the calculated molecular weight (1928.76).

Chapter 2. Screening of CPP

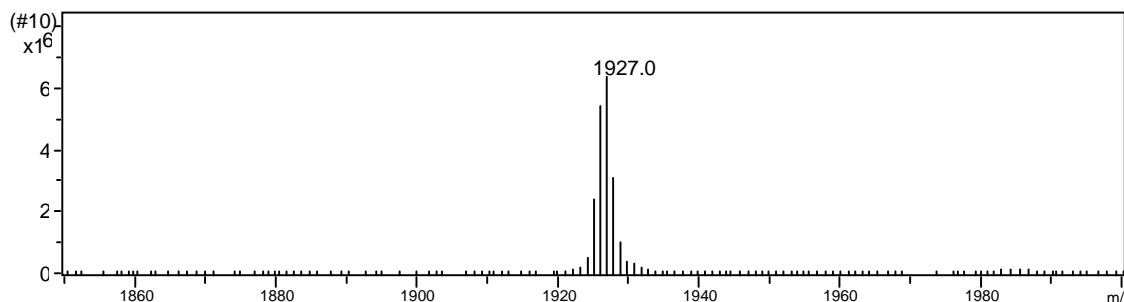


Figure 11. Isotopic pattern of Gd-DTPA-Lys(FITC)-NLS-OH

Table 1. ESI-MS Data of CPP conjugated MR contrast agents

| Contrast agent | Amino sequence | HPLC purity (%) | Molecular weight | ESI-MS |
|------------------------------------|-----------------|-----------------|------------------|-------------------------------|
| Gd-DTPA-L-Tat ₄₉₋₅₇ | RKKRRQRRR | 91 | 2385.71 | 796.6, 597.4, 478.3, 398.9 |
| Gd-DTPA-D-Tat ₅₇₋₄₉ | rrrqrrkkr | 90 | 2385.71 | 796.3, 597.4, 478.2, 398.8 |
| Gd-DTPA-PTD-4 | YARAAARQ ARA | 90 | 2250.44 | 1126.0, 750.9, 563.5 |
| Gd-DTPA-NLS | PKKKRKV | 93 | 1928.76 | 964.4, 643.8, 483.0 |
| Gd-DTPA-Orn-D-Tat ₅₇₋₄₉ | rrrorrkkr | 92 | 2371.72 | 791.7, 593.9, 475.4, 396.4 |
| Gd-DOTA-L-Tat ₄₉₋₅₇ | RKKRRQRRR | 92 | 2397.78 | 800.2, 600.2, 480.4, 400.5 |
| Gd-DOTA-D-Tat ₅₇₋₄₉ | rrrqrrkkr | 94 | 2397.78 | 800.3, 600.4, 480.7, 400.6 |
| Gd-DOTA-Orn-D-Tat ₅₇₋₄₉ | rrrorrkkr | 96 | 2383.80 | 796.2, 596.5, 477.7, 398.4 |

2.2.2 Determining the concentration and relaxivity of CPP conjugated contrast agents in aqueous solution

The relative purities of CPP conjugated contrast agents were analyzed by HPLC, and the resulting purities of all contrast agents were higher than 90%. However, the exact purities of the contrast agents can not be determined by HPLC. Because the final products were purified by HPLC using 0.1%TFA in H₂O/ACN as eluent, there is a high probability that TFA binds to positive charged amino residues as counter-anion. However, the exact nature and quantity of the counter-anion can not be determined by HPLC, thus, the real content of the contrast agent should be determined after they are dissolved in solvents. As every contrast agent molecule contains one FITC and one Gd chelate, the real concentration of these CPP conjugates could be determined by UV-Vis absorption at 485nm of Fluorescein for the standard curve ($\epsilon=81000 \text{ cm}^2/\text{mol}$) (Table 2). Determination of the concentration of CPP conjugates by UV-Vis absorption allowed for the calculation of the molar concentration without knowing the exact identity of the counter-anions.

Table 2. Determining the concentration of CPP conjugated MR CAs in aqueous solution

| Contrast agent | Calculated concentration (mM) | Measured concentration (mM) | Purity (%) |
|------------------------------------|-------------------------------|-----------------------------|------------|
| Gd-DTPA-L-Tat ₄₉₋₅₇ | 10 | 4.154 | 42 |
| Gd-DTPA-D-Tat ₅₇₋₄₉ | 10 | 4.101 | 41 |
| Gd-DTPA-PTD-4 | 10 | 2.560 | 26 |
| Gd-DTPA-NLS | 10 | 5.312 | 53 |
| Gd-DTPA-Orn-D-Tat ₅₇₋₄₉ | 10 | 4.813 | 48 |
| Gd-DOTA-L-Tat ₄₉₋₅₇ | 10 | 4.069 | 41 |
| Gd-DOTA-D-Tat ₅₇₋₄₉ | 10 | 4.051 | 41 |
| Gd-DOTA-Orn-D-Tat ₅₇₋₄₉ | 10 | 4.141 | 41 |

Calculated concentration was obtained by adding certain mg of CPP conjugates in aqueous solution; measured concentration was obtained by UV-Vis absorption.

Chapter 2. Screening of CPP

Relaxivity measurements were acquired by taking the slope of a plot of the R_1 relaxation rate versus concentration, where relaxivity (r_1) is a measure of the ability of a contrast agent to shorten T_1 (Table 3). MR measurements of the contrast agents in aqueous solution were performed at 3T at room temperature ($\sim 21^\circ\text{C}$). The results of MR measurement demonstrated that the relaxivity of CPP conjugated Gd(III) chelates are in the range of 6-9 $\text{mM}^{-1} \text{s}^{-1}$, except Gd-DTPA-NLS ($5.0 \text{ mM}^{-1} \text{ s}^{-1}$) and Gd-DOTA-D-Tat₅₇₋₄₉ ($14.2 \text{ mM}^{-1} \text{ s}^{-1}$).

Table 3. Relaxivity (r_1) of CPP conjugated MR contrast agents

| Abbreviation | Contrast agent | Relaxivity ($\text{mM}^{-1} \text{ s}^{-1}$) |
|--------------|------------------------------------|--|
| CA1 | Gd-DTPA-L-Tat ₄₉₋₅₇ | 8.8 |
| CA2 | Gd-DTPA-D-Tat ₅₇₋₄₉ | 7.1 |
| CA3 | Gd-DTPA-PTD-4 | 8.8 |
| CA4 | Gd-DTPA-NLS | 5.0 |
| CA5 | Gd-DTPA-Orn-D-Tat ₅₇₋₄₉ | 6.3 |
| CA6 | Gd-DOTA-L-Tat ₄₉₋₅₇ | 7.1 |
| CA7 | Gd-DOTA-D-Tat ₅₇₋₄₉ | 14.2 |
| CA8 | Gd-DOTA-Orn-D-Tat ₅₇₋₄₉ | 7.1 |

MR measurements of the contrast agents in aqueous solution were performed at 3T at room temperature ($\sim 21^\circ\text{C}$).

2.2.3 *In vitro* studies of Gd-DTPA conjugates with L-Tat₄₉₋₅₇, D-Tat₅₇₋₄₉, PTD-4 and NLS

At first, cell-penetrating peptides such as L-Tat₄₉₋₅₇, D-Tat₅₇₋₄₉, PTD-4 and NLS were selected to be conjugated with FITC and Gd-DTPA complexes respectively. The resulting contrast agents, Gd-DTPA-Lys(FITC)-L-Tat₄₉₋₅₇ (**CA1**), Gd-DTPA-Lys(FITC)-D-Tat₅₇₋₄₉ (**CA2**), Gd-DTPA-Lys(FITC)-PTD-4 (**CA3**) and Gd-DTPA-Lys(FITC)-NLS (**CA4**) were

tested *in vitro* to study their intracellular delivery ability. These four CPPs were selected because HIV Tat peptide is one of the most studied and widely applied cell penetrating peptides; PTD-4 is one of the best artificially designed protein transduction domains according to the amphipathic model; NLS is one of the specific sequences that provide translocation into the nucleus. Although TAT, PTD-4 and NLS have been extensively employed for *in vitro* and *in vivo* delivery of different cargos into cells, little is known of the relative efficacy, toxicity and uptake mechanism of individual CPP, factors that will be critical in determining the optimal CPP sequence for intracellular MR contrast agent design.

Cellular uptake of these compounds was confirmed by fluorescence microscopy and spectroscopy in NIH/3T3 mouse fibroblasts plated in 96well plates as well as by MR analyses in Eppendorf tubes (please see the cellular uptake assay in chapter 4). In brief, cells were treated with contrast agents at various concentrations in complete medium for 18 hours. After cells were washed or extracellular fluorescence was quenched, internalized fluorescence was measured in a multiplate reader. Subsequently, fluorescence microscopy was performed with the same cells to observe the cellular localization.

Toxicity via the reduction of the cell number was measured by counterstaining the cell nuclei with the DNA dye Hoechst 33342TM in the fluorescence reader. These values were also used to correlate the measured the measured CA fluorescence to the cell number per well.

For MR imagings, exponentially growing fibroblasts were labeled with the contrast agents for 18 hrs. Cells were repeatedly HBSS washed, trypsinized and re-suspended in 1.5 mL Eppendorf tubes at the rate of 1×10^7 cells in 500 μ L complete DMEM. MRI of the cell pellets was conducted at 300 MHz on a vertical 7T/60 cm Bruker MRI Biospec system using T1-weighted spin-echo sequence at room temperature ($\sim 21^\circ\text{C}$). The axial slice of interest was positioned through the cell pellet.

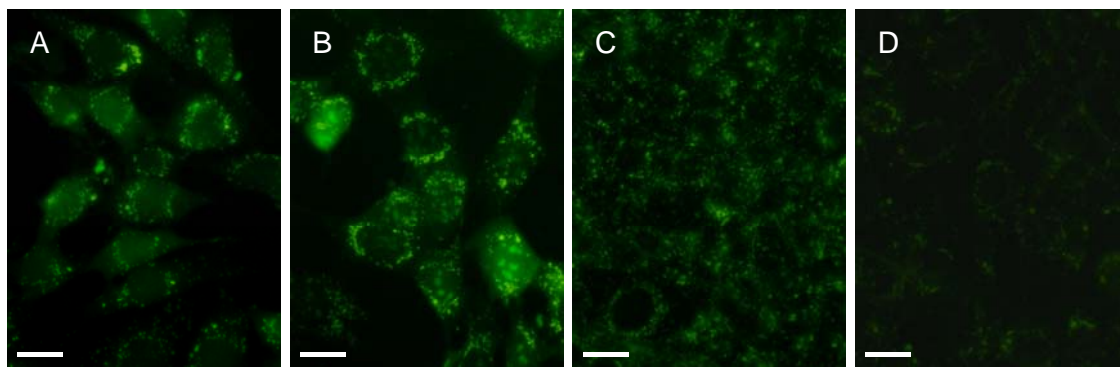


Figure 12. Fluorescence microscopic images of NIH/3T3 cells after loading with contrast agents for 18 hours.

A: 20 μ M CA1; B: 20 μ M CA2; C: 20 μ M CA3; D: 20 μ M CA4; bars represent 20 μ m

Fluorescence microscopic images showed that all of these four contrast agents could be delivered efficiently into NIH/3T3 fibroblasts cells (Figure 12). This as well as spectroscopic data demonstrated that the uptake of CPP conjugates decreased in following order **CA2 > CA1 > CA3 > CA4**.

However, examination of cellular toxicity showed following order **CA3 > CA2 > CA1 > CA4**. Overall, comparison of the uptake and toxicity suggests that D-Tat₅₇₋₄₉ proves to be a useful cell-penetrating peptide for the development of new intracellular MR contrast agents.

The results of T₁- and T₂-weighted MR measurements demonstrate that the uptake of agents **CA1** and especially **CA2** was sufficient to enhance significantly relaxation rates R₁ and R₂ in cells (Figure 13). Therefore, D-Tat₅₇₋₄₉ peptide was confirmed as an efficient CPP for the intracellular delivery of MR contrast agents.

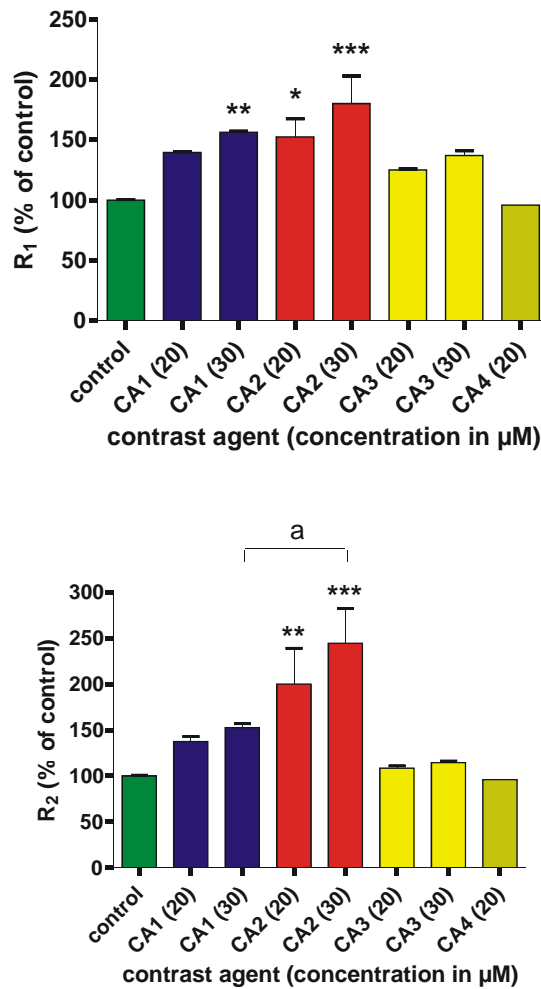


Figure 13. Changes in relaxation rates R_1 and R_2 in the cells after internalization of contrast agents.

Values are means \pm SEM, $n=2-5$; * $p<0.05$, ** $p<0.01$, *** $p<0.001$, statistically significant different compared to control; a $P<0.05$ statistical significant difference.

2.2.4 *In vitro* comparison studies of Gd-DTPA and Gd-DOTA conjugates of L-Tat₄₉₋₅₇, D-Tat₅₇₋₄₉, and Orn- D-Tat₅₇₋₄₉

Piwnica-Worms et al reported that intracellular uptake values increased up to 13-fold (78), when the chirality of the Tat peptide sequence was changed from L to D. Furthermore, length, sequence, and type of chelating domain all impacted peptide uptake into cells. They demonstrated that the highest level of uptake was found in Orn-D-Tat peptide by introduction of modifications in the sequence like replacement of glutamine (q) with ornithine (Orn, o). In addition, our preliminary studies demonstrate that Tat peptide especially D-Tat₅₇₋₄₉ is very efficient to deliver Gd-DTPA complex into NIH/3T3 cells. In order to study the relative intracellular uptake efficiency in detail, we planned to synthesize in parallel the Gd-DTPA complexes of L-Tat₄₉₋₅₇ and its derivatives, D-Tat₅₇₋₄₉ and Orn-D-Tat₅₇₋₄₉.

It was reported that DTPA-metal complexes had a lower thermodynamic stability compared to DOTA complexes if one of the N-acetate side chains was used for coupling via amide bond. Especially lower pH-values enhanced this effect. In addition, Aime's group (32) reported that the lower stability of the Gd-DTPA-BMA complex was responsible for a shift in the dissociation equilibrium that resulted in the net transfer of Gd³⁺ ions on the cell membrane followed by a slower internalization process and accompanied by a drastic decrease in cell viability. On the other hand, Meade et al. (47) reported that NIH/3T3 transduction appears to be Gd(III) chelator dependent, preferring DTPA- to DOTA-based contrast agents. Therefore, Gd-DOTA conjugates with L-Tat, D-Tat and D-Orn-Tat were synthesized and comparatively studied with corresponding Gd-DTPA conjugate.

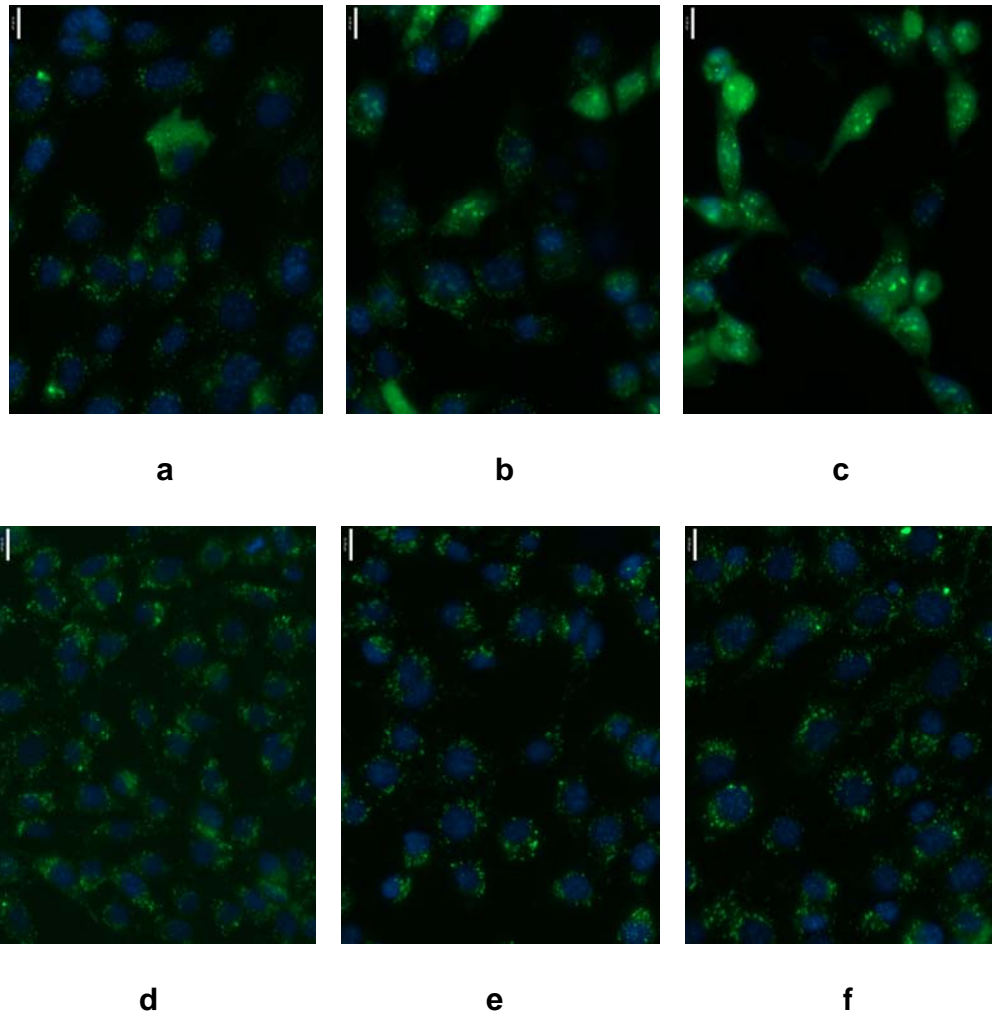


Figure 14. Microscopic images of NIH/3T3 cells incubated for 18 hrs with 20 μ M of Gd-DTPA-Lys(FITC)-L-Tat₄₉₋₅₇ (a), Gd-DTPA-Lys(FITC)-D-Tat₅₇₋₄₉ (b), Gd-DTPA-Lys(FITC)-Orn-D-Tat₅₇₋₄₉ (c), Gd-DOTA-Lys(FITC)-L-Tat₄₉₋₅₇ (d), Gd-DOTA-Lys(FITC)-D-Tat₅₇₋₄₉ (e) and Gd-DOTA-Lys(FITC)-Orn-D-Tat₅₇₋₄₉ (f). Bars represent 16 μ m. Green: CA, Blue: H33342 (nuclei)

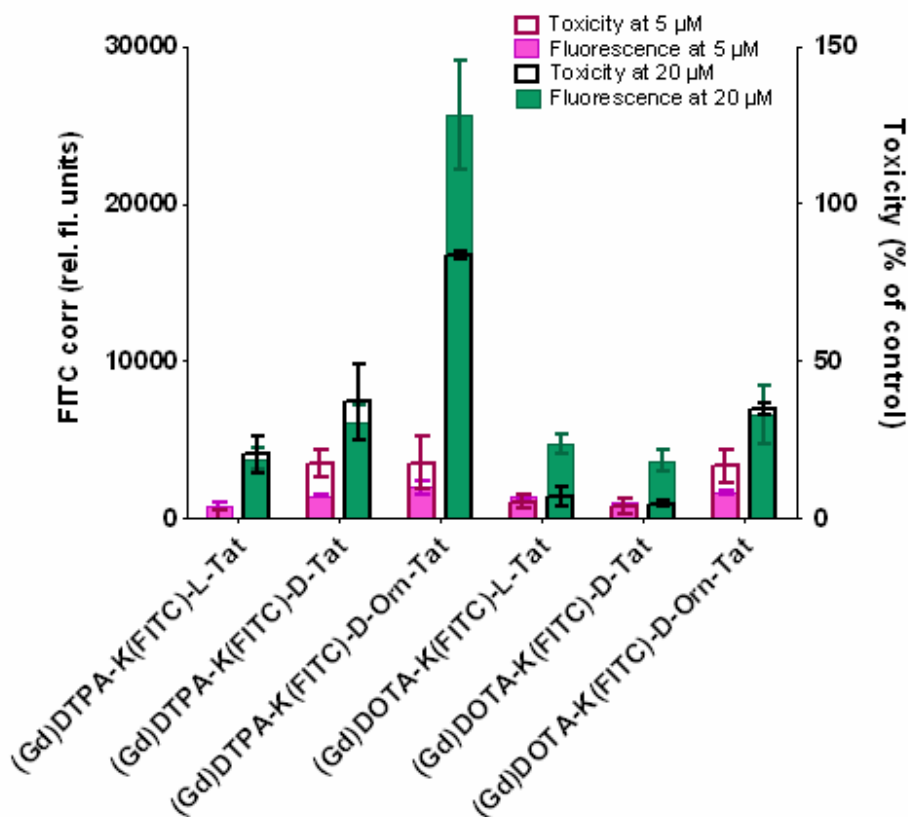


Figure 15. Fluorescence and toxicity of cells after incubation with 5 and 20 μM of various Tat conjugated CAs for 18 hrs. Values are means ± SEM (n=3).

The results of fluorescent studies demonstrated that modifications of the native CPP sequence enhanced the uptake of the corresponding contrast agents. Thus, their intracellular delivery efficiency showed following order L-Tat ≤ D-Tat < D-Orn-Tat in both Gd-DTPA and Gd-DOTA complexes. However, the cellular toxicity showed the same order of L-Tat ≤ D-Tat < D-Orn-Tat (Figure 15).

Interestingly, Gd-DTPA-CPP conjugates enter NIH/3T3 cells more efficiently than corresponding Gd-DOTA-CPP conjugates. These results could be a function of overall molecular charge or three-dimensional chelator conformations. The Gd-DTPA-D-Orn-Tat shows the best intracellular delivery ability; however, it also expressed the highest cytotoxicity. When applied at 20 μM, Gd-DTPA-D-Orn-Tat showed a significant increased cellular toxicity (Figure 14, Figure 15). Therefore, comparison of the uptake

and toxicity suggests that D-Tat₅₇₋₄₉ proves to be the optimal vector among the Tat peptide derivatives for the intracellular delivery of MR contrast agents.

2.3. Discussion

2.3.1 Synthesis of CPP conjugated, dual-labeled Gd(III)-based MR contrast agents

2.3.1.1 Optimization of the coupling scheme for Fluorescein labeling

At beginning, we tried to couple FITC with Fmoc-Lysine in solution. After purification by HPLC, the product Fmoc-Lys(FITC)-OH can be applied as a building block to be conjugated with CPPs. With several tests, we found there are some difficulties in this scheme: First, it is very difficult to obtain highly purified Fmoc-Lys(FITC)-OH compound at gram scale. Fmoc-Lys(FITC)-OH is very difficult to be re-crystallized in solutions, it has to be purified by RP-HPLC. But the solubility of this compound is very low in 0.1% TFA in water/ACN. Therefore, it is very difficult to obtain highly pure product in relative large scale. Second, there is an unprotected phenol hydroxyl group in FITC. When coupling Fmoc-Lys(FITC)-OH with CPP, side products were formed which are derived from the carboxyl group coupling with phenol group in FITC. Fischer et al. took great efforts to extend the applicability of carboxyfluorescein in solid-phase synthesis (81). They also found similar problems with coupling of the carboxyl group to the phenol group in carboxyfluorescein. In addition, they suggested that treatment of the resin with 20% piperidine in DMF could remove the over-coupling side products. However, this could not be confirmed in our systems. Referred from literature, we have developed and optimized the coupling scheme that enables us to label Lys on resin smoothly. Under eight times excess of DIEA, FITC couples completely with the ϵ -NH₂ group of Lys in 7 hours; and ESI-MS has demonstrated that there is no over-coupling side product formed.

2.3.1.2 Conjugate DTPA dianhydride with peptides

DTPA dianhydride is highly active, therefore, it can be coupled with free $-\text{NH}_2$ group very fast. Unfortunately, there are two anhydride groups in every molecule of DTPA

Chapter 2. Screening of CPP

dianhydride. Under normal coupling condition, there are a lot of side products formed, including double coupled product in which one DTPA coupled with two peptide sequences at both ends of DTPA, or hydrazine coupled on one end during the next Dde deprotect step with hydrazine, because hydrazine is highly nucleophilic reagent. To optimize the reaction condition, we tried to decrease the reaction speed in low temperature. The formation of side products was reduced dramatically when the reaction was controlled at 0-5 °C. And the coupling can be finished in 2~3 hours. Since we can not cool the temperature to 0-5 °C on the peptide synthesizer, this step can only be performed in a small glass flask. The second anhydride group was hydrolyzed (DMF: water: DIEA = 90:5:5) after DTPA dianhydride conjugated with peptide to prevent the formation of hydrazine coupled side product. The best scheme to avoid the double coupled side products is using tert-butyl protected DTPA (four of the five carboxyl groups in DTPA were protected by tert-butyl) as the building block (kindly provided by Prof. K.-H. Wiesmueller). With protected DTPA, the yield of the objective product is much higher than that with DTPA dianhydride.

2.3.1.3 Formation of Gd-complexes

Gd-DOTA-CPP complexes can be formed smoothly under the conditions of pH 6.5, 60°C in 12h with 1eq GdCl₃.6H₂O. But there are many donor atoms on the peptide that might offer alternative coordination sites to the lanthanide ion. Initially, the complexes were dialyzed for 48 h after the CPP conjugated ligands were coordinated with gadolinium. But the resulting compounds showed very high r₁ relaxivity (e.g.197.7 mM⁻¹ s⁻¹ for Gd-DOTA-D-Tat; data not shown) in solution MR tests. We considered that possibly unspecifically bound Gd³⁺ (i.e. not chelated by DOTA-ligand) was still present in the preparation even after dialysis. The Gd-DOTA complexes are very stable even in an acidic environment. Thus, the unstable bound Gd(III) can be separated from Gd-DOTA-CPP complexes by RP-HPLC with 0.1%TFA in H₂O/ACN.

However, the coordinating condition and stability of Gd-DTPA-CPP complexes are different from that of Gd-DOTA complexes. Gd³⁺ could be chelated with DTPA-CPP ligand at room temperature. But Gd-DTPA-CPP complexes are not as stable as Gd-DOTA-CPP complexes, because one carboxyl group of DTPA was used for coupling to

the peptide. Thus, if purified by RP-HPLC with 0.1%TFA in H₂O/CAN, some of Gd was released from DTPA. We have tried to dialyze the chelating mixture to remove free Gd³⁺. However, even after 72h, there was still free Gd³⁺ observed with xylenol orange indicator. Finally, we purified Gd-DTPA-CPPs by RP-HPLC with 0.05%TFA in H₂O/ACN. The ESI-MS confirmed that Gd³⁺ is still chelated with DTPA, and the MR measurement demonstrated the unspecific bound Gd(III) was removed.

2.3.1.4 Relaxivity of CPP conjugated MR contrast agents

The r_1 relaxivity of CPP conjugated Gd(III) chelates are in the range of 6-9 mM⁻¹ s⁻¹ at 3 T, except Gd-DTPA-NLS (5.0 mM⁻¹ s⁻¹) and Gd-DOTA-D-Tat₅₇₋₄₉ (14.2 mM⁻¹ s⁻¹). These results are in accordance with published literature for monomeric chelates. Meade et al reported the r_1 relaxivity of Gd-DTPA-(Arg)₈ is 6.8 mM⁻¹ s⁻¹ at 3T (46); and Piwnica-Worms et al reported the r_1 relaxivity of Gd-DOTA-D-Tat is 7.94 mM⁻¹ s⁻¹ at 4.7T (82). In addition, Ranganathan et al. (83) have shown that the relaxivity per Gd(III) correlates well with molecular weight for a series monomeric and multimeric Gd(III) chelates. They demonstrated that increases in relaxivity correlate approximately with increasing molecular weight for spherical molecules. For example, when the molecular weight of Gd(III) complexes are in the range of 2,200 to 2,400, their r_1 relaxivities at 20MHz are in the range of 8.4 to 8.8 mM⁻¹ s⁻¹ per Gd(III). Indeed, most of our CPP conjugated Gd(III) complexes have their molecular weight in the range of 2,200 to 2,400; and their r_1 relaxivity are in the range in of 6-8.8 mM⁻¹ s⁻¹. The r_1 relaxivity NLS conjugated Gd-DTPA is 5.0 mM⁻¹ s⁻¹; this is correlate with its molecular weight (1929). These results demonstrated that the r_1 relaxivity of these CPP conjugated Gd(III) complexes are reliable considering their molecular weight. However, the r_1 relaxivity of Gd-DOTA-D-Tat₅₇₋₄₉ (14.2 mM⁻¹ s⁻¹) is exceptionally high. We have synthesized and measured four batches of Gd-DOTA-D-Tat₅₇₋₄₉. The r_1 relaxivity values were still in the range of 13~14 mM⁻¹ s⁻¹. The reason of this exceptional value is still under investigation.

There are some differences in the value of relaxivity from batch to batch of the same CPP conjugated Gd(III) chelates. This might be because TFA bind with positive charged amino residue as the counter-anions and the real concentration of these MR contrast agent were determine by the UV-Vis absorption of FITC. Relaxivity measurements were

Chapter 2. Screening of CPP

acquired by taking the slope of a plot of R_1 versus concentration. Although every molecule of the CPP conjugated ligand includes only one FITC and one ligand group, the content of Gd(III) might differ from batch to batch. There is still the possibility that some of the ligands have not completely chelated with Gd(III), or that free Gd(III) still remaining unspecifically in the CPP, considering many donor atoms on the peptide which might offer alternative coordination sites to the lanthanide ion. Therefore, other methods which can determine Gd(III) directly (such as ICP-MS) would be better to quantify the Gd(III) content in the ligands. And the resulting relaxivity would be more reliable than our current method. (Determination of Gd(III) by ICP-MS is under progress by the collaboration group at the University of Bremen)

2.3.2 Intracellular delivery of CPP conjugated MR contrast agents

Efficient delivery of diagnostic compounds to the cell interior using CPPs has enabled novel applications in molecular imaging. Peptide-based imaging agents in particular are desired for molecular imaging applications because of their potential for specific detection of a target, great flexibility in design, facile synthesis, and the availability of well-characterized chelation cores for incorporation of imaginable metals, such as technetium (^{99m}Tc) (44) for nuclear imaging and gadolinium (Gd) for MRI (47).

We have synthesized a series of Gd-DTPA or Gd-DOTA complexes, which were conjugated with L-Tat₄₉₋₅₇, D-Tat₅₇₋₄₉, Orn-D-Tat₅₇₋₄₉, PTD-4 and NLS, respectively, and tested their intracellular delivery *in vitro*. The biological evaluation showed some advisable results about their relative efficacy, toxicity and possible uptake mechanism, which will be critical in determining the optimal CPP sequence for intracellular MR contrast agent design.

Both the MR and the fluorescence results from our biological studies confirmed that Tat peptide and its derivatives are efficient in the intracellular delivery of MR contrast agents. HIV Tat peptide is the most intensively studied and widely applied cell penetrating peptides. An endocytic uptake had already been demonstrated for the entire HIV-1 Tat protein in 1991. However, the precise intracellular uptake mechanism of Tat peptide still appears controversial and requires further investigations. Contradictory results are often obtained. They could result from experimental variations in, for example, the diversity of the Tat peptide sequence used to promote the translocation activity, the wide variety of

cell lines studied, the differing protocols applied to investigate the entry mechanism or the high diversity of cargoes, all of which might influence the behavior of Tat peptide during the cellular entry process (78). In the case of delivering MR contrast agents, Meade et al. (47) reported that the variables of Gd (III) chelator (DOTA or DTPA) and cell type (NIH/3T3, RAW264.7, or MDCK) could be attributed to the variable uptake of MR contrast agents. NIH/3T3 and RAW264.7 transduction appears to be Gd(III) chelator dependent, preferring DTPA- to DOTA-based contrast agents. This result is demonstrated in our cell biological studies also: Gd(III)-DTPA complexes were more efficient to enter NIH/3T3 cells than Gd(III)-DOTA complexes. However, the cytotoxicity of Gd(III)-DTPA complexes were also higher than that of Gd(III)-DOTA complexes. These results could be a function of overall molecular charge or three- dimensional chelator conformations.

Our comparison studies of the uptake and toxicity on NIH/3T3 cells suggest that D-Tat₅₇₋₄₉ contrast agent could label cells sufficient to enhance significantly relaxation rates R_1 and R_2 for MR measurements, and without effecting cell bioavailability when concentration less than 20 μ M were applied. Therefore, D-Tat₅₇₋₄₉ peptide proves to be a useful cell-penetrating peptide for the further development of new intracellular MR contrast agents.

2.4. Summary

1). Two synthesis schemes were developed in comparison to synthesize the CPPs conjugated MR contrast agents: fragment conjugation scheme and on-line continuous solid-phase synthesis scheme. The continuous solid-phase synthesis scheme was proved to be optimal compared to fragment conjugation scheme in the synthesis of CPP conjugates.

2). Eight intracellular MR contrast agents, which are Gd-DTPA-Lys(FITC)-L-Tat₄₉₋₅₇-OH, Gd-DTPA-Lys(FITC)-D-Tat₅₇₋₄₉-OH, Gd-DTPA-Lys(FITC)-Orn-D-Tat₅₇₋₄₉-OH, Gd-DTPA-Lys(FITC)-NLS-OH, Gd-DTPA-Lys(FITC)-PTD-4-OH, Gd-DOTA-Lys(FITC)-L-Tat₄₉₋₅₇-OH, Gd-DOTA-Lys(FITC)-D-Tat₅₇₋₄₉-OH and Gd-DOTA-Lys(FITC)-Orn-D-Tat₅₇₋₄₉-OH, were synthesized by continuous solid phase synthesis scheme. The key intermediates and final products were characterized by ESI-MS. The detected molecular ions were consistent with the calculated molecular weight. The r_1 relaxivity of these contrast agents in aqueous solution are in the range of 6-9 $\text{mM}^{-1} \text{s}^{-1}$ at 3 T, except Gd-DTPA-NLS ($5.0 \text{mM}^{-1} \text{s}^{-1}$) and Gd-DOTA-D-Tat₅₇₋₄₉ ($14.2 \text{mM}^{-1} \text{s}^{-1}$).

3). Fluorescence microscopy imaging as well as spectroscopy data in NIH/3T3 cells plated in 96well plates demonstrated that the delivery efficiency showed following order Orn-D-Tat > D-Tat > L-Tat > PTD-4 > NLS.

4). Both the MR and the fluorescence results confirmed that the Tat peptide and its derivatives are efficient in the intracellular delivery of MR contrast agents. Our studies on uptake and toxicity in NIH/3T3 cells suggest that D-Tat₅₇₋₄₉ contrast agent could label cells sufficiently to enhance significantly relaxation rates R_1 and R_2 in MR measurements, thus D-Tat₅₇₋₄₉ peptide proves to be a useful vector for the development of novel intracellular MR contrast agents.

5). The design of a reliable intracellular delivery system offers a powerful tool to label cells with MR contrast agents. The properties of the Gd(III) complexes described in this chapter are well suited for facilitating the study of biological activity *in vivo* by MRI

Chapter 3: Design, synthesis and *in vitro* evaluation of antisense PNA conjugated intracellular MR contrast agents

3.1 Research design

To be useful as a probe, an antisense PNA must target a unique mRNA sequence in the objective cells. The targeted mRNA should be highly abundant in cells to ensure good detection sensitivity and selectivity for MR imaging. Therefore, as a proof of principle we chose the mRNA of the red fluorescent dsRed protein as target. The gene for this protein, originating from a coral of the *Discosoma* genus, is widely used as a transfection marker in model systems, such as yeast, *E. coli*, *C.elegans*, and zebrafish. Furthermore, Nagy et al. (84) developed a system which expresses dsRed protein in mouse embryonic stem cells, embryos and adult animals (Figure 16). Thus, this model system can be applied in future for *in vitro* and *in vivo* studies.

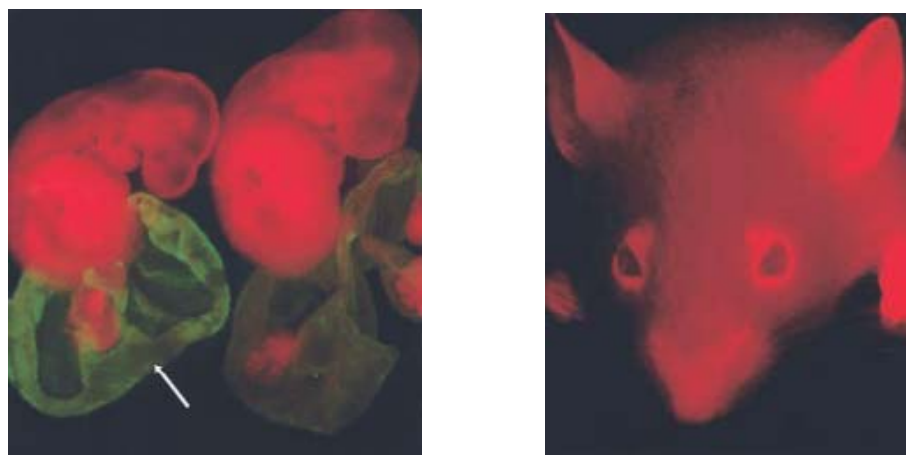


Figure 16. Red fluorescent protein expression in mouse embryos and adult animals (Vintersten et al., *Genesis*. **2004**; 40(4): 241-6)

The CPP and PNA fragments will be synthesized by solid phase by the Fmoc mediated scheme. Synthetically, PNAs incorporate repetitive elements, which are readily amenable to assemble via automated solid phase synthesizer. Specifically, protecting group strategies, solid phase peptide synthesis protocols, de-protection methods and purification procedures developed for peptide synthesis are adapted to the synthesis of PNAs.

Chapter 3. Synthesis of PNA Conjugates

Furthermore, the use of Fmoc protection offers several advantages, including milder synthesis conditions, improved monomer solubility, high coupling efficiencies and facilitated purification of the final product.

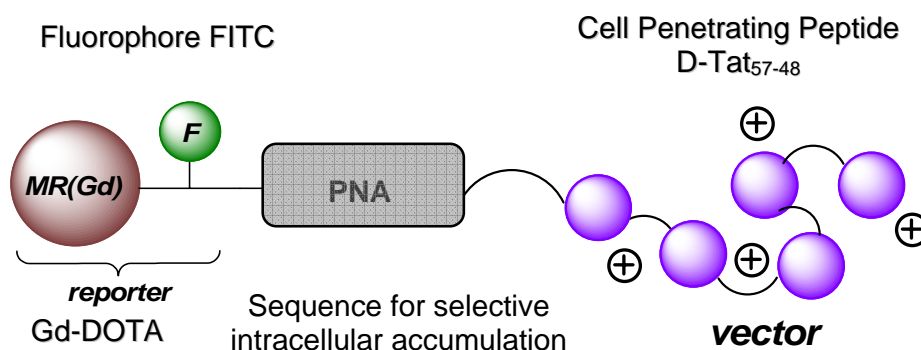


Figure 17. Schematic structure of targeted intracellular CA

This chapter aims to design and synthesize intracellular MR contrast agents, which conjugate PNA with cell penetrating peptides, Gd-DOTA and FITC (Figure 17). The designed antisense contrast agent will include three functional domains: first, CPP helps intracellular delivery of the contrast agent; second, PNA fragment is the antisense to the mRNA of dsRed, which specifically bind with complementary sequence in mRNA of dsRed; third, Gd-DOTA and FITC forms reporter domain for fluorescent optical imaging as well as MR imaging.

In vitro cell biological evaluations were made on normal NIH/3T3 mouse fibroblasts and a transgenic cell line to test the internalization of these compounds into cells, their biocompatibility and specificity using MR and fluorescent optical imaging techniques. Furthermore, the intracellular content of the antisense PNA contrast agents was determined by MR after the labeled cells were treated by concentrated acid. The specificity of the antisense PNA contrast agents to the target sequence was demonstrated by an *in vitro* hybridizing-ELISA test. These preliminary studies on the antisense probes, designed for imaging mRNA transcription by MRI, support some helpful data for the further rational design and modification of intracellular targeted MR contrast agents.

3.2 Results

3.2.1 Design of antisense PNA-CPP conjugates

In chapter one, we demonstrated that conjugates of Gd-DTPA or Gd-DOTA with cationic CPP, such as Tat peptide and its derivatives, could be internalized into cells in sufficient quantities to enhance contrast in MR images. Cell biological tests demonstrated that the modified CPP D-Tat₅₇₋₄₉: (retro-inverso sequence with D-amino acids); improved intracellular delivery with acceptable biocompatibility when compared to natural CPP. Therefore, we selected D-Tat₅₇₋₄₉ as a vehicle for the intracellular delivery of the PNA conjugates in the current study.

Recently, it was shown that DTPA-metal complexes had a lower thermodynamic stability compared to DOTA complexes if one of the N-acetate side chains is used for coupling via amide bond (85). Especially lower pH-values enhanced this effect. In addition, Aime's (32) group reported that the lower stability of the Gd-DTPA-BMA complex was responsible for a shift in the dissociation equilibrium that resulted in the net transfer of Gd³⁺ ions on the cell membrane followed by a slower internalization process and accompanied by a drastic decrease in cell viability. Therefore, Gd-DOTA was selected as the MR contrast agent.

Two PNA conjugates were designed after a BLAST (Basic Local Alignment and Search Tool) database search: The sequence of anti-dsRed PNA is tcc gtg aac ggc (corresponding to base 61 to 72 of dsRed cDNA sequence) marked red in Figure 18, which specifically targets to the mRNA of dsRed. This sequence of 12 bases is unique for dsRed and has no significantly similar sequence in mouse genome. While the nonsense PNA (gtt cag agt cta) does not correspond to any known mammalian gene or sequence of the dsRed gene (Figure 19).

Chapter 3. Synthesis of PNA Conjugates

atggcctcct ccgaggacgt catcaaggag ttcattgctt tcaaggtgcg
 catggagggc **tccgtgaacg** **gc**cacgagtt cgagatcgag ggcgagggcg
 agggccgccc ctacgagggc acccagaccg ccaagctgaa ggtgaccaag
 ggcggccccc tgccttcgc ctgggacatc ctgtccccc agttccagta
 cggctccaag gtgtacgtga agcaccgccg cgacatcccc gactacaaga
 agctgtcctt ccccgagggc ttcaagtggg agcgcgtgat gaacttcgag
 gacggcggcg tggtgaccgt gaccacggac tcttcctgc aggacggctc
 cttcatctac aaggtgaagt tcatcggcgt gaacttcccc tccgacggcc
 ccgtaatgca gaagaagact atgggctggg aggcctccac cgagcgcctg
 taccctccgc acggcgtgct gaagggcgag atccacaagg cctgaagct
 gaaggacggc ggccactacc tggtgaggtt caagtccatc tacatggcca
 agaagcccgt gcagctgccc ggctactact acgtggactc caagctggac
 atcacctccc acaacgagga ctacaccatc gtggagcagt acgagcgcgc
 cgagggccgc caccacctgt tcttg

Figure 18. cDNA sequence of dsRed and the selected fragment (red) for the antisense MR contrast agent. The red marked sequence is specific for dsRed and is selected to design the PNA sequence antisenses to mRNA of dsRed.

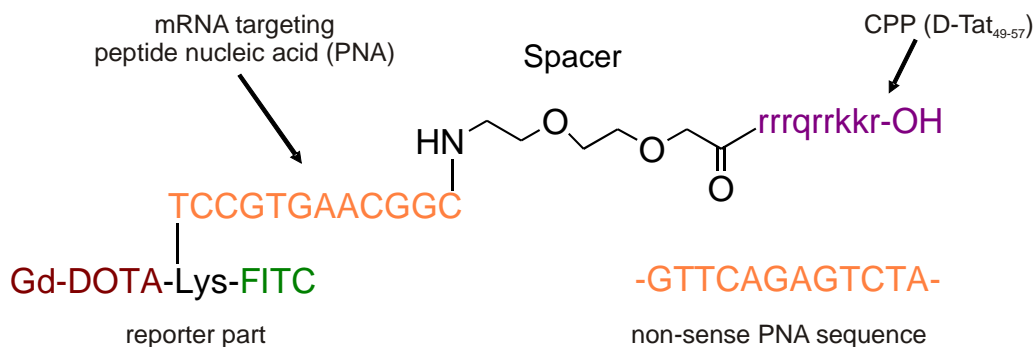
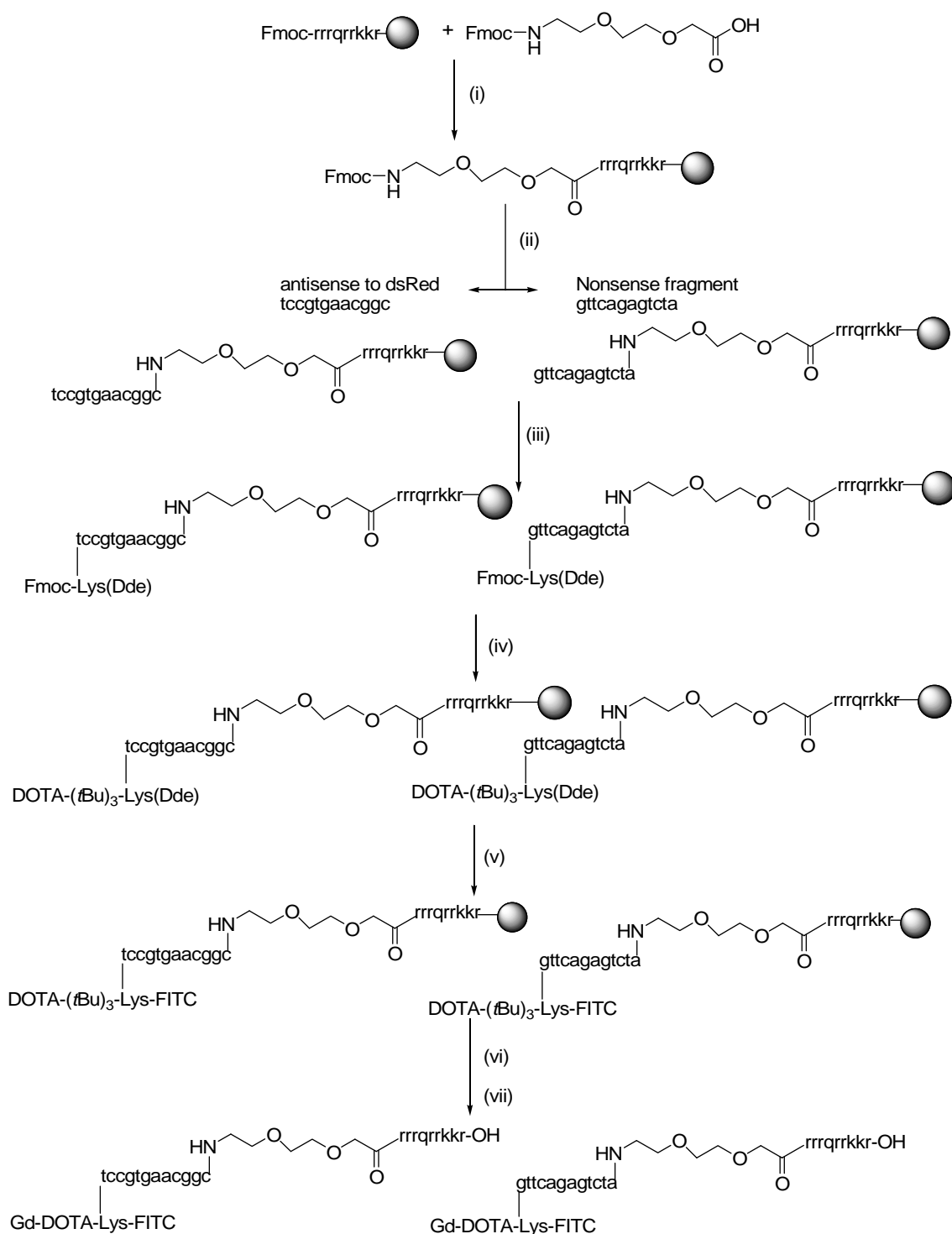


Figure 19. Schematic structure of antisense dsRed mRNA targeting contrast agent (dsRed CA) and nonsense contrast agent (nonsense CA)

Chapter 3. Synthesis of PNA Conjugates



Scheme 3. Synthesis of PNA conjugated MR contrast agent.

Reagents and conditions: (i) Fmoc-AEEA-OH, HATU, DIEA, DMF; (ii) Fmoc/Bhoc protected monomers, HATU, DIEA, DMF; (iii) Fmoc-Lys(Dde)-OH, HATU, DIEA,

Chapter 3. Synthesis of PNA Conjugates

DMF; (iv) DOTA-(tBu)₃-OH, HATU, DIEA, DMF, 2 h; (v) FITC, DIEA, DMF, 7 h; (vi) TFA: m-Cresol: TIS: H₂O (90:5:2.5:2.5), 4 h; (vii) GdCl₃·6H₂O, 60 °C, 12 h;

3.2.2 Synthesis of Gd-DOTA-Lys(FITC)-PNA-CPP conjugates

The conjugates were synthesized by a continuous solid phase synthesis scheme using Fmoc/Bhoc chemistry for PNA synthesis (Scheme 3). First, D-Tat₅₇₋₄₉ was synthesized on Wang resin at a low level of substitution (0.30 mmol/g) like described in chapter 2. Then, PNA building blocks were coupled continuously through an AEEA spacer. A Fmoc-Lys(Dde)-OH residue was applied as second spacer. Afterwards, Fmoc group was deprotected selectively; and DOTA tris(*tert*-butyl) ester was coupled on the α -NH₂ group of Lys. Finally, the Dde group was removed by treatment with 2% hydrazine in DMF and FITC was coupled on the ϵ -NH₂ group of Lys under the addition of DIEA (8eq).

The advantage of this scheme was that all coupling reactions were performed under mild conditions preventing the formation of side products, such as excess coupling on the phenol group of FITC. Because of this continuous scheme, the whole coupling process can also be carried out by a fully automated synthesizer.

After purified by semi-preparative reversed-phase HPLC, the products were characterized by ESI-MS: for anti-dsRed PNA conjugate, detected molecular ions at $m/z = 1126.3$ ((M+5H)⁵⁺), 938.9 ((M+6H)⁶⁺), 805.0 ((M+7H)⁷⁺), and 704.3 ((M+8H)⁸⁺) were consistent with the calculated mass of the desired product (5628.2) (e.g. Figure 20). For nonsense PNA conjugate, detected molecular ions at $m/z = 1129.1$ ((M+5H)⁵⁺), 941.1 ((M+6H)⁶⁺), 806.9((M+7H)⁷⁺), and 706.1 ((M+8H)⁸⁺) were consistent with the calculated mass of the desired product (5642.4).

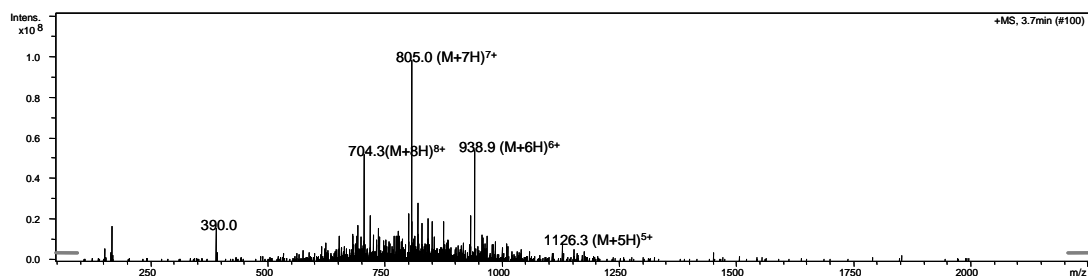


Figure 20. ESI-MS Spectrum of anti-dsRed PNA ligand

3.2.3 Chelating with gadolinium and purification

PNA conjugates were successfully chelated with Gd^{3+} under mild conditions (at $60^{\circ}C$ for 12 h). After chelating with gadolinium, the complexes were characterized by ESI-MS: From anti-dsRed PNA complex, detected molecular ions at $m/z = 964.7 ((M+6H)^{6+})$, $826.9 ((M+7H)^{7+})$, $723.8 ((M+8H)^{8+})$, and $643.1 ((M+9H)^{9+})$ were consistent with the calculated mass of the desired product (5782.4) (in the following called dsRed CA) (e.g. Figure 21). For nonsense PNA complex, detected molecular ions at $m/z = 1159.7 ((M+5H)^{5+})$, $966.7 ((M+6H)^{6+})$, $829.1((M+7H)^{7+})$, and $725.7 ((M+8H)^{8+})$ were consistent with the calculated mass of the desired product (5796.6; nonsense CA). These mass spectra demonstrated that the PNA conjugates successfully chelated with gadolinium.

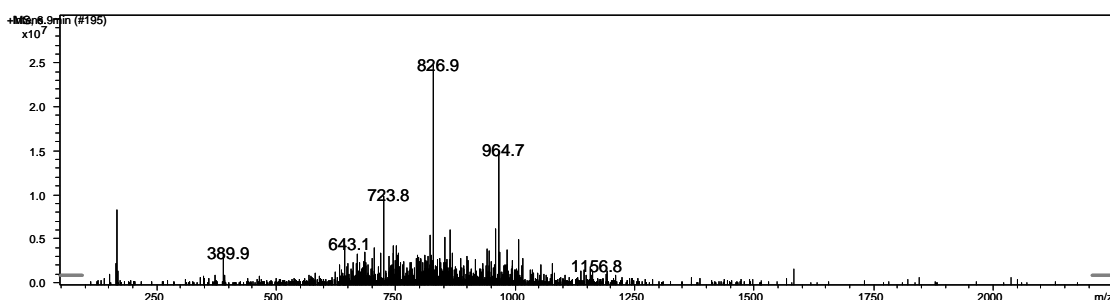


Figure 21. ESI-MS spectrum of anti-dsRed contrast agent

Before biological testing, the compounds were purified carefully to separate free gadolinium and other inorganic salts. Initially, the chelating mixtures were dialyzed for 48 h. But the compounds still showed very high R_1 and especially R_2 relaxation rates in cell MR tests (210 and 813 % of control for $1 \mu M$, respectively; data not shown). We ascribed this to the possibility that some Gd^{3+} not chelated by DOTA-ligand but weakly bound to other potential chelating moieties (amide in peptide and PNA backbone, amino groups in the nucleobases, etc) in the peptide/PNA complex was still present in the preparation even after dialysis. Thus, we modified the purification process. The chelating mixtures were purified first by HPLC to separate the unstable bound Gd^{3+} , and subsequently, the compounds were dialysed to remove other impurities. After this purification the observed relaxivities of both CA in water were between 3.4 and 5.3 (mM^{-1}

Chapter 3. Synthesis of PNA Conjugates

$^1\text{sec}^{-1}$). These values are in the expected range for compounds with one DOTA-complexed gadolinium (10). The relaxivity was not further decreasing in a competitive assay with free DTPA indicating the complete removal of unspecifically bound Gd^{3+} during the additional purification steps.

3.2.4 Determining the concentration and relaxivity of PNA conjugated contrast agents

Because the final products were purified by HPLC using 0.1%TFA in $\text{H}_2\text{O}/\text{ACN}$ as eluent, there is as well a high probability for the PNA conjugated contrast agents that TFA interacts with positive charged amino residues as the counter-anions. Thus, the real concentrations of CPP conjugates were determined by UV-Vis absorption of the fluorescence moiety.

Table 4. Determination of the concentration of PNA conjugated MR CAs

| Contrast agent | Calculated concentration (mM) | Measured concentration (mM) | Purity (%) |
|----------------|-------------------------------|-----------------------------|------------|
| dsRed CA | 5 | 2.941 | 59 |
| Nonsense CA | 5 | 3.383 | 67 |

Relaxivity measurements were acquired by taking the slope of a plot of R_1 versus the determined concentration. Relaxivity measurements of contrast agents were performed in the concentration range of 0 – 30 μM at 300 MHz at room temperature ($\sim 21^\circ\text{C}$). Contrast agents were diluted in water and 1ml aliquots were transferred to Eppendorf cups. The observed relaxivities of dsRed contrast agent and nonsense contrast agent in water were 3.3 and 5.3 ($\text{mM}^{-1}\text{sec}^{-1}$), respectively. These values are in the expected range for compounds with one DOTA-complexed gadolinium.

Table 5. Relaxivity of PNA conjugated contrast agents

| Contrast agent | PNA sequence | Relaxivity ($\text{mM}^{-1}\text{s}^{-1}$) |
|----------------|-----------------|--|
| dsRed CA | tcc gtg aac ggc | 3.4 |
| Nonsense CA | gtt cag agt cta | 5.3 |

3.2.5 *In vitro* fluorescence studies on NIH/3T3 embryonic mouse fibroblasts

To determine whether these synthesized PNA-peptide conjugates are internalized into cells and to evaluate the distribution of the compounds in subcellular compartments, fluorescence spectroscopy and fluorescence microscopic studies were performed with both contrast agents at first on NIH/3T3 embryonic mouse fibroblasts. The NIH/3T3 cells are not containing any target molecule for both PNA conjugated contrast agents.

The results of fluorescence spectroscopy (Figure 22) showed that both contrast agents could enter efficiently into 3T3 cells in a concentration dependent manner from 0.5 μM to 9.0 μM . At concentrations higher than 5.0 μM , the cytotoxicity of these compounds increased dramatically (data not shown). No significant differences between the two compounds were observable, as expected for a cell line without any target mRNA. Therefore, further results were shown solely of the dsRed CA and at concentrations below 5.0 μM .

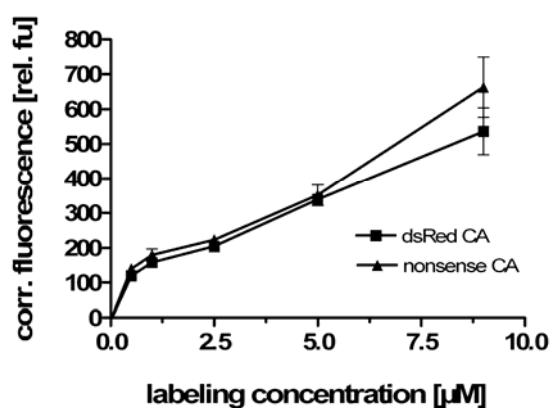


Figure 22. Cell internalization of dsRed and nonsense CA into 3T3 cells measured by fluorescence spectroscopy. Cells were incubated with contrast agents at various concentrations in complete medium for 18 h. External fluorescence was quenched with trypan blue and subsequent washes with HBSS; Values are means \pm SEM, $n=3-10$ with six replicates each.

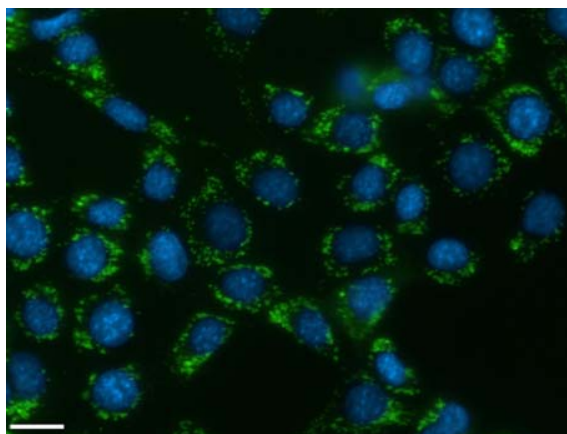


Figure 23. Fluorescence microscopic images displaying the cellular localization of dsRed CA in 3T3 cells

Cells were incubated with dsRed CA at 5 μM in complete medium for 18 h, cell nuclei were counterstained by Hoechst 33342 and external fluorescence was quenched with trypan blue and subsequent washes with HBSS.

dsRed CA: green (FITC fluorescence); nuclei: blue (Hoechst 33342); bar represents 20 μm .

Fluorescence microscopy imaging (Figure 23) demonstrated that the dsRed CA (green) could enter cells and was located predominately in vesicles around the nucleus (blue) whereas no uptake into the nucleus was observed. The vesicular distribution indicates a predominantly endosomal uptake mechanism of dsRed CA. We observed only few cells with low cytosolic fluorescence at higher concentrations might be indicating a slow release from these endocytic vesicles in our model system.

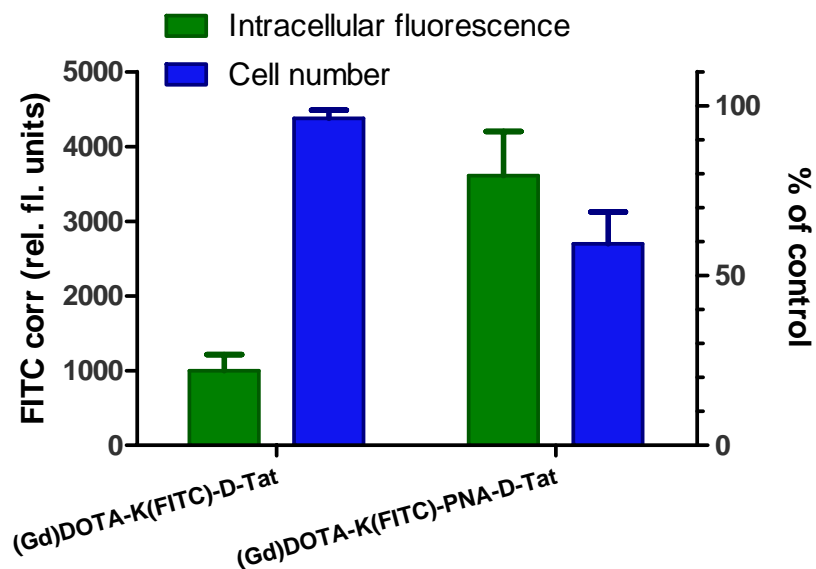


Figure 24. CA fluorescence (left Y-axis) and cell number (right Y-axis) in 3T3 cells after incubation with 5 μM of Gd-DOTA-Lys(FITC)-D-Tat₅₇₋₄₉ and Gd-DOTA-Lys(FITC)-PNA-D-Tat₅₇₋₄₉ for 18 hrs. Values are means \pm SEM (n=3).

The intracellular uptake of Gd-DOTA-Lys(FITC)-PNA-D-Tat₅₇₋₄₉, Gd-DOTA-Lys(FITC)-D-Tat₅₇₋₄₉ and Gd-DOTA-Lys(FITC)-PNA were compared to visualize the influence of the contrast agent structure on the internalization. Whereas Gd-DOTA-Lys(FITC)-PNA without CPP was very poorly internalized (data not shown), Gd-DOTA-Lys(FITC)-D-Tat₅₇₋₄₉ showed efficient intracellular uptake at concentration of 20-30 μM (see chapter 2). However, Gd-DOTA-Lys(FITC)-PNA-D-Tat₅₇₋₄₉ could label cells very efficiently allowed at concentrations as low as 0.5-5 μM . Figure 24 shows the comparison of the fluorescence spectroscopic results for the incubation of 3T3 cells with 5 μM of Gd-DOTA-Lys(FITC)-D-Tat₅₇₋₄₉ and Gd-DOTA-Lys(FITC)-PNA-D-Tat₅₇₋₄₉, respectively. The PNA-CPP conjugate showed much better internalization compared to the only CPP coupled contrast agent, but accompanied by an increased cytotoxicity indicated by the reduced cell number. These results suggest that there should be a synergistic effect between CPP and PNA sequence. Gd-DOTA-Lys(FITC)-PNA-D-Tat₅₇₋₄₉ is the best intracellular MR contrast agent in all our synthesized probes until now.

3.2.6 *In vitro* MR studies on NIH/3T3 embryonic mouse fibroblasts

Cellular uptake of the PNA conjugated contrast agents was also confirmed by *in vitro* MR studies at 300 MHz. After loading with dsRed CA, the relaxation rate $R_{1,cell}$ inside 3T3 cells (Figure 25) increased linearly with the applied (extracellular) labeling concentration of contrast agent (from 0.1 μM to 1.0 μM). Up to now, we are still developing a method to quantify the exact concentration of gadolinium inside the cells after the labeling period of 18 h. Thus, in a first approach the apparent “intracellular” relaxation rates are plotted against the extracellularly applied concentration. Nevertheless, the measured intracellular relaxation rate increased significantly after loading with 0.5 μM and 1 μM dsRed contrast agent. Contrast enhancement in T_1 -weighted MR images of cells was also observable at these low concentrations, exemplarily is shown for a single experiment in Figure 26. The results of the MR measurements are summarized in Table 6, also illustrating that already at 0.5 μM applied concentration, a statistically significant increase of the intracellular relaxation rate $R_{1,cell}$ and thus a contrast enhancement was detectable. No significant effect on T_2 was observable at these low concentrations (data not show).

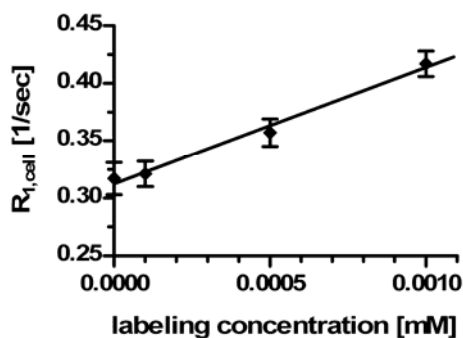


Figure 25. Relaxation rate $R_{1,cell}$ in 3T3 cells after loading with dsRed CA. After treated with dsRed CA for 18 h, cells were trypsinized, centrifuged and re-suspended in 1.5 mL Eppendorf tubes at 1×10^7 cells/500 μL in complete DMEM for MR studies. The measured relaxation rates were plotted vs. the extracellularly applied labeling concentration. Control: cells incubated with culture medium without CA.

Control (cells without CA) 0.5 μM dsRed CA 1 μM dsRed CA

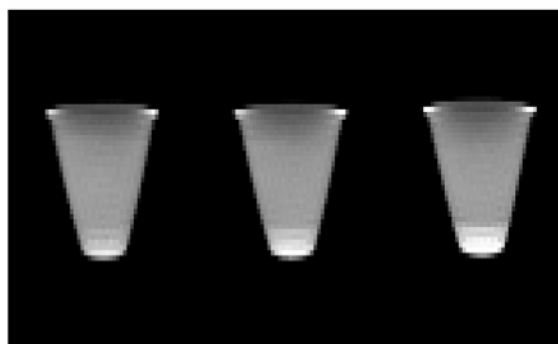


Figure 26. T_1 weighted MR images of 3T3 cells after loading with dsRed CA for 18 h. Sagittal images were obtained with a field of view $14 \times 6.9 \text{ cm}^2$, matrix 256×256 , slice thickness 2 mm, SW 100 kHz, TE 9.2 ms, TR 1500 ms, 26 averages for T_1 weighted images. Control: cells incubated with culture medium without CA.

Table 6. Intracellular relaxation rates $R_{1,\text{cell}}$ in 3T3 cells after loading with dsRed CA for 18 h.

| Labeling concentration [μM] | 0.5 | 1.0 | 2.5 |
|--|--------------------|--------------------|--------------------|
| $R_{1,\text{cell}}$ [% of control] | $112 \pm 0.5^{**}$ | $132 \pm 3.7^{**}$ | $144 \pm 1.9^{**}$ |
| n | 3 | 3 | 2 |

Values are means \pm SEM; **: $p < 0.01$ statistically different as compared to control ($100 \pm 0.6 \%$), ANOVA with Dunnett's post test; n: number of experiments, each with two replicates.

3.2.7 Determination of intracellular Gd^{3+} content

In order to determine the real intracellular relaxivity of the antisense PNA contrast agent, the content of probe should be measured via Gd(III) . According to the literature (32), the intracellular Gd^{3+} content can be determined by a MR method: After incubated with MR

Chapter 3. Synthesis of PNA Conjugates

contrast agent, the cells were recovered enzymatically with trypsin/EDTA mixture as was usually done for cell detachment. Then the collected cells were treated with 6M HCl at 120°C overnight. Upon this treatment, all Gd can be solubilized as free aquo-ion. By measuring the relaxation rates of these solutions by MR and in comparison to a standard curve, it is possible to determine its concentration.

At first, we made the parallel standard curves with or without cells: For preparing the standard curve in solution without cells, different concentrations of GdCl₃ diluted in 6M HCl and heated at 120°C overnight (Figure 27). For preparing the standard curve in solution with cells, different concentrations of GdCl₃ were mixed with 10⁷ cells and treated with 12M HCl (V/V=1:1, the final concentration of HCl is 6M) at 120°C overnight. Afterwards, the relaxation rate were measured by MR. The resulting standard curves were made by plotting R₁ versus concentration (Figure 28).

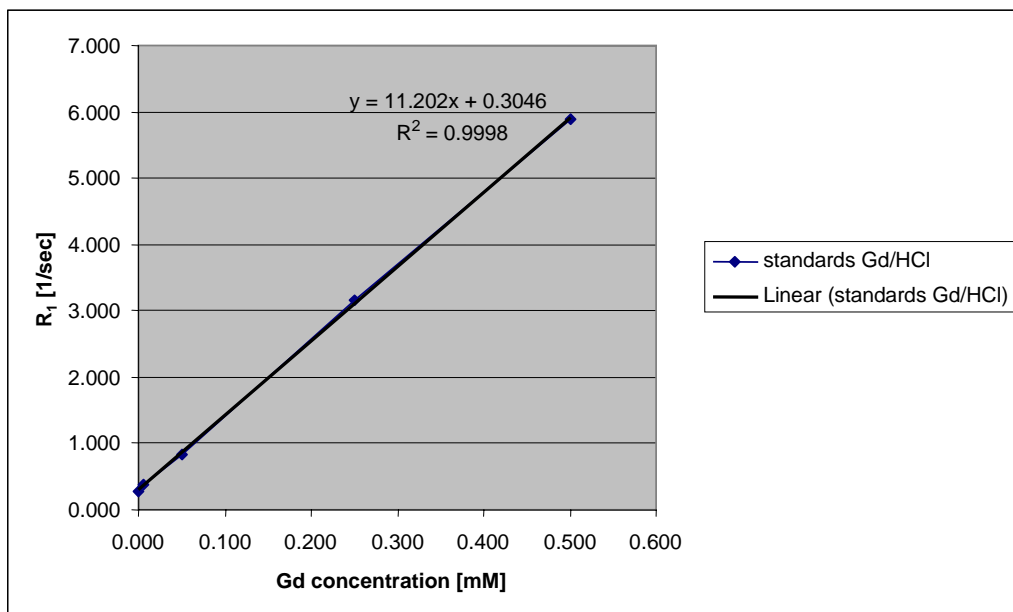


Figure 27. Gd(III) relaxation standard curve in 6M HCl.

Different concentrations of GdCl₃ in 6M HCl were prepared and heated at 120°C overnight. MR measurement was performed at 300MHz.

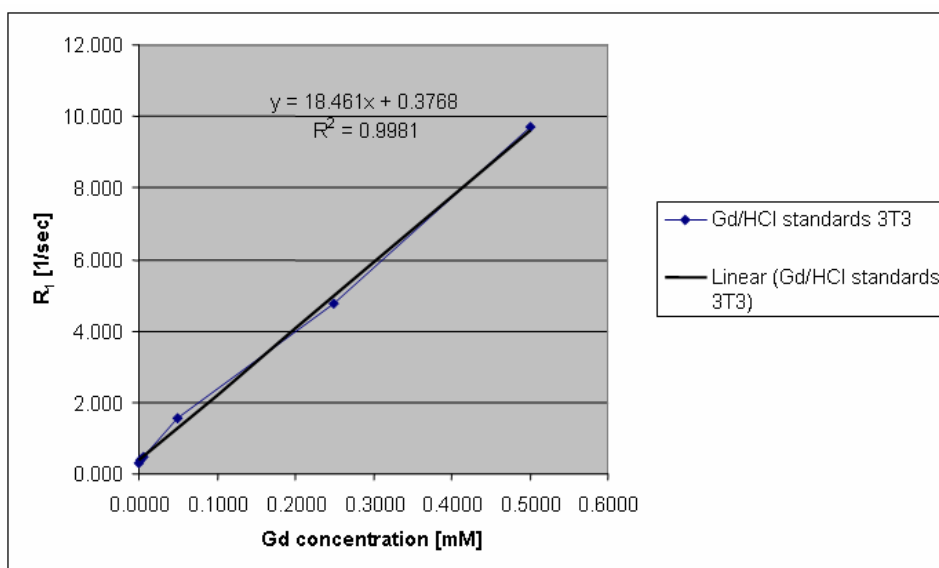


Figure 28. Gd(III) relaxation standard curve with cell background (6M HCl in medium). Different concentrations of GdCl₃ in the mixture of 10⁷ cells were prepared and heated at 120°C overnight. MR measurement was performed at 300MHz.

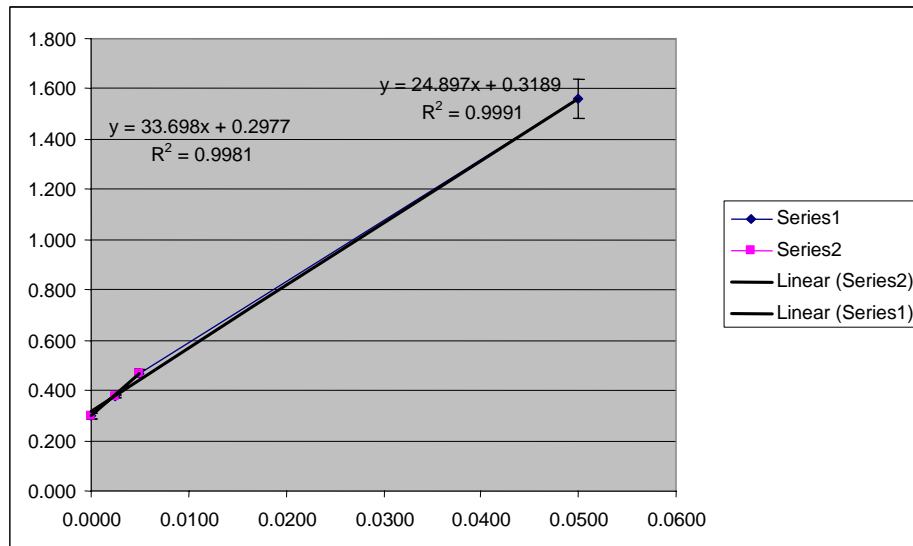


Figure 29. Gd(III) relaxation standard curve at low concentration (0.5μM-50μM) with cell background (6M HCl in medium). Different concentrations of GdCl₃ in the mixture of 10⁷ cells with 6M HCl were prepared and heated at 120°C overnight. MR measurement was performed at 300MHz.

Chapter 3. Synthesis of PNA Conjugates

Comparing the standard curves, there is a significant difference between the relaxation value of Gd(III) in water or in cell medium. Especially at low concentrations of 0.5 μM -5 μM (Figure 29), the relaxivity for low Gd(III) concentrations in cell lysates ($33.7 \text{ mM}^{-1} \text{ s}^{-1}$) is almost three times higher than that of Gd(III) in aqueous 6M HCl ($11.2 \text{ mM}^{-1} \text{ s}^{-1}$). The relaxation rates for the labeled cells were located in this low range. If the intracellular content of Gd(III) was calculated according the relaxivity of Gd(III) in 6M HCl, the resulting value were unreasonably high.

Thus, the intracellular content of Gd(III) should be calculated according to the relaxivity of Gd(III) in cell lysates. The resulting intracellular Gd(III) contents were in the range of 10^{-9} - 10^{-8} mol Gd/ 10^7 cells, which is in agreement with the values from literature (82). The volume of 3T3 fibroblasts can be estimated by a centrifuge measurement in special tubes. The resulting volume of 1×10^7 NIH/3T3 mouse fibroblasts was estimated to approx 28 μl . Thus, we can determine the real intracellular relaxivity of dsRed CA by taking the slope of a plot of R_1 versus intracellular contrast agent concentration. The resulting intracellular relaxivity of dsRed CA is $2.5 \pm 0.3 \text{ mM}^{-1} \text{ s}^{-1}$ (Figure 30).

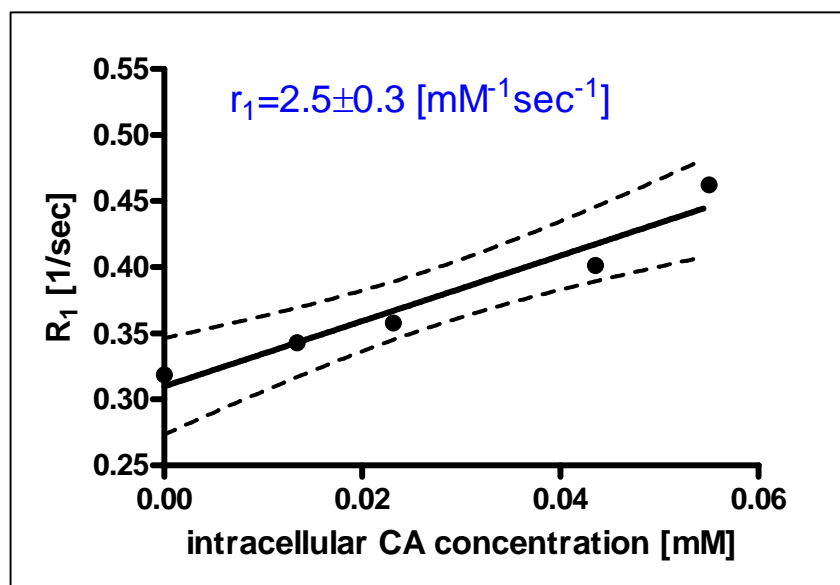


Figure 30. Determination of intracellular relaxivity of dsRed CA by MR measurements of cell lysates and Gd standards. (Estimated volume of 1×10^7 3T3 fibroblasts: $28 \pm 2 \mu\text{l}$). Dashed lines show the 95% confidence interval.

3.2.8 *In vitro* test of antisense PNA hybridizing with target sequence

An *in vitro* binding assay was performed to demonstrate the antisense specificity of dsRed contrast agent according to a protocol supported by Corning Costar Company. A target oligodeoxynucleotide sequence was immobilized in DNA-BIND™ 96-well plates. Then dsRed CA and nonsense CA were hybridized with the immobilized oligo-DNA sequence (Figure 31). The amount of hybridized contrast agent was determined by an ELISA assay, which can quantify the concentration of FITC by an antibody (86). This *in vitro* PNA-DNA binding assay confirmed that there is a significant higher specificity of the antisense dsRed CA in comparison to its nonsense counterpart (Figure 32). However, there are several positively charged amino acid residues in the D-Tat peptide which was conjugated to the PNA fragment. These positively charged amino acid residues can bind with the negatively charged backbone of DNA. Therefore, some nonspecific hybridization between the nonsense CA and the target sequence was observable. This nonspecific binding would be reduced dramatically, and specific binding would be increased significantly if the non-complementary sequence in the target oligo-DNA would be shorter (data not shown).

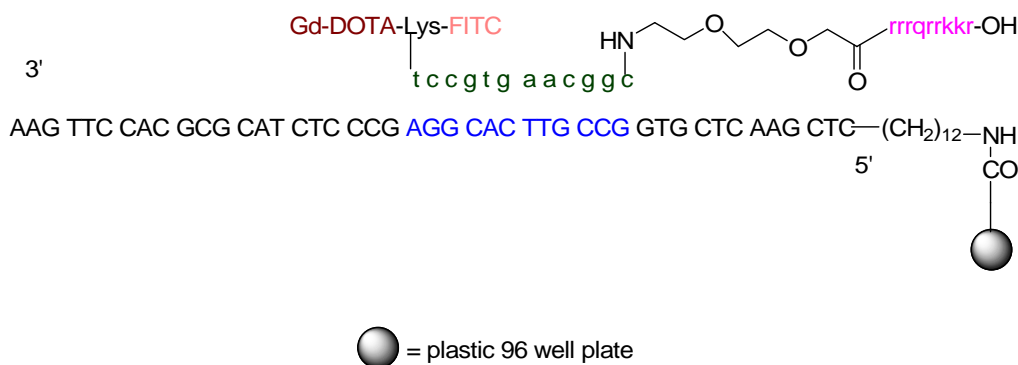


Figure 31. Schematic structure of antisense dsRed contrast agent hybrid with an immobilized artificial target sequence.

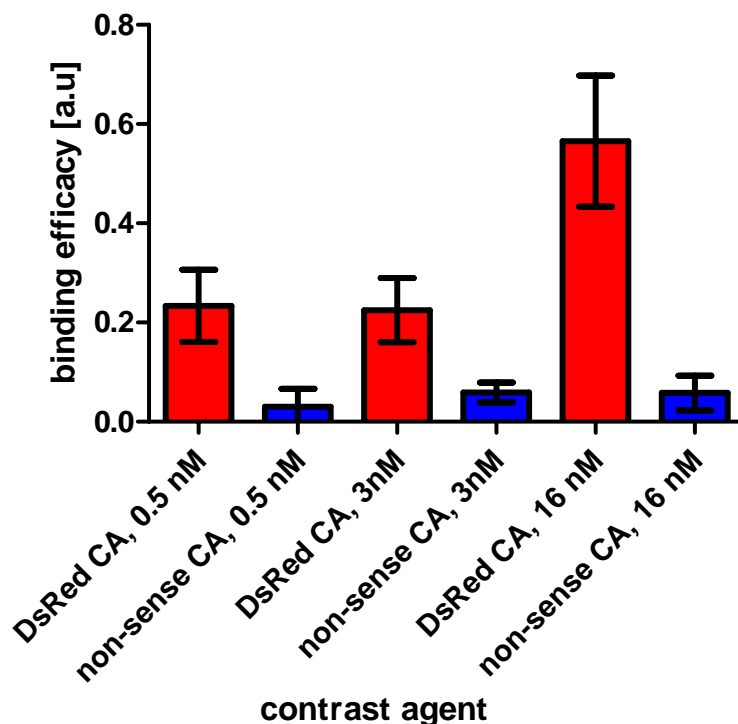


Figure 32. *In vitro* hybridization efficacy of the PNA-CPP conjugated CAs with an artificial DNA target sequence

3.2.9 *In vitro* biological studies on a transgenic cell line expressing dsRed

In order to study the antisense specificity of the dsRed contrast agent in cells, a transgenic dsRed expressing cell line (mouse fibrosarcoma cell line expressing dsRed gene was kindly provided by M. Erieson, University of Minnesota) containing the target mRNA was incubated with dsRed CA and nonsense CA. Fluorescence studies demonstrated that both dsRed CA and nonsense CA enter the transgenic cells efficiently. A significantly higher contrast enhancement could be observed at labeling concentrations more than 1 μ M. However, no specific accumulation of the antisense dsRed CA in comparison to the non-sense CA could be detected in the target containing dsRed cells.

Fluorescence microscopy imaging of these cells showed an exclusive endosomal localization of the contrast agent (Figure 33). Since the target mRNA is located in the cytosol, the vesicular entrapment prevents a specific interaction between the CA and the target. Thus, further modifications of the contrast agents are required to achieve the release from endosomes or a direct uptake into the cytosol.

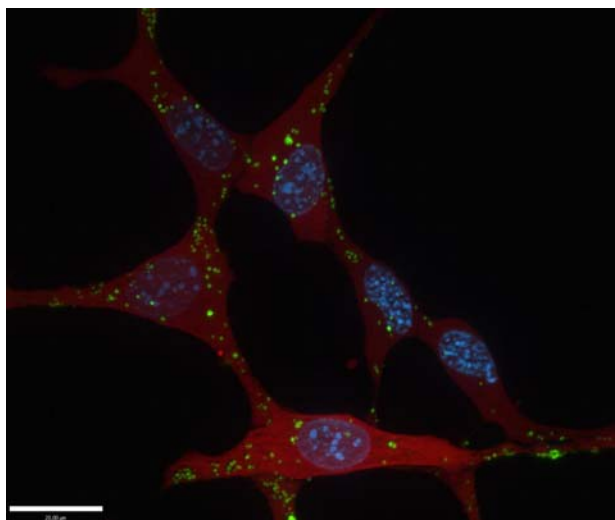


Figure 33. Endosomal localization of dsRed CA in dsRed expressing cells (Contrast agent is trapped inside the endosomes and cannot interact with target. dsRed CA: green (FITC fluorescence); nuclei: blue (Hoechst 33342); dsRed protein: red; bar represents 20 μm .)

3.3 Discussion

3.3.1 PNA synthesis and cleavage

This chapter described the design and synthesis of two PNA-CPP conjugated MR contrast agents: one is an antisense contrast agent to mRNA of dsRed; while the other one is a nonsense contrast agent as control. They were synthesized by a continuous solid phase synthesis scheme. Synthetically, PNAs incorporate repetitive elements. Therefore, PNA synthesis is comparable to the peptide synthesis. Specifically, protecting group strategies, solid phase synthesis protocols, de-protection methods and purification procedures developed for peptide synthesis might be applicable to the synthesis of PNAs and their analogs with only slight modifications. However, some key notes should be emphasized in the synthesis of PNAs:

- 1) The chemical structures of PNA monomers are much more complex than amino acid residues. In order to avoid interactions, such as steric hindrance effect, between growing PNA chains that can terminate the synthesis, we started the synthesis by downloading the capacity of the resin. Since the Wang resin, which is commercially available from Novabiochem Company, usually have high substitutions (0.5-0.6mmol/g), it is necessary to download their substitutions to the range between 0.2-0.3mmol/g. Kilk et al reported that the solid support should have substitution of between 0.01 and 0.2 mmol/g (67), and a lysine in the C-terminus of PNA improves PNA solubility and thus is more suitable for resin downloading than PNA monomers. In our synthesis scheme, D-tat peptide is synthesized on resin at first. Since Lysine is the second amino residue from the C-terminus of D-Tat peptide, we also downloaded the substitution of Wang resin by Lysine. The standard PNA EXPEDITETM column supplied by Applied Biosystems usually contains 2 μ mol per column. This is too less for us to be applied in our synthesis scheme. Because MRI is less sensible than radiolabelling imaging method, we need higher amounts for MR measurements. Thus, the PNA-CPP conjugated MR contrast agents should be synthesized at about 20-30 μ mol scales to ensure enough products for MR measurements. Therefore, we determined to synthesize PNA fragments manually on Wang resin with substitutions of between 0.2-0.3mmol/g.

- 2) Unlike peptides, upon Fmoc deprotection, PNA can undergo an alkaline pH-dependent N-acyl transfer rearrangement that converts the primary N-terminus into an unreactive amide (87). Therefore, piperidine reactions should be carried out in precise controlled cycles when PNAs were synthesized manually. During our PNA synthesis procedure, Fmoc was deprotected by 20% piperidine in DMF in 2 x 5 min; while in peptide synthesis, 2 x 10 min is usually performed in Fmoc deprotection. Gallazzi et al. (88) suggested deprotecting Fmoc in precise 1min by 20% piperidine in DMF two cycles. The PNA synthesis protocol supplied by Applied Biosystems (89) suggests the deprotection of the Fmoc group by 20% piperidine in DMF in 2 x 2.5 min. However, when we tried this procedure, the Fmoc group was not completely removed in 2.5 min. (After aliquots of the resin-bound PNAs being cleaved and Bhoc-deprotected with H₂O/TIS/m-Cresol/ TFA (2.5:2.5:5:90) for 4 h, the products were checked by ESI-MS, and some of Fmoc protected products still could be observed). This difference might be due to the different solid supports. Wang resin is applied in our PNA synthesis scheme, while Fmoc-XAL PEG PS resin was used by Gallazzi and Applied Biosystems. Therefore, we adjusted the deprotection scheme to 2 x 5min, and the desired sequences could be prepared in their entirety.
- 3) The exocyclic amines of the PNA monomers (A, C and G) are protected by the (Bhoc) protecting group. The Bhoc group can be removed with TFA in the presence of the scavenger m-Cresol. Thus, the cleavage cocktail for PNA is different from the cleavage condition for peptide. During our synthesis procedures, the cleavage cocktail for PNA is H₂O/TIS/m-Cresol/TFA (2.5:2.5:5:90), and the cleavage condition for peptide is H₂O/TIS/TFA (2.5:2.5:95). Actually, the cleavage cocktail of H₂O/TIS/TFA (2.5:2.5:95) was tried in our preliminary PNA test synthesis experiments. It could remove the Bhoc group too. However, the water solubility of the product is not as good as that of the product cleft by the m-Cresol containing cocktail.

3.3.2 Determining the relaxivity of PNA conjugated contrast agents in solution and in labeled cells.

The observed relaxivities of dsRed CA and nonsense contrast agents in water were 3.3 and 5.3 ($\text{mM}^{-1}\text{sec}^{-1}$), respectively. To our best knowledge, there was no reported relaxivity value for the PNA-CPP conjugated MR contrast agent. Therefore, compare to the relaxivity of Gd(III)-DOTA complex ($r_1 = 4.2 \text{ mM}^{-1}\text{sec}^{-1}$ at 20MHz, 25°C) (10), the observed relaxivities of dsRed CA and nonsense contrast agents are in the expected range for compounds with one DOTA-complexed gadolinium. However, there are some differences in the value of relaxivity from batch to batch of the same PNA conjugated Gd(III) chelates (as was observed from the contrast agents without PNA in chapter 2). This might be because the TFA bind with positive charged amino residue and the exocyclic amines of the PNA monomers as the counter-anions. The real concentration of these MR contrast agent were determine by the UV-Vis absorption of FITC; and relaxivity measurements were acquired by taking the slope of a plot of R_1 versus concentration. Although every molecule of the CPP conjugated ligand includes one FITC and one ligand group, the containing of Gd(III) may be a little different. There is still possibility that some of the ligands have not completely chelated with Gd(III) or there might be some of free Gd(III) still remaining in the PNA-CPP conjugate, considering many donor atoms on the peptide which might offer alternative coordination sites to the lanthanide ion (please see the discussion in chapter 2).

3.3.3 Intracellular uptake of PNA conjugated MR contrast agent

Antisense PNA conjugated with different cell penetrating peptides (such as PTD-4 or poly-D-lysine) and radiometal complexes (such as ^{111}In , ^{90}Y or ^{64}Cu) has been reported as nuclear imaging probes (PET and SPECT) (61, 62). The utilization of such conjugates as contrast agents for MR imaging is very limited, probably because the accumulation of the PNA imaging probes in the targeting cells could barely reach the MR detectable level. Heckl et al. (64) developed a MR contrast agent combining a Gd^{3+} -complex with antisense PNA targeting the *c-myc* mRNA and the Antennapedia peptide. With this contrast agent, an increase in MR signal intensity and prolonged retention in tumor cells highly expressing this gene was observed *in vitro* and *in vivo*. But the applied concentration of contrast agent (0.5 mM) in that study was about 1000x higher compared

to the lowest concentration of dsRed CA in our experiments which is showing a significant increase in relaxation rate $R_{1,\text{cell}}$ within 3T3 cells. The difference is likely attributable to the different cell penetrating peptides and the Gd^{3+} moiety used. Thus, our synthesized dsRed contrast agent has an excellent potential to be used as targeted contrast agent for MR imaging in cells expressing the dsRed gene.

In order to demonstrate the antisense specificity of dsRed contrast agent, an *in vitro* binding assay was performed. After dsRed CA and nonsense CA were hybridized with the immobilized target oligo-DNA sequence, there is a significant higher specificity of the antisense dsRed CA in comparison to its nonsense counterpart. These results demonstrate that the antisense dsRed CA has the potential to bind specifically with its complementary target sequence.

Further studies on a transgenic cell line have been performed in order to prove the specific accumulation in cells by targeting the mRNA. A significantly higher contrast enhancement could be observed at labeling concentrations above 1 μM . However, no specific accumulation of the antisense dsRed CA in comparison to the non-sense CA could be detected in the target containing dsRed cells. Fluorescence microscopy imaging of these cells showed an exclusive endosomal localization of the contrast agent. Indeed, many studies have reported that cellular uptake of most CPP conjugates (such as Tat peptide or polyarginine) occurs mainly through endocytotic pathways, and most CPP conjugate is retained in the endosomal compartments of the cell (37). Since the target mRNA is located in the cytosol, the vesicular entrapment prevents a specific interaction between the contrast agent and the target. Thus, endosomal trapping and escape of CPP conjugates is one of the main rate-limiting steps which substantially limit the efficacy of CPP-mediated delivery of cargoes such as PNA. Therefore, further modifications of the contrast agents are required to achieve the release from endosomes or a direct uptake into the cytosol.

Treatments with endosome disruption agents, such as chloroquine, Ca^{2+} , sucrose or photosensitizers, facilitate the escape of CPP conjugates from endosomal compartments and their release into the cytoplasm might improve the antisense effects by two orders of magnitude. Nielsen et al (90) recently summarized these protocols of CPP-mediated, PNA delivery-assisted endosome-disruption agents. The protocols provide efficient and

Chapter 3. Synthesis of PNA Conjugates

fairly simple methods for the cytosolic and/or nucleic internalization of antisense PNA *in vitro*. However, these protocols are unlikely to be applied *in vivo*. In 2006, Takeuchi et al. (91) reported some interesting results about the direct and rapid cytosolic delivery using cell penetrating peptides conjugate and pyrenebutyrate. The addition of pyrenebutyrate resulted in direct membrane translocation of the peptides yielding in diffuse cytosolic distribution within a few minutes. However, there is a limitation in this approach since it is not applicable in the presence of a medium or serum. The competition with various ionic species in the medium would hamper the interaction of the arginine with pyrenebutyrate.

Additional studies are necessary for developing CPPs with better penetration properties, especially directly into the cytoplasmic compartment. One of the strategies is to incorporate endosomolytic peptides into delivery constructs (92). Generally these are Asp- and Glu-rich peptides, for example, the so-called GALA peptide, that selectively adopt amphipathic structures when the acidic residues become protonated at the low pH in late endosomes, leading to membrane rupture and release to the cytoplasm. Polycationic polyethyleneimine (PEI) based delivery systems appear to possess intrinsic endosomolytic activity, although the mechanistic reasons are not well understood (35). The use of an influenza virus hemagglutinin derived pH-sensitive fusogenic peptides that destabilize lipid membranes at low pH has also been shown to ameliorate macropinosome entrapment of Tat protein fusion constructs (93).

Referred from these studies, we now try to modify D-Tat₄₉₋₅₇ with pyrenebutyrate or endosomolytic peptide GALA to achieve the cytosolic delivery. A series of novel compounds, which covalently link Tat peptide with one or more copy of pyrenebutyrate residues or GALA peptide, has been designed and synthesized; further screening tests are under progress.

The fact that the pAntp CPP vector can enhance endosomal escape of cationic polymethacrylate-DNA complexes indicates that at least some CPPs also possess innate endosomolytic activity (94). Some members of our group are currently working on developing new and novel CPPs towards achieving this goal. Their preliminary results demonstrate that leakage from endosomes or a direct uptake into the cytoplasm is achievable (Deepti Jha, et al. personal communication).

3.3.3 Antisense imaging by MRI

As summarized by Weissleder (63), the major prerequisites for visualizing specific molecules or molecular mechanisms *in vivo* include: i) the availability of stable, nontoxic and high-affinity probes; ii) the ability of these probes to overcome biological delivery barriers; iii) the use of amplification strategies to increase the signal to background ratio; and iv) the availability of fast and high-resolution imaging techniques. Regarding these prerequisites, our proposal to image mRNA transcription by MRI using antisense PNA-CPP conjugated MR contrast agents, is rational:

First, MRI offers excellent three-dimensional spatial resolution, complete body coverage, and the opportunity to determine additional physiologic parameters noninvasively which has the ability to combine both functional and morphological imaging (2, 3). All these characterize MRI to contain considerable potential for molecular imaging.

Second, PNA is a leading agent among ‘third generation’ antisense and antigene agents. It is extremely stable in biological fluids. PNA oligomers with mixed bases sequences form duplexes (by Watson-Crick base-pairing) with complementary DNA and RNA with higher thermal stability than corresponding DNA-DNA or DNA-RNA complexes and without sacrificing sequence specificity (59). Actually, our PNA-DNA binding assay confirmed that there is a significant higher specificity of the dsRed antisense contrast agent in comparison to its nonsense counterpart.

Third, our synthesized PNA conjugated contrast agents are very efficient to overcome cell membrane. A subtoxic labeling concentration of 0.5 μM is sufficient to enhance MR imaging contrast significantly.

Therefore, we are making considerable progress in the development of antisense MR contrast agent, despite its obvious complexities. Unfortunately, antisense technology is proving to be much more complicated and challenging than was expected. There are still two main concerns regarding the antisense MR imaging: namely that the mechanism of localization may not be suitable for antisense interaction and that the degree of accumulation will be impractically low for imaging. The first concern about the localization of contrast agent has been discussed earlier (in the discussion of the intracellular uptake of PNA conjugated MR contrast agent), and our group is currently working on developing novel CPPs towards achieving this goal. As to the second

Chapter 3. Synthesis of PNA Conjugates

concern, there are some inspiring studies about the specific accumulation of antisense probes in recent years. Hnatowich et al. (95) reported the statistically significantly higher accumulations of antisense DNAs in cancer cells compared to control DNAs. From cell culture results such as using the number of cells per well and the known specific activity of the radiolabeled DNA, it may be calculated that the specific accumulation (i.e. antisense minus control DNA) is approximately 10^5 - 10^6 antisense DNA molecules per cell after 10-24hrs of incubation (and corresponds to an increase in concentration of antisense oligomers from nM in the media to mM concentration in the cytoplasm). These specific accumulations are many orders of magnitude over the steady-state target mRNA concentrations that are usually assumed to be in the range of 1-1000 copies per cell. One approach that may result in increased specific accumulation is to consider the mRNA target. It has been suggested that the antisense DNA may be acting in some manner to preserve its target mRNA (e.g. PNA do not activate RNase H degradation of mRNA (59)). If so, the mRNA turnover rate would be more important for successful targeting than the steady-state mRNA level as an increased transcription rate would increase the cellular concentration of the target mRNA if stabilized by the antisense DNA or PNA. If this hypothesis is correct, an increased accumulation of antisense DNA or PNA may be expected as the number of target mRNAs increase while accumulations in non-target tissues would presumably remain unchanged.

Very recently, Liu et al. (96) reported some very interesting results about antisense imaging of cerebral mRNA transcripts in live animals. They coupled SPIONs to phosphorothioate-modified oligo-DNA (sODN) with sequence complementary to c-fos and β -actin mRNA. In animals that were administered SPION-cfos and amphetamine, retention of the antisense probes was significantly elevated in the nucleus accumbens, striatum, and medial prefrontal cortex of the forebrain. Control groups that received a SPION conjugate with a random sequence probe showed no retention. This study demonstrated that SPION-sODN conjugates can detect active transcriptions of specific mRNA in living animals by MRI.

3.4. Outlook

Antisense imaging mRNA transcription by MRI, which promises that any tissue with a unique gene expression can be specifically visualized *in vivo*, is an outstanding important subject in molecular imaging. If antisense imaging were to achieve even a fraction of its promise, the results could well lead a revolution in diagnostic medicine. It has been more than 10 years since the first molecular imaging with a tumor-targeting antisense radioprobe was performed in an animal model of cancer. Progress in this area has been limited by formidable challenges of surmounting biological barriers to detect low concentrations of target mRNA. However, numerous recent advances, such as new antisense analogues, novel drug delivery technologies and better understanding of the antisense mechanism, offer a renewed anticipation that real-time, *in vivo* antisense imaging will be widely demonstrated. Further modifications of our antisense PNA conjugated MR contrast agents are needed to meliorate their targeting character, such as: 1) covalently link peptide vector with endosomolytic peptide or compounds, or developing novel CPPs to enhance the cytosolic delivery. 2) multistep labeling or pretargeting schemes which link a macromolecular contrast agent (Gd nanoparticles or dendrimers, etc) with CPP to increase MR contrast. Thus, the antisense PNA conjugated MR contrast agent will become a powerful tool for the molecular imaging of endogenous gene expression.

3.5 Summary

1. Two MR contrast agents, conjugated to PNA and cell penetrating peptide, were synthesized by a continuous solid phase synthesis scheme and characterized by ESI-MS.
 2. The intracellular uptake was confirmed by fluorescence absorption spectroscopy, transmission fluorescence microscopy and MR imaging on NIH/3T3 mouse fibroblasts as well as on transgenic dsRed cells.
 3. Concentration-dependent uptake (most probably by endocytosis) was observed. A subtoxic labeling concentration of 0.5 μM is sufficient to enhance significantly MR imaging contrast.
 4. The intracellular content of Gd(III) was calculated according the relaxivity of Gd(III) in cell lysates. The resulting intracellular Gd(III) contents are at the range of $10^{-9}\sim 10^{-8}$ mol Gd/ 10^7 cells. The intracellular relaxivity of dsRed CA is $2.5 \pm 0.3 \text{ mM}^{-1}\text{sec}^{-1}$.
 5. An *in vitro* PNA-DNA binding assay confirmed that there is a significant higher specificity of the dsRed antisense contrast agent in comparison to its nonsense counterpart.
 6. Further studies on the transgenic cell line expressing the target mRNA showed a significantly higher contrast enhancement at labeling concentrations above 1 μM . However, no specific accumulation of the antisense dsRed CA in comparison to the nonsense CA could be detected in the target containing dsRed cells.
 7. Fluorescence microscopy studies have shown an exclusive endosomal localization of the contrast agents. Since the target mRNA is located in the cytosol, the vesicular entrapment prevents a specific interaction between the CA and the target. Thus, further modifications of the contrast agents are required to achieve the release from endosomes or a direct uptake into the cytosol.
- In conclusion, the synthesized PNA conjugated contrast agents are very efficient to label cells for MR as well as fluorescent imaging.

Chapter 4. Experimental

4.1 General

All reagents were HPLC or peptide synthesis grade. DMF, DCM, ACN, TFA, methanol, and FITC were obtained from Acros Organics (Heidelberg, Germany). All standard, protected Fmoc amino acid derivatives, 2-(1H-benzotriazol-1-yl)-1,1,3,3-tetramethyluronium hexafluoro-phosphate (HBTU), pre-loaded Wang resin and 1-hydroxybenzotriazole (HOBt) were obtained from Novabiochem (Nottingham, UK). All Fmoc/Bhoc protected monomers and 2-(1-H-7-azabenzotriazol-1-yl)-1,1,3,3-tetramethyluronium hexafluorophosphate (HATU) for PNA synthesis were obtained from Applied Biosystems (Darmstadt, Germany). 1,4,7,10-tetraazacyclododecane (cyclen) was obtained from Strem Chemicals (Newburyport, USA).

Analytical and semipreparative RP-HPLC was performed at room temperature on a Varian PrepStar Instrument (Australia) equipped with PrepStar SD-1 pump heads. UV absorbance was measured using a ProStar 335 photodiode array detector at 260 nm. A Varian Polaris C18-Ether column (4.6 × 250 mm, particle size 5 μm, particle pore diameter 100 Å) was used for analytical RP-HPLC. For semipreparative HPLC, a Varian Polaris C18-Ether column (21.2 × 250 mm, 5 μm, 100 Å) was used.

CPP and PNA conjugates were analyzed using a linear gradient of water (0.1% TFA) (solvent A)/ACN (0.1% TFA) (solvent B) from 10% B to 90% B within 30 min (flow rate: 1 ml/min).

CPP and PNA conjugates were purified by semi-preparative RP-HPLC. Gradient systems were adjusted according to the elution profiles and peak profiles obtained from the analytical HPLC chromatograms.

ESI-MS was performed on ion trap SL 1100 system (Agilent, Germany).

4.2 Synthesis of CPP conjugated, dual-labeled Gd(III)-based MR contrast agents

Peptide synthesis was performed by solid-phase Fmoc/tBu-chemistry using a Heidolph Synthesis 1 synthesizer (Schwabach, Germany). Wang resin was used as a solid support at a substitution level of 0.50-0.60 mmol/g. The side chain of Arg was Pbf protected, Gln

Chapter 4. Experimental

was Trt protected, and Tyr was tBu protected. Fmoc-protected amino acids (four-fold excess) were activated in situ by HBTU/HOBt. The Fmoc protecting group was removed by 20% piperidine in DMF. The resin was washed with DMF after each coupling and deprotection step. All chemical steps were followed by a Kaiser test on the resin (97), and the resulting colorimetric reaction indicated the presence of free primary amines after Fmoc deprotection and the absence of primary amines after the coupling steps.

4.2.1 Gd-DTPA-Lys(FITC)-L-Tat₄₉₋₅₇-OH (1)

L-Tat₄₉₋₅₇ peptide synthesis was performed manually by solid-phase Fmoc/tBu-chemistry using a Heidolph Synthesis 1 synthesizer. Polystyrene-based Wang resin containing an Fmoc protected arginine residue (0.2g, 0.58 mmol/g) was swelled in DCM for 30 min and washed four times with peptide synthesis grade DMF. The resin was treated twice with a solution of 20% piperidine (3mL) in DMF for 10 min, and was washed four times with DMF. In a separate vial, Fmoc protected amino acid (4eq), HBTU (3.6eq), HOBt (3.6eq) were dissolved in DMF (2mL), and DIEA (8eq) was added. The resulting solution was added to the resin and allowed to react under N₂ for 30 min. The resin was drained and rinsed for times with DMF. This procedure was repeated until a Fmoc protected Tat₄₉₋₅₇ peptide (amino sequence: RKKRRQRRR) bound to Wang resin was obtained. An aliquot of the resin-bound peptide was deprotected the Fmoc group with 20% piperidine, and cleaved with H₂O/TIS/TFA; ESI-MS analysis was performed to confirm that the observed masses $m/z = 670.5 ((M+2H)^{2+})$, $447.5 ((M+3H)^{3+})$, $335.9 ((M+4H)^{4+})$, and $268.9 ((M+5H)^{5+})$ were consistent with the calculated molecular weight (1339.6) of the Tat peptide.

The resin-bound peptide was deprotected with piperidine, coupled with one Fmoc-Lys(Dde)-OH residue. After additional deprotection with piperidine, DTPA dianhydride (4eq) was coupled on the α -NH₂ group of Lys under base catalysis of DIEA (8eq). The resin was drained and rinsed four times with DMF. An aliquot of the resin-bound DTPA-Lys(Dde)-Tat was cleaved with H₂O/TIS/TFA; ESI-MS analysis was performed to confirm that the observed masses $m/z = 1004.6 ((M+2H)^{2+})$, $670.0 ((M+3H)^{3+})$ were consistent with the calculated molecular weight (2007.31) of the DTPA-Lys(Dde)-Tat-OH.

The resin-bound DTPA-Lys(Dde)-Tat was treated twice with hydrazine hydrate (2% in DMF, 2 min) to remove the Dde group. Then FITC was reacted with the ϵ -NH₂ group of Lys (resin:FITC:DIEA= 1:4:8) within 7 hours. The solvent was removed and the resin was washed with DMF, DCM and methanol alternatively four times. After dried under vacuum, DTPA-Lys(FITC)-L-Tat-OH was cleaved off the resin using TFA/TIS/H₂O (95:2.5:2.5, v/v/v). Crude products were precipitated by adding cold MTBE. The precipitated product was collected by centrifugation and exposed to the TFA cleavage cocktail (TFA/TIS/H₂O (95:2.5:2.5, v/v/v)) for 10h. After precipitated again in cold MTBE, the product was collected by centrifugation and dissolved in tBuOH/H₂O (4:1, v/v) and lyophilized. The sample was analyzed on an analytical column with detection at UV 218nm, using a water (0.1% TFA) (solvent A)/ACN (0.1% TFA) (solvent B) gradient from 10% B to 90% B within 30 min (flow rate: 1 ml/min). And then, DTPA-Lys(FITC)-L-Tat-OH was purified by semi-preparative RP-HPLC. Gradient systems were adjusted according to the elution profiles and peak profiles obtained from the analytical HPLC chromatograms. The ligand DTPA-Lys(FITC)-L-Tat₄₉₋₅₇-OH was characterized by ESI-MS. Detected molecular ions at $m/z = 1117.0$ ((M+2H)²⁺), 745.1 ((M+3H)³⁺), 559.1 ((M+4H)⁴⁺), and 461.7 ((M+5H)⁵⁺) were consistent with the calculated mass of the desired product (2232.13).

The purified product was dissolved in 5 mL H₂O, one equivalent of GdCl₃.6H₂O was added, and the pH was adjusted to 6.5 with 1N NaOH. The reaction mixture was stirred at room temperature for 24h. The pH was periodically checked and adjusted to 6.0-7.0 using a solution of 1N NaOH and 1N HCl as needed. The mixtures were purified first by HPLC using a water (0.05% TFA) (solvent A)/ACN (0.05% TFA) (solvent B) gradient to separate the unstable bound Gd³⁺. Afterwards, the product was dialyzed (Float-A-Lyzer, cellulose ester membranes, MWCO: 1,000; Spectrum Laboratories, Inc.) to remove inorganic impurities. The solution was lyophilized and yellow to orange solids were obtained. The absence of free Gd³⁺ was checked with xylenol orange indicator. Finally, the product Gd-DTPA-Lys(FITC)-L-Tat-OH (**1**) was characterized by ESI-MS. Detected molecular ions at $m/z = 796.6$ ((M+3H)³⁺), 597.4 ((M+4H)⁴⁺), 478.3 ((M+5H)⁵⁺), and 398.9 ((M+6H)⁶⁺) were consistent with the calculated mass of the desired product (2385.02) (Figure 34).

Chapter 4. Experimental

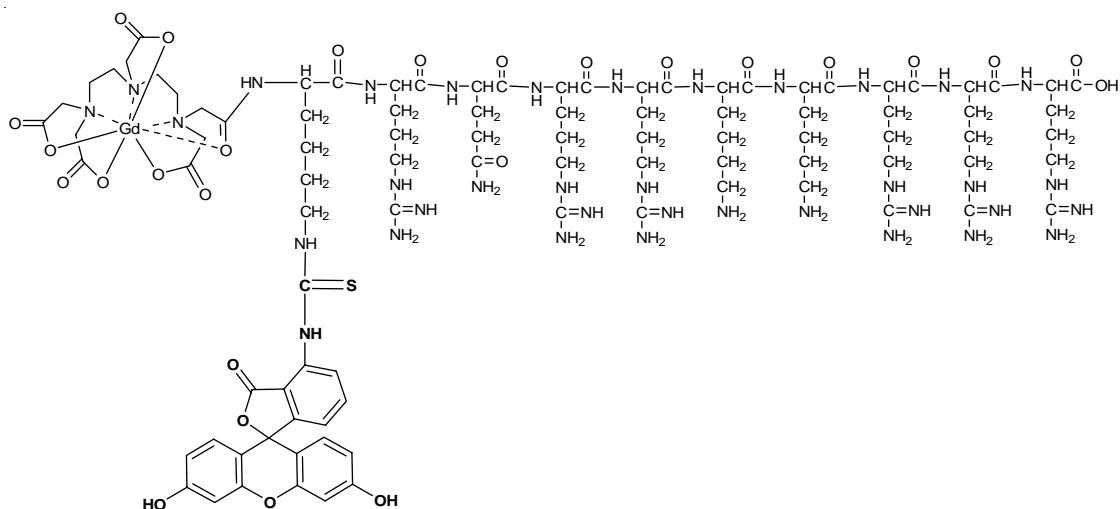


Figure 34. Chemical structure of Gd-DTPA-Lys(FITC)-L-Tat-OH (**1**)

4.2.2 Gd-DTPA-Lys(FITC)-D-Tat₅₇₋₄₉-OH (**2**)

2 was synthesized with the same synthesis scheme as **1**, substituting the L-form of amino acid residues to the D-form and reversing the amino acid sequence. Therefore the amino acid sequence in **2** is rrrqrrkkr. The ligand DTPA-Lys(FITC)-D-Tat₅₇₋₄₉-OH was characterized by ESI-MS. Detected molecular ions at $m/z = 1117.1 ((M+2H)^{2+})$, $745.3 ((M+3H)^{3+})$, $559.0 ((M+4H)^{4+})$, and $461.5 ((M+5H)^{5+})$ were consistent with the calculated mass of the desired product (2232.13).

After chelated with Gd^{3+} , the final product was characterized by ESI-MS also. Detected molecular ions at $m/z = 796.3 ((M+3H)^{3+})$, $597.4 ((M+4H)^{4+})$, $478.2 ((M+5H)^{5+})$, and $398.8 ((M+6H)^{6+})$ were consistent with the calculated mass of the desired product (2385.02) (Figure 35).

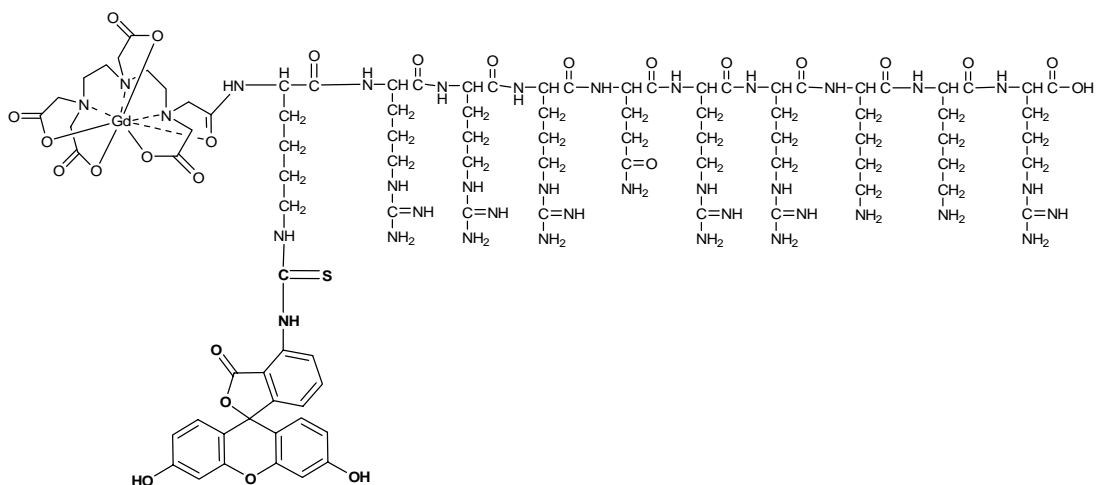


Figure 35. Chemical structure of Gd-DTPA-Lys(FITC)-D-Tat₅₇₋₄₉-OH (**2**)

4.2.3 Gd-DTPA-Lys(FITC)-Orn-D-Tat₅₇₋₄₉-OH (**3**)

3 was synthesized with the same synthesis scheme as **2**, substituting the amino acid residue Gln by Orn. Therefore the amino acid sequence in **3** is rrrorrkkrr. The ligand DTPA-Lys(FITC)-Orn-D-Tat₅₇₋₄₉-OH was characterized by ESI-MS. Detected molecular ions at $m/z = 740.4$ ($(M+3H)^{3+}$), 555.2 ($(M+4H)^{4+}$), and 444.6 ($(M+5H)^{5+}$) were consistent with the calculated mass of the desired product (2218.50).

After chelated with Gd^{3+} , the final product was characterized by ESI-MS also. Detected molecular ions at $m/z = 791.5$ ($(M+3H)^{3+}$), 593.9 ($(M+4H)^{4+}$), 475.3 ($(M+5H)^{5+}$), and 396.2 ($(M+6H)^{6+}$) were consistent with the calculated mass of the desired product (2371.04) (Figure 36).

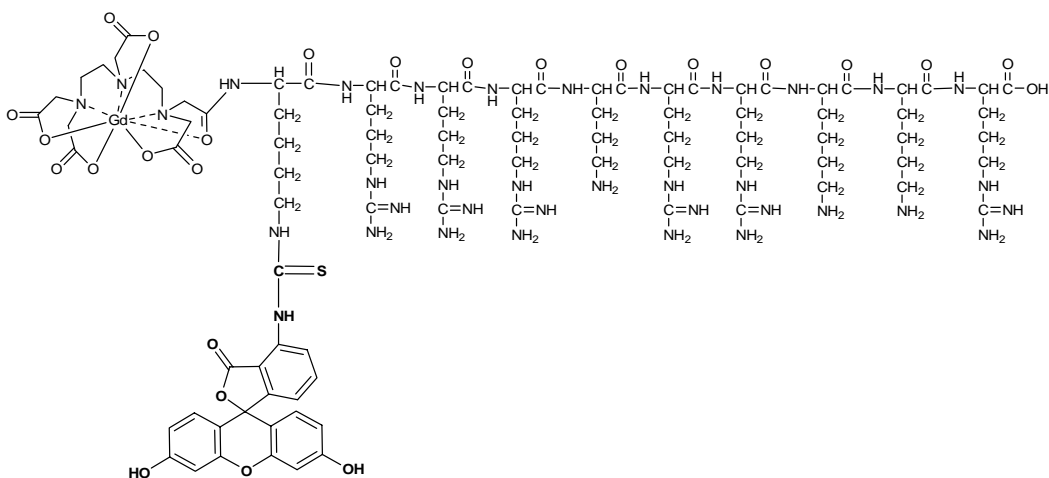


Figure 36. Chemical structure of Gd-DTPA-Lys(FITC)-Orn-D-Tat₅₇₋₄₉-OH (**3**)

4.2.4 Gd-DTPA-Lys(FITC)-NLS-OH (4)

4 was synthesized with the same synthesis scheme as **1**. The amino acid sequence in **4** is PKKKRKV. The ligand DTPA-Lys(FITC)-NLS-OH was characterized by ESI-MS. Detected molecular ions at $m/z = 889.1 ((M+2H)^{2+})$, $592.9 ((M+3H)^{3+})$, and $445.2((M+4H)^{4+})$ were consistent with the calculated mass of the desired product (1776.02).

After chelated with Gd^{3+} , the final product was characterized by ESI-MS also. Detected molecular ions at $m/z = 964.4((M+2H)^{2+})$, $643.8 ((M+3H)^{3+})$, and $483.0 ((M+4H)^{4+})$ were consistent with the calculated mass of the desired product (1928.76) (Figure 37).

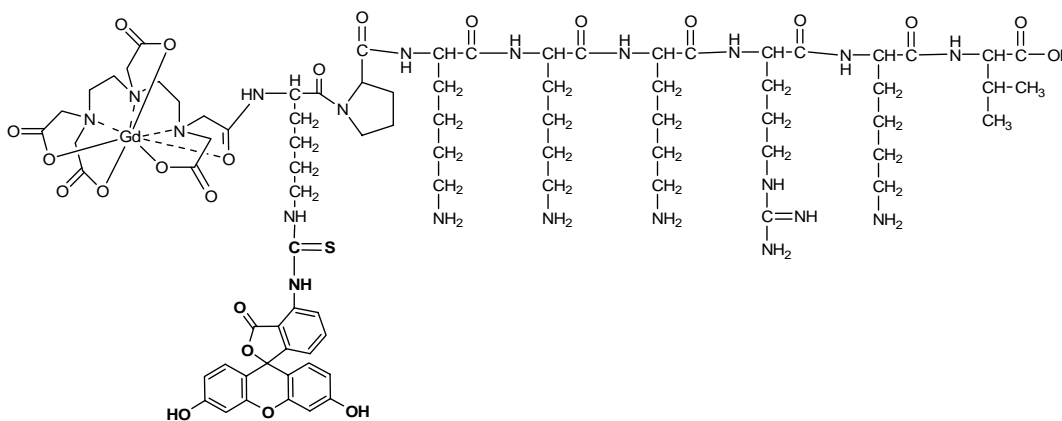


Figure 37. Chemical structure of Gd-DTPA-Lys(FITC)-NLS-OH (**4**)

4.2.5 Gd-DTPA-Lys(FITC)-PTD-4-OH (5)

5 was synthesized with the same synthesis scheme as **1**. The amino acid sequence in **5** is YARAAARQARA. The ligand DTPA-Lys(FITC)-PTD-4-OH was characterized by ESI-MS. Detected molecular ions at $m/z = 1049.6 ((M+2H)^{2+})$, $700.2 ((M+3H)^{3+})$, $525.3 ((M+4H)^{4+})$, and $420.4 ((M+5H)^{5+})$ were consistent with the calculated mass of the desired product (2097.23).

After chelated with Gd^{3+} , the final product was characterized by ESI-MS also. Detected molecular ions at $m/z = 750.8 ((M+3H)^{3+})$, $563.3 ((M+4H)^{4+})$ and $450.8 ((M+5H)^{5+})$, were consistent with the calculated mass of the desired product (2249.81) (Figure 38).

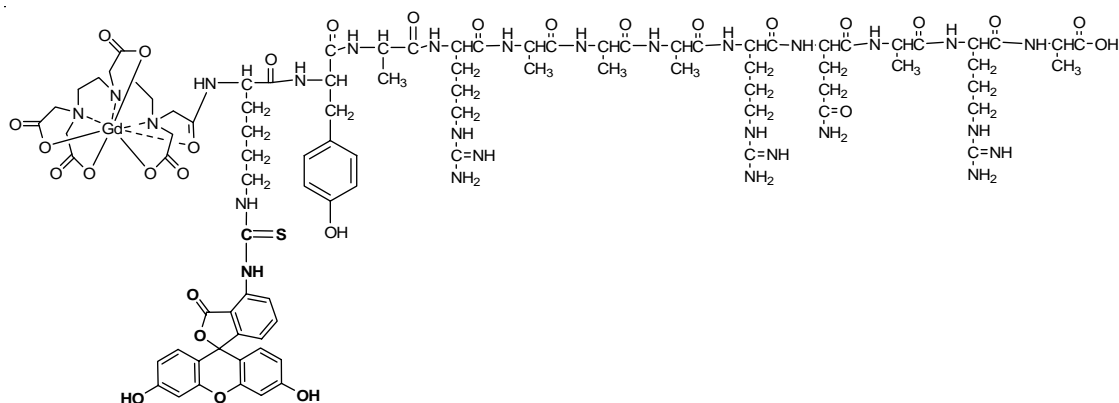


Figure 38. Chemical structure of Gd-DTPA-Lys(FITC)-PTD-4-OH (5)

4.2.6 Synthesis of 4,7,10-tricarboxymethyl-*tert*-butyl ester 1,4,7,10-tetraaza cyclododecane-1-acetate (DOTA-(*t*Bu)₃)

Please see reference (98) for the details of synthesis DOTA-(*t*Bu)₃. In brief:

- (1) 1,4,7,10-tetraazacyclododecane-1-carboxymethyl-benzylester (**D1**): To a stirred solution of 1,4,7,10-tetraazacyclododecane (cyclen) in acetonitrile was added dropwise benzyl bromoacetate (0.5eq.) in acetonitrile. Reaction completed at room temperature for 2h.
- (2) 1,4,7,10-tetraazacyclododecane-4,7,10-tricarboxymethyl-*tert*-butylester-1-carboxymethyl-benzylester (**D2**): To a stirred solution of **D1** in acetonitrile K₂CO₃ (4eq.) was added followed by the dropwise addition of *tert*-butyl bromoacetate (4eq.) in acetonitrile within 30 min. Reaction completed at room temperature for 48 h.
- (3) 4,7,10-tricarboxymethyl-*tert*-butyl ester 1,4,7,10-tetraazacyclododecane-1-acetate (**D3**): Pd/C (10% Pd) was added to a solution of **D2** in MeOH, and hydrogenation was conducted for 4h at normal pressure. The catalyst was removed by filtration through Celite. The solvent was removed by a rotary evaporator. The resulting yellowish oil was purified by column chromatography (silica gel, 10% MeOH in DCM) to afford the product **D3**. ESI-MS (+): calcd C₂₈H₅₂N₄O₈; m/z 572.38; found 573.3 (M+H)⁺; 595.3 (M+Na)⁺.

4.2.7 Gd-DOTA-Lys(FITC)-L-Tat₄₉₋₅₇-OH (6)

L-Tat₄₉₋₅₇ peptide was synthesized as described above. Then the resin-bound peptide was deprotected with piperidine, and coupled with one Fmoc-Lys(Dde)-OH residue. After deprotection with piperidine, DOTA tris(*tert*-butyl) ester was coupled on the α -NH₂ group of Lys (coupling condition: DOTA-(*t*Bu)₃ : HATU : DIEA = 4: 3.6: 8). The resin was drained and rinsed four times with DMF. The resin-bound DTPA-Lys(Dde)-Tat was treated twice with hydrazine hydrate (2% in DMF, 2 min) to remove the Dde group. Then FITC was reacted with the ϵ -NH₂ group of Lys (resin:FITC:DIEA= 1:4:8) within 7 hours. Further procedures including the cleavage, HPLC analysis and purification are progressed the same as for (1). The ligand DOTA-Lys(FITC)-L-Tat₅₇₋₄₉-OH was characterized by ESI-MS. Detected molecular ions at $m/z = 748.6 ((M+3H)^{3+})$, 561.9 $((M+4H)^{4+})$, 449.8 $((M+5H)^{5+})$, and 374.9 $((M+6H)^{6+})$ were consistent with the calculated mass of the desired product (2244.56).

The ligand DOTA-Lys(FITC)-L-Tat₅₇₋₄₉-OH was dissolved in 5 mL H₂O, one equivalent of GdCl₃.6H₂O was added, and the pH was adjusted to 6.5 with 1N NaOH. The reaction mixture was stirred at 60°C for 12 h. The pH was periodically checked and adjusted to 6.0-7.0 using a solution of 1N NaOH and 1N HCl as needed. The mixtures were purified first by HPLC using a water (0.05% TFA) (solvent A)/ACN (0.05% TFA) (solvent B) gradient to separate the unstable bound Gd³⁺. Afterwards, the product was dialyzed (Float-A-Lyzer, cellulose ester membranes, MWCO: 1,000; Spectrum Laboratories, Inc.) to remove inorganic impurities. The solution was lyophilized and yellow to orange solids were obtained. The absence of free Gd³⁺ was checked with xylenol orange indicator. After chelated with Gd³⁺, the final product was characterized by ESI-MS. Detected molecular ions at $m/z = 800.1((M+3H)^{3+})$, 600.3 $((M+4H)^{4+})$, 480.6 $((M+5H)^{5+})$, and 400.4 $((M+6H)^{6+})$ were consistent with the calculated mass of the desired product (2397.08) (Figure 39).

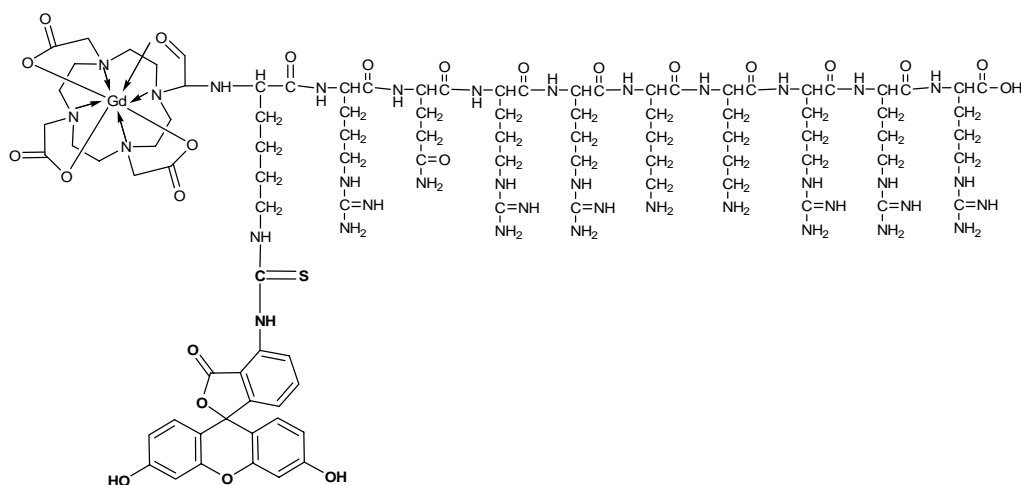


Figure 39. Chemical structure of Gd-DOTA-Lys(FITC)-L-Tat₅₇₋₄₉-OH (**6**)

4.2.8 Gd-DOTA-Lys(FITC)-D-Tat₅₇₋₄₉-OH (**7**)

7 was synthesized with the same synthesis scheme as **6**, substituting the L-form of amino acid residues by the D-form and reversed the amino acid sequence. Therefore the amino acid sequence in **7** is rrrqrrkkr. The ligand DOTA-Lys(FITC)-D-Tat₅₇₋₄₉-OH was characterized by ESI-MS. Detected molecular ions at $m/z = 748.6 ((M+3H)^{3+})$, $561.9 ((M+4H)^{4+})$, $449.8 ((M+5H)^{5+})$, and $374.9 ((M+6H)^{6+})$ were consistent with the calculated mass of the desired product (2244.56). After chelated with Gd^{3+} , the final product was characterized by ESI-MS also. Detected molecular ions at $m/z = 800.7((M+3H)^{3+})$, $600.4 ((M+4H)^{4+})$, $480.5 ((M+5H)^{5+})$, and $399.3 ((M+6H)^{6+})$ were consistent with the calculated mass of the desired product (2397.08) (Figure 40).

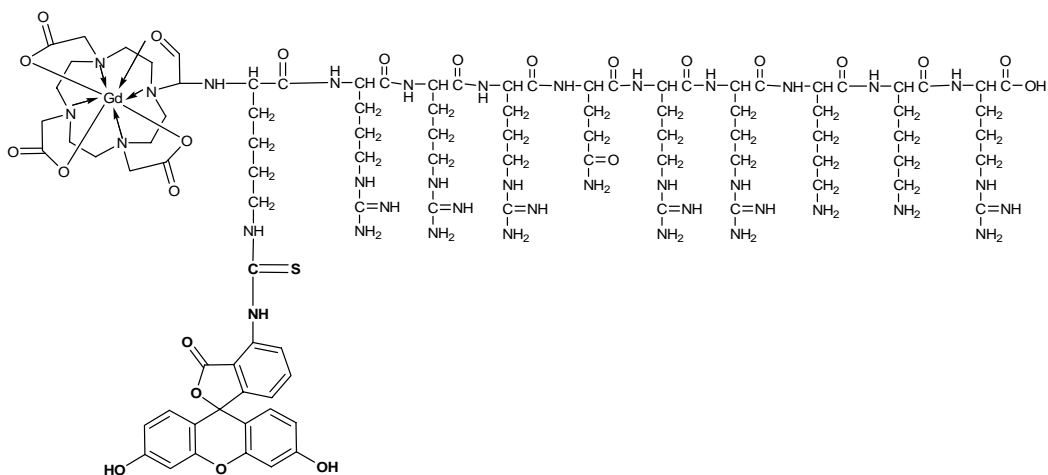


Figure 40. Chemical structure of Gd-DOTA-Lys(FITC)-D-Tat₅₇₋₄₉-OH (**7**)

4.2.9 Gd-DOTA-Lys(FITC)-Orn-D-Tat₅₇₋₄₉-OH (**8**)

8 was synthesized with the same synthesis scheme as **7**, substituting the amino acid residue Gln by Orn. Therefore the amino sequence in **8** is rrrorrkk_r. The ligand DOTA-Lys(FITC)-Orn-D-Tat₅₇₋₄₉-OH was characterized by ESI-MS. Detected molecular ions at $m/z = 744.3 ((M+3H)^{3+})$, $558.3 ((M+4H)^{4+})$, and $447.0 ((M+5H)^{5+})$ were consistent with the calculated mass of the desired product (2229.21). After chelated with Gd^{3+} , the final product was also characterized by ESI-MS. Detected molecular ions at $m/z = 796.2((M+3H)^{3+})$, $596.5 ((M+4H)^{4+})$, $477.7 ((M+5H)^{5+})$, and $398.4 ((M+6H)^{6+})$ were consistent with the calculated mass of the desired product (2383.10) (Figure 41).

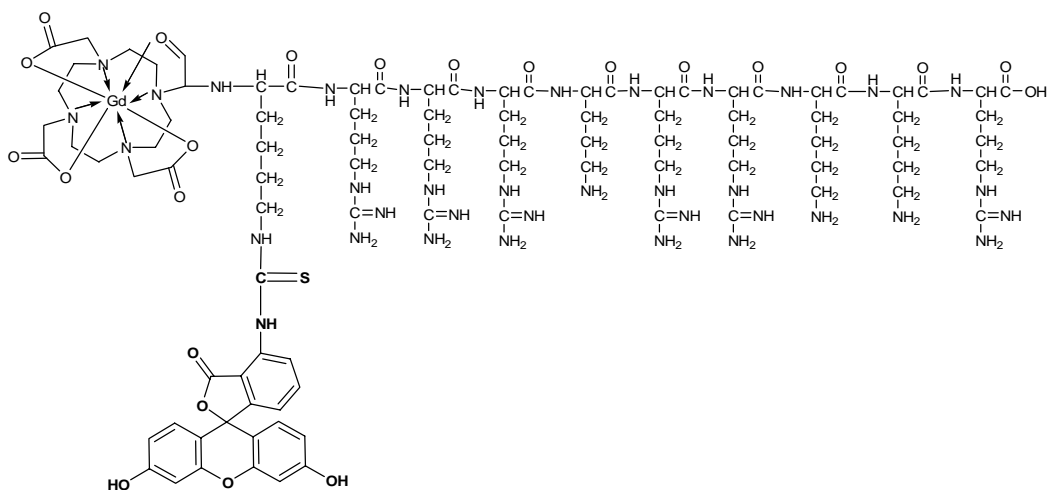


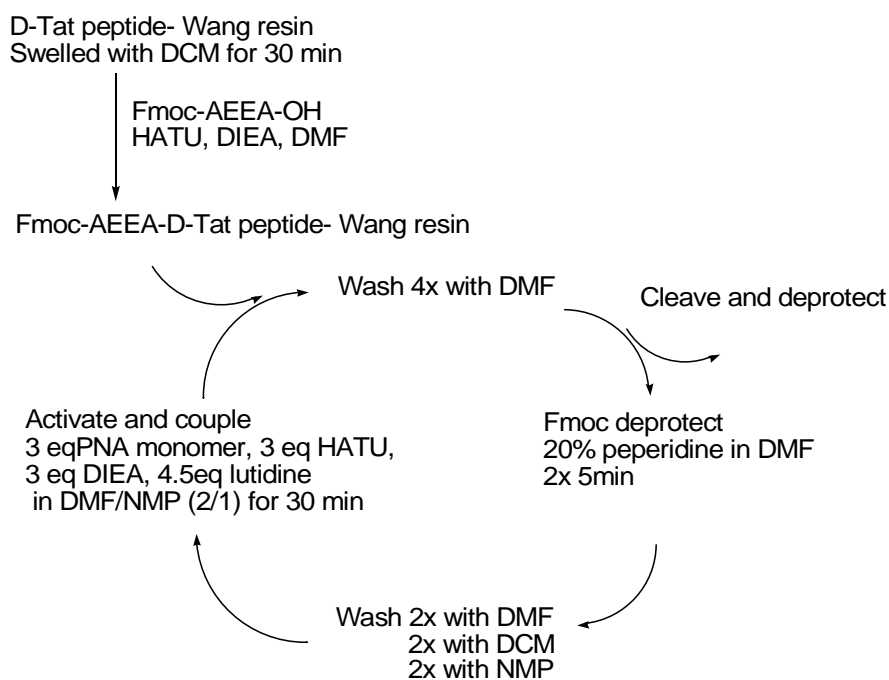
Figure 41. Chemical structure of Gd-DOTA-Lys(FITC)-Orn-D-Tat₅₇₋₄₉-OH (**8**)

4.3 Synthesis of PNA-CPP conjugated MR contrast agents

4.3.1 PNA synthesis

Syntheses of dsRed-PNA (tcc g_tg aac ggc) and nonsense PNA (g_tt cag agt cta) were performed in continuous solid phase synthesis after coupling of an AEEA spacer to the D-Tat₅₇₋₄₉ bound on Wang resin (Scheme-4). The synthesis protocol of D-Tat₅₇₋₄₉ and coupling of AEEA spacer is the same as peptide synthesis. Fmoc/Bhoc chemistry was used with the following PNA monomers: Fmoc-A(Bhoc)-OH, Fmoc-C(Bhoc)-OH, Fmoc-G(Bhoc)-OH, and Fmoc-T-OH. Each cycle of elongation consisted of (1) Fmoc deprotection with 20% piperidine in DMF for 2 cycles of 5 min at room temperature, (2) washing with DMF, DCM, and twice with NMP for 1min each at room temperature, (3)

coupling using a molar ratio of resin/monomer/HATU/DIEA/2,6-lutidine = 1.0:3.0:2.7:3.0:4.5; 3 min on preactivation followed by 30 min coupling at room temperature, (4) capping with 2 mL of 5% acetic anhydride/6% 2,6-lutidine in DMF for 5 min at room temperature, and (5) washing with NMP, DCM, and twice with DMF for 1 min each at room temperature. All chemical steps were followed by a Kaiser test on the resin, and the resulting colorimetric reaction indicated the presence of free primary amines after Fmoc deprotection and the absence of primary amines after the coupling and capping steps. After 3, 6, 9, and 12 cycles, aliquots of the resin-bound PNAs were cleaved and Bhoc-deprotected with H₂O/TIS/m-Cresol/ TFA (2.5:2.5:5:90) for 4 h, and ESI-MS analysis was performed to confirm that the observed masses were consistent with the calculated molecular weights of the Fmoc-protected intermediates.



Scheme-4. PNA synthesis cycle

4.3.2 Conjugate DOTA tris(*tert*-butyl) ester (DOTA-(tBu)₃) with PNA-CPP conjugates

The resin-bound PNA-CPP conjugates were deprotected with 20% piperidine in DMF, and coupled with one Fmoc-Lys(Dde)-OH residue. After Fmoc deprotection with piperidine, DOTA tris(*tert*-butyl) ester was coupled on the α -NH₂ group of Lys.

4.3.3 Labeling PNA-CPP conjugate with FITC

The resin-bound DOTA-(tBu)₃-Lys(Dde)-PNA was treated with hydrazine hydrate (2% in DMF, 2 min) to remove the Dde group. Then FITC was reacted with the ϵ -NH₂ group of Lys (resin:FITC:DIEA= 1:4:8) within 12 hours.

The PNA-peptide conjugates were cleaved off the resin using TFA/m-Cresol/TIS/H₂O (90:5:2.5:2.5, v/v/v). Crude products were precipitated by adding cold diethyl ether. The precipitated product was collected by centrifugation and re-suspended in cold diethyl ether. After purified by semi-preparative reversed-phase HPLC, the products were lyophilized to give yellow powders. The products were characterized by ESI-MS: for anti-dsRed PNA conjugate, detected molecular ions at $m/z = 1126.3 ((M+5H)^{5+})$, $938.9 ((M+6H)^{6+})$, $805.0 ((M+7H)^{7+})$, and $704.3 ((M+8H)^{8+})$ were consistent with the calculated mass of the desired product (5628.2). For nonsense PNA conjugate, detected molecular ions at $m/z = 1129.1 ((M+5H)^{5+})$, $941.1 ((M+6H)^{6+})$, $806.9((M+7H)^{7+})$, and $706.1 ((M+8H)^{8+})$ were consistent with the calculated mass of the desired product (5642.4).

4.3.4 Chelating with gadolinium

The PNA-CPP conjugated ligand was dissolved in 5 mL H₂O, one equivalent of GdCl₃.6H₂O was added, and the pH was adjusted to 6.5 with 1N Na₂CO₃. The reaction mixture was stirred at 60°C for 12 h. The pH was periodically checked and adjusted to 6.0-7.0 using a solution of 1N Na₂CO₃ and 1N HCl as needed. The mixtures were purified first by HPLC using a water (0.05% TFA) (solvent A)/ACN (0.05% TFA) (solvent B) gradient to separate the unstable bound Gd³⁺. Afterwards, the reaction mixture was dialyzed (Float-A-Lyzer, cellulose ester membranes, MWCO: 2,000; Spectrum Laboratories, Inc.) to remove other impurities. The solution was lyophilized and yellow to orange solids were obtained. The absence of free Gd³⁺ was checked with

xylenol orange indicator and by a MR based competitive ligand assay with DTPA. The complexes were characterized by ESI-MS: From anti-dsRed PNA complex, detected molecular ions at $m/z = 964.7 ((M+6H)^{6+})$, $826.9 ((M+7H)^{7+})$, $723.8 ((M+8H)^{8+})$, and $643.1 ((M+9H)^{9+})$ were consistent with the calculated mass of the desired product (5782.4) (dsRed CA). For nonsense PNA complex, detected molecular ions at $m/z = 1159.7 ((M+5H)^{5+})$, $966.7 ((M+6H)^{6+})$, $829.1((M+7H)^{7+})$, and $725.7 ((M+8H)^{8+})$ were consistent with the calculated mass of the desired product (5796.6; nonsense CA). These mass spectra demonstrated that the PNA-CPP conjugates were successfully chelated with gadolinium.

4.4 Cellular uptake assay

Experiments on cells were done in 96 well microplates by inoculation of NIH/3T3 mouse embryonic fibroblasts (1×10^4 cells/well) cultured in Dulbecco's Modified Eagle's Medium (DMEM) supplemented with 10% fetal bovine serum, 4 mM L-glutamine, 100 $\mu\text{g}/\text{mL}$ streptomycin and 100 U/mL penicillin (all purchased from Biochrom AG, Germany). After 24 h, cells were incubated with various concentrations of MR contrast agents for additional 18 h. Cells were washed with Hanks' balanced salt solution (HBSS; Biochrom AG, Germany) and extracellular fluorescence was quenched by incubating with cold trypan blue (0.05% in PBS) for 3 min followed by repeated washes with HBSS. Cell-related FITC fluorescence (Ex 485 nm/Em 530 nm) was evaluated in a multiplate reader (BMG Labtech, Germany). Subsequently, fluorescence microscopy was performed with the same cells on a Zeiss Axiovert 200 M (Germany), to observe the cellular localization (Figure 42). Instead of the first washing, cells could be incubated with Bisbenzimid 33342 (Hoechst 33342), a nuclear stain, for 30 min prior to trypan blue quenching. This can be used as counterstaining of the cell nuclei as well as for the evaluation of cytotoxicity, since the fluorescence (Ex 360 nm/Em 485 nm) is proportional to the cell number.

In some of the first experiments, evaluation of cytotoxicity was done by addition of propidium iodide (PI) and a detergent with subsequent fluorescent reading (Ex 530 nm/Em 645 nm). By combination of the two fluorescence readings FITC and Hoechst or PI, a correlation is established between the FITC fluorescence and the total cell number per well. Both methods have given quantitatively the same results, only that the absolute

Chapter 4. Experimental

values of the corrected FITC fluorescence are lower in the case of PI (see Figure 22/24). Experiments were run at least three times for each concentration with six replicates. Statistical analysis was performed by Student's *t*-test or ANOVA with Dunnett's post test. P values < 0.05 were considered significant.

Experimental protocol on mouse fibrosarcoma cell line expressing dsRed gene was similar to that of NIH/3T3 mouse embryonic fibroblasts. But the culture medium of dsRed cell line was changed to NCTC135 supplemented with 10% DonorHouse serum instead of DMEM culture medium supplemented with 10% fetal bovine serum for NIH/3T3 cell line.

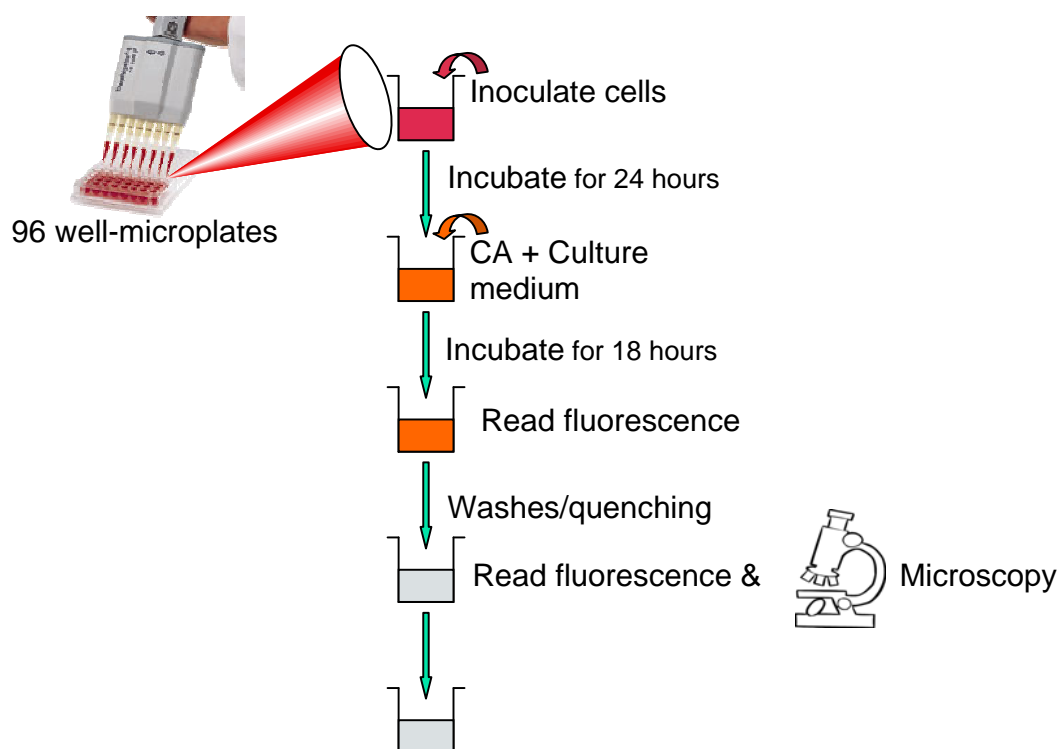


Figure 42. Experimental protocol for fluorescence studies

4.5 Determination of intracellular Gd^{3+} content

Exponentially growing 3T3 cells were labeled with 0.1 – 2.5 μ M PNA-CPP-CA in 175 cm^2 tissue culture flasks for 18 h. After repeated washes with Hanks' buffered saline, cells were trypsinized, centrifuged and re-suspended in 1.5 mL Eppendorf tubes at 1×10^7 cells in 500 μ L complete DMEM. 500 μ L of 37% HCl was added and left at 120°C

overnight to lyse the cells completely. Upon this treatment all Gd(III) was solubilized as free aquo-ion. By measuring the relaxation rates of these solutions at 300 MHz, it is possible to determine its concentration according to the literature (32). To prepare standard samples in aqueous HCl solution: different concentrations of GdCl₃ prepared in 500 µL distilled water at first. And then 500 µL of 12M HCl was added. The resulting GdCl₃ in 6M HCl solution was heated at 120°C overnight. To prepare standard samples in medium with Cells: different concentrations of GdCl₃ prepared with 1×10^7 cells in 500 µL complete DMEM. 500 µL of 12M HCl was added and left at 120°C overnight to lyse the cells completely. Standard curves were acquired by taking the slope of a plot of the R₁ relaxation rate versus concentration of Gd(III).

4.6 In vitro test of antisense PNA hybridizing with target sequence

The target oligo-DNA sequence (5'-CTC GAA CTC GTG GCC CAC GGA GCC CTC CAT GCG CAC CTT GAA GCG CAT GAA CTC CTT GAT-3'), synthesized from MWG-Biotech AG, was amino-modified with a C12 linker at the 5' end. According to the DNA-BINDTM application guide, the oligo-DNA was coupled to DNA-BINDTM 96-well plate (10mM phosphate buffer, pH 8.5, at 4°C, overnight). Different concentrations of dsRed CA and nonsense CA were prepared in hybridizing buffer (10mM phosphate buffer, pH6.5). The contrast agents were co-incubated with immobilized DNA at 37°C for 1h, and then at room temperature overnight. Non-binding contrast agent was washed out with 10mM phosphate buffer, the content of hybrid contrast agents were determined by ELISA measurement, according to the procedures described in literature (86).

4.7 In vitro MR studies

For MR imaging of cells, exponentially growing 3T3 cells were labeled with 0.1 – 2.5 µM PNA-CA in 175 cm² tissue culture flasks for 18 h. After repeated washes with Hanks' buffered saline, cells were trypsinized, centrifuged and re-suspended in 1.5 mL Eppendorf tubes at 1×10^7 cells in 500 µL complete DMEM. Cells were allowed to settle before making MR measurements. Tubes with medium only, cells without MR contrast agent, and cells re-suspended in medium containing the extracellular contrast agent Magnevist[®] (Schering, Germany) at 50 µM served as controls.

Chapter 4. Experimental

MR imaging of the cell pellets was performed at 300 MHz using T_1 - and T_2 -weighted spin-echo sequences at room temperature ($\sim 21^\circ\text{C}$).

The axial slice of interest was positioned through the cell pellet. Experimental parameters for T_1 were: field of view $17 \times 6.9 \text{ cm}^2$, matrix 512×256 , slice thickness 1.5 mm, SW 70 kHz, TE 14.6 ms, TR 70-7000 ms, 2 averages (logarithmic time steps, 80 images). For T_2 , similar parameters were used, but TR = 10 s and TE = 15-600 ms (linear time steps, 40 echoes). Sagittal images were obtained with a field of view $14 \times 6.9 \text{ cm}^2$, matrix 256×256 , slice thickness 2 mm, SW 100 kHz, TE 9.2 ms, TR 1500 ms, 26 averages for T_1 weighted images, and a field of view $14 \times 6.9 \text{ cm}^2$, matrix 256×256 , slice thickness 2 mm, SW 100 kHz, TE 80 ms, TR 10000 ms, 6 averages for T_2 weighted images.

Relaxivity measurements of contrast agents were performed in the concentration range of 0 – 30 μM using the same experimental setup. CAs were diluted in water and 1ml aliquots were transferred to Eppendorf cups.

To examine the dependence of the relaxivity on the magnetic field strength, additional T_1 -measurements were performed at a frequency of 123 MHz and a magnetic field of 3 T. For these experiments, an inversion recovery sequence was used to obtain images from a 1 mm thick slice through the samples. The inversion time was varied from 23 ms to 3000 ms in about 12 steps. The images were read out with a turbo spin echo technique, acquiring 5 echoes per scan. The repetition time TR was 10 s to make ensure complete relaxation between the scans. A resolution of 256×256 voxels over a Field-of-view of $110 \times 110 \text{ mm}^2$ was reached. Six averages were acquired within less than 25 min.

4.8 Data analysis

The *fitting* to relaxivity curves was performed with self-written routines in MATLAB 6.5 R13 (The Mathworks Inc.). The series of T_1 and T_2 relaxation data were fitted to the following equations: a) T_1 series with varying $t = TR$: $S = S_0 (1 - a \times \exp(-t / T_1))$. b) T_2 series with varying $t = TE$: $S = S_0 \exp(-t / T_2) + b$. Nonlinear least-squares fitting of three parameters S_0 , T_1/T_2 , and a/b was done for each voxel with the Gauss-Newton method (MATLAB function `nlinfit`). For each fitted parameter, the 95% confidence intervals were calculated (MATLAB functions `nlparci`, `nlpredci`) and used as an error estimate of

the fitted relaxation times T_1/T_2 and S_0 (initial signal at $t = 0$). The fit procedure resulted in parameter maps of T_1 , T_2 , S_0 and corresponding error maps σ_{T1} , σ_{T2} , σ_{S0} .

Image-regions around the tubes were defined as Regions of Interest (ROIs), and the means and distribution width of the relaxation times of voxels in these regions were calculated: An *iterative* Gaussian fit was used to determine mean and standard deviation (SD) of a distribution with outliers. For this purpose, a distribution histogram was first fitted to a Gaussian to estimate mean and SD. The tails of the distribution were then discarded by using a threshold of three SDs. A repeated fit proved to be robust and converged to the 'true' Gaussian mean and width of the distribution barring the outliers, observed as a result of the non-linear fit of noisy voxels. The processing of the relaxation data thus resulted in specific $R_{1,2} = 1/T_{1,2}$ values for each tube sample including the standard deviation in the selected ROI ensemble. The ensemble error matched closely the errors of a single-voxel fit, which showed that no further systematic errors were introduced by the image encoding. Finally, the relaxivity $r_{1,2}$ was calculated from the slope of $R_{1,2}(c)$ versus the concentration c of the contrast agent by an error-weighted linear regression.

For the inversion recovery experiments at 3 T, the regions of interest were again defined inside the sample tubes. The values from all voxels inside each ROI were averaged; the resulting relaxation curves were used to fit the equation $M_0 \cdot (1 - 2 \cdot \exp(-T_I/T_1))$, using the nonlinear least squares technique implemented in MATLAB.

References

References

- 1) Weissleder R and Mahmood U. Molecular imaging. *Radiology*, **2001**; 219: 316-333.
- 2) Buxton RB. *Introduction to Functional Magnetic Resonance Imaging*; Cambridge University Press, **2002**
- 3) Johnson GA., Benveniste H, Black RD, et al. Histology by magnetic resonance microscopy. *Magn Reson Q.* **1993**; 9:1-30
- 4) Smith B. R., Johnson G. A., Groman E. V., Linney E. Magnetic resonance microscopy of mouse embryos. *Proc Natl Acad Sci USA*, **1994**; 91: 3530-3533.
- 5) Cassidy P. J. and Radda G. K. Molecular imaging perspectives. *J. R. Soc. Interface*, **2005**; 2: 133-144.
- 6) Saini S. Advances in contrast-enhanced MR imaging: Principles. *AJR*, **1991**; 156: 236-239.
- 7) Vlaardingerbroek M. T. and Boer J. A. J. *Magn. Res. Imaging. Theory and practice*. Springer Verlag, Germany, **1996**
- 8) Merbach A. E. and Toth E. *The chemistry of contrast agents in medical magnetic resonance imaging*. John Wiley & Sons, Ltd., New York, **2001**.
- 9) Lauffer RB. Paramagnetic metal complexes as water proton relaxation agents for NMR imaging: theory and design. *Chem. Rev.* **1987**; 87:901-927.
- 10) Caravan P., Ellison J. J., McMurry T. J., and Lauffer R. B. Gadolinium (III) chelates as MRI contrast agents: Structure, dynamics, and applications. *Chem. Rev.* **1999**, 99, 2293-2352.
- 11) Koenig SH, and Brown RD. Relaxometry of magnetic resonance imaging contrast agents. *Magn. Reson. Annu.* **1987**; 263-286.
- 12) Sherry AD, Cacheris WP, Kuan KT. Stability constants for Gd³⁺ binding to model DTPA-conjugates and DTPA-proteins: implications for their use as magnetic resonance contrast agents. *Magn Reson Med.* **1988**; 8:180-90.
- 13) Weissleder R., Elizondo G., Wittenberg J., et al. Ultrasmall superparamagnetic iron oxide: characterization of a new class of contrast agents for MR imaging. *Radiology*, **1990**, 175: 489-493.

- 14) Bulte J. W. M. and Kraitchman D. L. Iron oxide MR contrast agents for molecular and cellular imaging. *NMR in Biomed.* **2004**; 17: 484-499.
- 15) Brasch R. C. Li K. C. Husband J. E., et al. In vivo monitoring of tumor angiogenesis with MR imaging. *Acad Radiol.* **2000**, 7: 812-823.
- 16) Bremer C., Mustafa M., Bogdanov A. J., et al. Steady-state blood volume measurements in experimental tumors with different angiogenic burdens a study in mice. *Radiology*, **2003**; 226: 214-220.
- 17) Jacques V, Desreux JF. New classes of MRI contrast agents. *Top. Curr. Chem.* **2002**; **221**: 123-163.
- 18) Allen M. J. and Meade T. J. Magnetic resonance contrast agents for medical and molecular imaging. *Met Ions Biol Syst.* **2004**; 42: 1-38.
- 19) Bogdanov A., Matuszewske L., Bremer C., et al. Oligomerization of paramagnetic substrates results in signal amplification and can be used for MR imaging of molecular targets. *Mol. Imaging.* **2002**; 1: 16-23.
- 20) Louie A. Y., Huber M. M., Ahrens E. T., et al. In vivo visualization of gene expression using magnetic resonance imaging. *Nat. Biotechnol.* **2000**; 18: 321-325.
- 21) Aime S., Barge A., Castelli D. D., et al. Paramagnetic lanthanide(III) complexes as pH-sensitive chemical exchange saturation transfer (CEST) contrast agents for MRI applications. *Magn. Reson. Med.* **2002**; 47: 639-648.
- 22) Wickline S. A., and Lanza G. M. Molecular imaging, targeted therapeutics and nanoscience. *J Cell Biochem.* **2002**; 39(suppl): 90-97.
- 23) Lanza G. M., Yu X., Winter P. M., et al. Targeted antiproliferative drug delivery to vascular smooth muscle cells with a magnetic resonance imaging nanoparticle contrast agent: implications for rational therapy of restenosis. *Circulation*, **2002**; 106: 2842-2847.
- 24) Flacke S., Fischer S., Scott M. J., et al. Novel MRI contrast agent for molecular imaging of fibrin: implications for detecting vulnerable plaques. *Circulation.* **2001**; 104: 1280-1285.

References

- 25) Winter P. M., Morawski A. M., Caruthers S. D., et al. Molecular imaging of angiogenesis in early-stage atherosclerosis with alpha (v) beta3-integrin-targeted nanoparticles. *Circulation*. **2003**; 108: 2270-2274.
- 26) Artemov D., Mori N., Ravi R., Bhujwala Z. M. Magnetic resonance molecular imaging of the HER-2/neu receptor. *Cancer Res*. **2003**; 63: 2723-2727.
- 27) Artemov D., Mori N., Okollie B., Bhujwala Z. M. MR molecular imaging of the Her-2/neu receptor in breast cancer cells using targeted iron oxide nanoparticles. *Magn Reson. Med*. **2003**; 49: 403-408.
- 28) Aime S., Cabella B. C., Crich S. G., and Gianolio E. Targeting cells with MR imaging probes based on paramagnetic Gd (III) chelates. *Current Pharmaceutical Biotechnology*, **2004**; 5: 509-518.
- 29) Walczak P, Kedziorek DA, Gilad AA, et al. Instant MR labeling of stem cells using magnetoelectroporation. *Magn. Reson. Med*. **2005**; 54: 769-774.
- 30) Crich SG, Lanzardo S, Barge A, et al. Visualization through magnetic resonance imaging of DNA internalized following in vivo electroporation. *Mol Imaging*. **2005**; 4: 7-17.
- 31) Tokumitsu H., Hiratsuka J., Sakurai Y., et al. Gadolinium neutron-capture therapy using novel gadopentetic acid-chitosan complex nanoparticles: in vivo growth suppression of experimental melanoma solid tumor. *Cancer letters*. **2000** ; 150: 177-182.
- 32) Cabella C., Crich S. G., Corpillo D., et al. Cellular labeling with Gd(III) chelates: only high thermodynamic stabilities prevent the cells acting as sponges' of Gd³⁺ ions. *Contrast Med. Mol. Imaging*, **2006**; 1: 23-29.
- 33) Wiener E. C., Konda S., Shadron A., et al. Targeting dendrimer-chelates to tumors and tumor cells expressing the high-affinity folate receptor. *Invest Radiol*. **1997**; 32 (12): 748-54.
- 34) Lewin M., Clement O., Belguise-Valladier P., et al. Hepatocyte targeting with Gd-EOB-DTPA: potential application for gene therapy. *Invest Radiol*. **2001**; 36: 9-14.

- 35) Fischer P. M. Cellular uptake mechanisms and potential therapeutic utility of peptidic cell delivery vectors: progress 2001-2006. *Medicinal Research Reviews*. **2006**; 3: 1-41.
- 36) Zorko M, Langel U. Cell-penetrating peptides: mechanism and kinetics of cargo delivery. *Advanced Drug Delivery Reviews*. **2005**; 57: 529-545.
- 37) Fischer R, Fotin-Mleczek M, Hufnagel H, and Brock R. Break on through to the other side—biophysics and cell biology shed light on cell-penetrating peptides. *Chembiochem*. **2005**, 6: 2126-2142.
- 38) Derossi D., Calvet S., Brunissen A., et al. Cell internalization of the third helix of the Antennapedia homeodomain is receptor-independent. *J Biol. Chem*. **1996**; 271: 18188-18193.
- 39) Wender P., Mitchell D., Pattabiraman K., et al. The design, synthesis, and evaluation of molecules that enable or enhance cellular uptake: peptoid molecular transporters. *Proc Natl Acad Sci USA*. **2000**; 97: 13003-13008.
- 40) Wender P., Rothbard J., Jessop T., et al. Oligocarbamate molecular transporters: Design, synthesis, and biological evaluation of a new class of transporters for drug delivery. *J Am Chem Soc*. **2002**; 124: 13382-13383.
- 41) Elliot G., O'Hare P. Intercellular trafficking and protein delivery by a Herpesvirus structural protein. *Cell*. **1997**; 88: 223-233.
- 42) Kubota S., Siomi H., Satoh T., et al. Functional similarity of HIV-1 rev and HTLV-1 rex protein. *Biochem Biophys Res Commun*. **1989**; 162: 963-970.
- 43) Fawell S, Seery J., Daikh Y., et al. Tat-mediated delivery of heterologous proteins into cells. *Proc Natl Acad Sci USA*. **1994**; 91: 664-668.
- 44) Liu S, Edwards D. ^{99m}Tc-labeled small peptides as diagnostic radiopharmaceuticals. *Chem. Rev*. **1999**; 99: 2235-3368.
- 45) Bhorade R, Weissleder R, Nakakoshi T, Moore A, and Tung CH. Macrocyclic chelators with paramagnetic cations are internalized into mammalian cells via a HIV-Tat derived membrane translocation peptide. *Bioconjugate. Chem*. **2000**; 11: 301-305.
- 46) Allen MJ, MacRenaris KW, Venkatasubramanian PN, Meade TJ. Cellular delivery of MRI contrast agents. *Chem Biol*. **2004**; 11: 301-307.

References

- 47) Endres PJ, MacRenaris KW, Vogt S, et al. Quantitative imaging of cell-permeable magnetic resonance contrast agents using X-ray Fluorescence. *Molecular Imaging*. **2006**; 5: 485-497.
- 48) Lewin M, MCarlesso N, Tung C, et al. Tat peptide-derivatized magnetic nanoparticles allow in vivo tracking and recovery of progenitor cells. *Nat Biotechnol*. **2000**; 18: 410-414.
- 49) Weissleder R, Moore A, Mahmood U, et al. In vivo magnetic resonance imaging of transgene expression. *Nat Med*. **2000**; 6(3): 351-5.
- 50) Blasberg R. Imaging gene expression and endogenous molecular processes: Molecular imaging. *J Cereb. Blood Flow Metab*. **2002**, 22: 1157-1146.
- 51) Belikova AM, et al. Synthesis of ribonucleosides and diribonucleoside phosphates containing 2-chloroethylamine and nitrogen mustard residues. *Tetrahedron Lett*. **1967**, 37: 3557-3562.
- 52) Crooke ST. Molecular mechanisms of action of antisense drugs. *Biochim Biophys. Acta*. **1999**; 1489: 31-44.
- 53) Dewanjee MK, et al. Non invasive imaging of c-myc oncogene messenger RNA with indium-111-antisense probes in a mammary tumor-bearing mouse model. *J. Nucl. Med*. **1994**, 35: 1054-1063.
- 54) Lewis, M.R. and Jia, F. Antisense imaging: and miles to go before we sleep? *J. Cell. Biochem*. **2003**, 90: 464-472
- 55) Miller PS. Development of antisense and antigene oligonucleotide analogs. In: Cohn WE, Moldave K, editors. *Nucleic acid research and molecular biology*, **1996**, 52: 261-291.
- 56) Nielsen PE, et al. PNA hybridizes to complementary oligonucleotides obeying the Watson-crick Hydrogen-bonding rules. *Nature*, **1993**, 365: 566-568.
- 57) Summerton J, Weller D. Morpholino antisense oligomers: Design, preparation, and properties. *Antisense Nucleic Acid Drug Dev*. **1997**, 7: 187-195.
- 58) Efimov VA, et al. Synthesis of polyacrylamides N-substituted with PNA-like oligonucleotide mimics for molecular diagnostic applications. *Nucleic Acids Res*. **1999**, 27: 4416-4426.

- 59) Nielsen PE. Applications of peptide nucleic acids. *Curr. Opin. Biotechnol.* **1999**, 1071-75.
- 60) Nielsen, P.E. Cellular delivery of peptide nucleic acid (PNA). *Advanced Drug Delivery Reviews.* **2003**, 55, 267-280.
- 61) Pardridge, M. et al. Antisense imaging of gene expression in the brain in vivo. *PNAS*, **2000**, 97, 26: 14709-14714
- 62) Tian X., Aruva MR, Qin W, Zhu W, Sauter ER, Thakur ML, and Wickstrom E. Noninvasive molecular imaging of MYC mRNA expression in human breast cancer xenografts with a [(99m)Tc] peptide-peptide nucleic acid-peptide chimera. *Bioconjugate Chem.* **2005**; 16: 70-79.
- 63) Weissleder, R. et al. Molecular imaging of gene therapy for cancer. *Gene therapy*, **2004**, 11: 1175-1187.
- 64) Heckl, S. et al. Intracellular visualization of prostate cancer using magnetic resonance imaging. *Cancer Research*, **2003**, 63: 4766-4722.
- 65) Venkatesan N and Kim BH. Peptide conjugates of oligonucleotides: synthesis and applications. *Chem. Rev.* 2006; 106: 3712-3761.
- 66) Koppelhus U, awasthi SK, Zachar V, Host HU, Nielsen PE. Cell-dependent differential cellular uptake of PNA, peptides and PNA-peptide conjugates. *Antisense Nucleic Acid Drug Dev.* **2002**, 12, 51-63.
- 67) Kilk K and Langel U. Cellular delivery of peptide nucleic acid by cell-penetrating peptides. *Methods in Molecular Biology.* **2006**; 298: 131-141.
- 68) Koning MC, Marel GA and Overhand M. Synthetic developments towards PNA-peptide conjugates. *Curr. Opin. Chem. Biol.* **2003**; 7: 764-740.
- 69) Juliano, R.L. et al. Conjugates of antisense oligonucleotides with the Tat and antennapedia cell-penetrating peptides: Effects on cellular uptake, binding to target sequences, and biologic actions. *Pharmaceutical Research*, **2002**, 19: 744-754
- 70) Andreu D, Albericio F, Sole NA, et al. *Formation of disulfide bonds in synthetic peptides and proteins. Peptide synthesis protocols.* Humana Press Inc;USA. **1994**; 91-169.

References

- 71) Zhang X, Ishihara T, Corey DR. Strand invasion by mixed base PNAs and a PNA-peptide chimera. *Nucleic Acids Res.* **2000**; 28: 3332-3338.
- 72) Good L, Awasthi SK, Dryselius R, et al. Bactericidal antisense effects of peptide-PNA conjugates. *Nat Biotechnol.* **2001**; 19: 360-364.
- 73) Neuner P, Gallo P, Orsatti L, et al. An efficient and versatile synthesis of bisPNA-peptide conjugates based on chemoselective oxime formation. *Bioconj. Chem.* **2003**; 14: 276-281.
- 74) De Koning MC, Filippov DV, Meeuwenoord N, et al. Synthesis of a PNA-peptide conjugate by chemical ligation. *Synlett.* **2001**; 10: 1516-1518.
- 75) Dawson PE, Muir TW, Clark-Lewis I, Kent SB. Synthesis of proteins by native chemical ligation. *Science* **1994**; 266: 776-779.
- 76) Bendifallah N, Rasmussen FW, Zachar V, et al. Evaluation of cell-penetrating peptides (CPPs) as vehicles for intracellular delivery of antisense peptide nucleic acid (PNA). *Bioconjug Chem.* **2006**; 17: 750-8.
- 77) Brooks H, Lebleu B, and Vives E. Tat peptide-mediated cellular delivery: back to basics. *Advanced Drug Delivery Reviews.* **2005**, 57: 559-577.
- 78) Gammon ST, Villalobos VM, Prior JL, et al. Quantitative analysis of permeation peptide complexes labeled with Technetium-99m: chiral and sequence-specific effects on net cell uptake. *Bioconj. Chem.* **2003**; 14: 368-376.
- 79) Lewis MR, Jia F, Gallazzi F, et al. Radiometal-labeled peptide-PNA conjugates for targeting bcl-2 expression: preparation, characterization, and in vitro mRNA binding. *Bioconjug. Chem.* **2002**, 6: 1176-1180.
- 80) Escriou V, Carriere M, Scherman D, and Wils P. NLS bioconjugates for targeting therapeutic genes to the nucleus. *Adv. Drug Deliv. Rev.* **2003**, 2: 295-306.
- 81) Fisher R, Mader O, Jung G, and Brock R. Extending the applicability of carboxyfluorescein in solid-phase synthesis. *Bioconjugate Chem.* **2003**, 14, 653-660.
- 82) Pranter AM, Sharma V, Garbow JR, et al. Synthesis and characterization of a Gd-DOTA-permeation peptide for magnetic resonance relaxation enhancement of intracellular targets. *Mol. Imaging.* **2003**; 2: 333-341.

- 83) Ranganathan RS, Fernandez ME, Kang SI, et al. New multimeric magnetic resonance imaging agents. *Invest. Radiol.* **1998**, 33, 779-797.
- 84) Vintersten K, Monetti C, Gertsenstein M, et al. Mouse in red: red fluorescent protein expression in mouse ES cells, embryos, and adult animals. *Genesis.* **2004**; 40(4): 241-6.
- 85) Hainsworth J, Harrison P, and Mather JS. Preparation and characterization of a DOTA-Lysine-Biotin conjugate as an effector molecule for pretargeted radionuclide. *Bioconjugate Chem.* 2005; **16**, 1468-1474.
- 86) Kelly KA, Reynolds F, Weissleder R, and Josephson L. Fluorescein isothiocyanate-hapten immunoassay for determination of peptide-cell interactions. *Anal Biochem.* **2004**, 15; 330(2):181-5.
- 87) Eriksson M, Christensen L, Schmidt J, et al. Sequence dependent N-terminal rearrangement and degradation of peptide nucleic acid in aqueous solution. *New J. Chem.* **1998**, 22, 1055-1059.
- 88) Gallazzi F, Wang Y, Jia F, et al. Synthesis of radiometal-labeled and fluorescent cell-permeating peptide-PNA conjugates for targeting the bcl-2 proto-oncogene. *Bioconjug. Chem.* **2003**, 14(6), 1083-1095.
- 89) *Expedite 8900 PNA chemistry user's guide*. [http:// docs. applied biosystems. com/pebiiodocs/00601308.pdf](http://docs.appliedbiosystems.com/pebiiodocs/00601308.pdf).
- 90) Shiraishi T and Nielsen PE. Enhanced delivery of cell-penetrating peptide-peptide nucleic acid conjugates by endosomal disruption. *Nature Protocols.* **2006**, 1, 1-4.
- 91) Takeuchi T, Kosuge M, Tadokoro A, et al. Direct and rapid cytosolic delivery using cell-penetrating peptides mediated by pyrenebutyrate. *ACS Chemical Biology.* **2006**, 5, 299-303.
- 92) Li W, Nicol F, Szoka FC, et al. A designed synthetic pH-responsive amphipathic peptide with applications in drug and gene delivery. *Adv. Drug Deliv. Rev.* **2004**, 7, 967-985.
- 93) Wadia JS, Stan RV, Dowdy SF. Transducible TAT-HA fusogenic peptide enhances escape of TAT-fusion proteins after lipid raft macropinocytosis. *Nature Medicine.* **2004**, 3, 310-315.

References

- 94) Christiaens B, Dubruel P, Grooten J, et al. Enhancement of polymethacrylate-mediated gene delivery by penetratin. *Eur. J. Pharm. Sci.* **2005**, 24, 525-537.
- 95) Hantowich DJ, Nakamura K. Antisense targeting in cell culture with radiolabeled DNAs – a brief review of recent progress --. *Annals of Nuclear Medicine.* **2004**, 5, 363-368.
- 96) Liu CH, Kim YR, Jia QR, Eichler F, Rosen BR, and Liu KP. Imaging cerebral gene transcripts in live animals. *J. Neuroscience*, **2007**, 3, 713-722.
- 97) Kay C, Lorthioir OE, Parr NJ, et al. Solid-phase reaction monitoring chemical derivatization and off-bead analysis. *Biotech. Bioeng. (Combin. Chem.)*, **2000/2001**, 71(2), 110-118.
- 98) Heppeler A, Froidevaux S, Macke HR, Jermann E, Powell P and Henning M. Radiometal-labeled macrocyclic chelator-derivatised somatostatin analogue with superb tumor-targeting properties and potential for receptor-mediated internal radiotherapy. *Chem. Eur. J.* **1999**, 5, 1974-1981.

Lebenslauf von Wu Su

1. Persönliche Informationen:

Name: Su Vorname: Wu

Geschlecht: männlich

Staatsbürgerschaft: Volksrepublik China

Geburtsdatum: 25. Oktober 1968

2. Ausbildung

Januar 2005 – jetzt: PhD Studium

Max-Planck Institut für biologische Kybernetik, Tübingen, Deutschland.

Forschungsbereich: Biologische Chemie

Titel der Arbeit: Design und Synthese von antisense Peptid-Nukleinsäure konjugierten MR Kontrastmitteln

September 1997 bis Juli 2000: Master degree of sciences

Department of Biological Chemistry, School of Life Sciences, Lanzhou University, Lanzhou, P.R. China.

Titel der Arbeit: Herstellung und Anwendung von Polymergekoppelten Ti-BINOL Komplexen als chirale Katalysatoren in der enantioselektiven Addition von Diethylzink an Aldehyde.

September 1986 bis Juli 1990: Bachelor degree of sciences

Department of Biology, Peking University, Beijing, P.R. China.

3. Beruflicher Werdegang

2000 bis 2004:

Wissenschaftlicher Assistent des Direktors und Forschungsgruppenleiter, Institute of Biological Chemistry, College of Biotechnology, East Chinese University of Sciences and Technology, Shanghai, P.R. China.

1990 bis 1997:

Forschungsassistent, Cancer Research Institute of Gansu Province, P.R. China.